

2016

Brain structural connectivity and neurodevelopment in post-Fontan adolescents

<https://hdl.handle.net/2144/19163>

"Downloaded from OpenBU. Boston University's institutional repository."

BOSTON UNIVERSITY
SCHOOL OF MEDICINE

Dissertation

**BRAIN STRUCTURAL CONNECTIVITY AND NEURODEVELOPMENT IN
POST-FONTAN ADOLESCENTS**

by

CHRISTOPHER G. WATSON

B.S., Massachusetts Institute of Technology, 2007

Submitted in partial fulfillment of the
requirements for the degree of
Doctor of Philosophy

2016

© 2016 by
CHRISTOPHER G. WATSON
All rights reserved

Approved by

First Reader

Lucia M. Vaina, M.D., Ph.D.
Professor of Biomedical Engineering

Second Reader

Michael J. Rivkin, M.D.
Associate Professor of Neurology
Harvard Medical School

Third Reader

P. Ellen Grant, M.D., M.S.
Associate Professor of Radiology
Harvard Medical School

DEDICATION

To Grandma, Grandpa, and Abuelita

ACKNOWLEDGMENTS

I would like to thank the members of the Cardiology, Neurology, Psychiatry, and Radiology teams responsible for making this project possible: the study coordinators, especially Dana Bernson, Lisa-Jean Buckley, and Carolyn Dunbar-Masterson, for running the study: recruiting and screening patients, getting detailed medical history data, and database work; David Wypij, Lisa Asaro, and Christian Stopp for all their help with statistics and data cleaning; Sasha Taylor and Madelyn Labella for acquiring the mountain of neuropsych data; Bob Mulkern, Sridhar Vajapeyam, Fotini, Rob, and Sue, for help on the MRI side of the study; and to David Wypij, Dave DeMaso, David Bellinger, Jane Newburger, and Michael Rivkin for leading all major aspects of the project. I particularly want to acknowledge David Wypij, David Bellinger, and Jane Newburger for their decades-long commitment to studying neurodevelopment in children with congenital heart disease. Your contributions to the field are nothing short of impressive.

I would like to thank my advisor, Lucia Vaina, and my committee members, Ellen Grant, Jason Bohland, and Eric Kolaczyk, for their advice on the direction my dissertation took and on matters related to data analysis, and for the courses I was able to take with them. Also deserving mention are Shelley Russek and Sandi Grasso, for all of the work they have done to make the GPN what it is today.

I give additional, special thanks to Michael Rivkin, who has been my supervisor and mentor since 2007. Thank you for giving me the opportunity to grow as a scientist, and for teaching me the ins and outs of research in a pediatric clinical setting. I would

not be where I am today were it not for the chance I was given to work in such a great children's hospital. And thank you for being so kind as to invite me into your home several times for Thanksgiving, and making me feel like a part of the family.

I would also like to thank all of my friends (friends?!) and classmates, for their implicit and explicit support over the years. In particular, to Bo Shi, for getting me the job as a Research Assistant in Dr. Rivkin's lab back in October 2007. Finally, I thank Melanie for sticking with me and supporting me over the last several months, in which I have been constantly stressed and sleep deprived. You helped me relax (without feeling guilty about it!) before I burned out, made my day-to-day life easier, and helped motivate me when I needed it the most.

My family deserves special mention, as they are responsible for the kind of person I have become, and for raising me in an environment which led me to higher education and clinical research. And of course, thank you to my parents for their support from a distance the 15 years I've lived in Boston. I also remember the family members who sadly died while I was in graduate school, and are not here to see me finish: Grandma (June 2013), Abuelita (May 2015), and Grandpa (June 2015).

This work was supported by R01 HL096825 from the National Heart, Lung, and Blood Institute (NHLBI), the Farb Family Fund, and the Kostin Family Innovation Fund.

**BRAIN STRUCTURAL CONNECTIVITY AND NEURODEVELOPMENT IN
POST-FONTAN ADOLESCENTS**

CHRISTOPHER G. WATSON

Boston University School of Medicine, 2016

Major Professor: Lucia M. Vaina, M.D., Ph.D., Professor of Biomedical Engineering

ABSTRACT

Congenital heart disease (CHD) is the most common congenital anomaly, with single ventricle (SV) defects accounting for nearly 10% of all CHD. SV defects tend to be the most severe forms of CHD: all patients born with SV require multiple open heart surgeries, often beginning in the neonatal period, ultimately leading to the Fontan procedure. Due to improvements in surgical procedures and medical care, more patients are surviving into adolescence and adulthood. Brain imaging and pathology studies have shown that patients with SV have differences in brain structure and metabolism even before the first surgery, and as early as *in utero*. Furthermore, a significant number of patients have new or more severe lesions after the initial surgery, and many still have brain abnormalities into early childhood. However, there are no detailed brain structural data of SV patients in adolescence. Our group recruited a large cohort of post-Fontan SV patients aged 10-19 years. Separate analyses of neuropsychological and behavioral outcomes in these patients show deficits in multiple areas of cognition, increased rates of attention deficit-hyperactivity disorder (ADHD), and increased use of remedial and/or special education services compared to a control group. Post-Fontan adolescents have more gross brain abnormalities, including evidence of chronic ischemic stroke.

Furthermore, there are widespread reductions in cortical and subcortical gray matter volume and cortical thickness, some of which are associated with medical and surgical variables. Diffusion tensor imaging (DTI) analyses show widespread areas of altered white matter microstructure in deep subcortical and cerebellar white matter. In this dissertation, I use graph theory methods to characterize structural connectivity based on gray matter (cortical thickness covariance) and white matter (DTI tractography), and examine associations between brain structure and neurodevelopment. I found that brain network connectivity differs in post-Fontan patients compared with controls, both at the global and regional level. Additionally, deficits in overall network structure were associated with impaired neurodevelopment in several domains, including general intelligence, executive function, and visuospatial skills. These data suggest that early neuroprotection should be a major focus in the care of SV patients, with the goal of improving long-term neurodevelopmental outcomes.

TABLE OF CONTENTS

DEDICATION	iv
ACKNOWLEDGMENTS	v
ABSTRACT	vii
TABLE OF CONTENTS	ix
LIST OF TABLES	xiv
LIST OF FIGURES	xvi
LIST OF ABBREVIATIONS	xviii
BACKGROUND	1
History: CHD and the brain	1
Single ventricle.....	3
Epidemiology	4
Types of SV	9
Fontan surgical course and outcomes	10
Staged palliation.....	11
Neurodevelopmental outcomes	13
Brain and neurologic outcomes.....	16
Graph theory and MRI	26

Gray matter networks	28
White matter networks	30
Graph theory associated with patient-specific variables	32
Preliminary studies	34
Patient characteristics and surgical history	34
Neuropsychological outcomes	36
Gray matter differences	37
White matter differences	38
Summary	39
GRAPH THEORY ANALYSIS OF GRAY MATTER NETWORKS IN POST- FONTAN CHILDREN AND ADOLESCENTS	49
Introduction	49
Methods	52
Subjects	52
MRI acquisition	53
Cortical thickness calculation	53
Network construction	54
Network metrics	55

Statistics	61
Results	62
Subjects	62
Network hubs	62
Network segregation	63
Small world	63
Network closeness.....	63
Permutation analysis	64
Robustness	65
Subgroup analysis	78
Discussion	89
Conclusions	94
GRAPH THEORY ANALYSIS OF WHITE MATTER NETWORKS IN POST- FONTAN CHILDREN AND ADOLESCENTS	95
Introduction.....	95
Methods.....	98
Subjects	98
MRI acquisition.....	98

DTI preprocessing and tractography	98
Network construction	99
Group differences in global- and vertex-level measures.....	101
Network-based statistic	102
Demographic and medical history variables	103
Results.....	104
Subjects	104
Global graph measures	104
Vertex-level differences	105
Associations with first operation.....	106
Network-based statistic	108
Discussion	125
Conclusions.....	128
 BRAIN STRUCTURAL CONNECTIVITY, SURGICAL HISTORY, AND NEURODEVELOPMENT IN POST-FONTAN CHILDREN AND ADOLESCENTS	129
Introduction	129
Methods.....	131
Gray matter networks	131

White matter networks	133
Neurodevelopmental outcomes	135
Surgical and medical history variables	136
Results	137
Gray matter networks	137
White matter networks	140
Discussion	152
Conclusions	156
CONCLUSIONS	157
BIBLIOGRAPHY	163
CURRICULUM VITAE	199

LIST OF TABLES

Table 1.1. Subject demographics.	40
Table 1.2. Surgical history.	41
Table 1.3. Type of Fontan procedure, full cohort	43
Table 1.4. Anatomic diagnosis, full cohort	43
Table 2.1. Subject demographics and education history	66
Table 2.2. Group differences in nodal efficiency.....	75
Table 2.3. Group differences in betweenness centrality	75
Table 2.4. Group differences in nodal efficiency, Norwood status	81
Table 2.5. Group differences in betweenness centrality, Norwood status	84
Table 2.6. Group differences in nodal efficiency, type of first operation.....	87
Table 2.7. Group differences in betweenness centrality, type of first operation	87
Table 2.8. Group differences in nodal efficiency, type of first operation.....	88
Table 2.9. Group differences in nodal efficiency, type of first operation.....	88
Table 3.1. Subject demographics and education history.....	109
Table 3.2. Group differences in vertex strength.....	111
Table 3.3. Group differences in vertex weighted nodal efficiency (L).....	113
Table 3.4. Group differences in vertex weighted nodal efficiency (R).....	114
Table 3.5. Group differences in vertex weighted shortest path length (L)	116
Table 3.6. Group differences in vertex weighted shortest path length (R)	117
Table 3.7. Associations between nodal efficiency and operative variables.....	119
Table 3.8. Associations between local efficiency and operative variables.....	120

Table 3.9. Associations between vertex strength and operative variables.....	123
Table 4.1. Associations between IC (LOO) and outcomes.....	138
Table 4.2. Associations between IC (AOP) and outcomes.....	139
Table 4.3. Associations between RC (LOO) and outcomes.....	141
Table 4.4. Associations between RC (AOP) and outcomes.....	143
Table 4.5. Associations between RC (LOO) and genetic abnormality.....	144
Table 4.6. Mediation between graph measures and neurodevelopmental outcomes	144
Table 4.7. Mediation between weighted nodal efficiency and neurodevelopmental outcomes	149
Table 4.8. Mediation between strength and neurodevelopmental outcomes	150
Table 4.9. Mediation between weighted local efficiency and neurodevelopmental outcomes	151

LIST OF FIGURES

Figure 1.1. Age at Fontan.....	42
Figure 1.2. Year of Fontan	44
Figure 1.3. Age at Fontan by diagnosis	45
Figure 1.4. Volumetric differences	46
Figure 1.5. Fractional anisotropy differences	47
Figure 1.6. Axial diffusivity differences	48
Figure 2.1. Hub regions in the Control group.....	67
Figure 2.2. Hub regions in the Fontan group	68
Figure 2.3. Hub regions across densities	69
Figure 2.4. Adjacency matrix for the Control group.....	70
Figure 2.5. Adjacency matrix for the Fontan group.....	71
Figure 2.6. Small-world (σ and ω) index against density.....	72
Figure 2.7. Global network measures against density.....	73
Figure 2.8. Vertices with significant between-group differences, nodal efficiency ...	74
Figure 2.9. Significant between-group differences, betweenness centrality.....	76
Figure 2.10. Robustness analysis.....	77
Figure 2.11. Significant differences in nodal efficiency (Norwood status).....	79
Figure 2.12. Vertices with significant between-group differences in betweenness centrality, Norwood status	80
Figure 2.13. Vertices with significant between-group differences in nodal efficiency, type of first operation.....	82

Figure 2.14. Vertices with significant between-group differences in betweenness centrality, type of first operation.....	83
Figure 2.15. Vertices with significant between-group differences in nodal efficiency, age at first operation	85
Figure 2.16. Vertices with significant between-group differences in betweenness centrality, age at first operation.....	86
Figure 3.1. Global network measures across thresholds.....	110
Figure 3.2. Group differences in vertex strength.....	112
Figure 3.3. Group differences in vertex weighted nodal efficiency	115
Figure 3.4. Group differences in vertex weighted shortest path length	118
Figure 3.5. Significant associations with nodal efficiency.....	121
Figure 3.6. Significant associations with local efficiency.....	122
Figure 3.7. Network-based statistic results	124
Figure 4.1. Fontan IC (LOO) and neurodevelopmental outcomes	145
Figure 4.2. Fontan IC (AOP) and neurodevelopmental outcomes	146
Figure 4.3. Significant associations with RC (LOO).....	147
Figure 4.4. Significant associations with RC (AOP).....	148

LIST OF ABBREVIATIONS

ACME	Average causal mediation effect
AD	Axial diffusivity
ADHD	Attention deficit-hyperactivity disorder
AI	Asymmetry index
AOP	Add-one-patient
AQ	Autism Spectrum Quotient
AUC	Area under the curve
AV	Atrioventricular
BCAS	Boston Circulatory Arrest Study
BCH	Boston Children's Hospital
BRIEF	Behavior Rating Inventory of Executive Function
BSID	Bayley Scales of Infant Development
BT	Blalock-Taussig
CADS-P	Conners' ADHD/DSM-IV Scales
CBF	Cerebral blood flow
CHD	Congenital heart disease
CI	Confidence interval
CPB	Cardiopulmonary bypass
DHCA	Deep hypothermic circulatory arrest
DILV	Double inlet left ventricle
D-KEFS	Delis-Kaplan Executive Function System

DKT	Desikan-Killiany-Tourville
DORV	Double outlet right ventricle
d-TGA	d-Transposition of the great arteries
DTI	Diffusion tensor imaging
EEG	Electroencephalography
FA	Fractional anisotropy
FDR	False discovery rate
FDT	FSL Diffusion Toolbox
FOV	Field of view
FSIQ	Full-scale intelligence quotient
FSL	FMRIB software library
GA	Gestational age
GE	General Electric
GLM	General linear model
GM	Gray matter
HLHS	Hypoplastic left heart syndrome
IC	Individual contribution
IQR	Interquartile range
ISVT	Infant Single Ventricle Trial
IVC	Inferior vena cava
LOO	Leave-one-out
MCA	Middle cerebral artery

MNI.....Montreal Neurological Institute
MP-RAGE..... Magnetization-prepared rapid acquisition gradient echo
MRI..... Magnetic resonance imaging
NAA N-acetyl-aspartate
NBS.....Network-based statistic
NIH.....National Institutes of Health
NIRS.....Near infrared spectroscopy
NYHANew York Heart Association
PA/IVS Pulmonary atresia with intact ventricular septum
PC.....Participation coefficient
PHN..... Pediatric Heart Network
PVL..... Periventricular leukomalacia
RC Regional contribution
RD Radial diffusivity
ROI.....Region of interest
RVPARight ventricle to pulmonary artery
SV..... Single ventricle
SVC.....Superior vena cava
SVRT Single Ventricle Reconstruction Trial
TTesla
TASToronto Alexithymia Scale
TCPC..... Total cavopulmonary connection

TE.....	Echo time
TI.....	Inversion time
TMS	Total Maturation Score
TR.....	Repetition time
TVPS.....	Test of Visual-Perceptual Skills
VSD.....	Ventricular septal defect
WAIS	Wechsler Adult Intelligence Scale
WIAT	Wechsler Individual Achievement Test
WISC.....	Wechsler Intelligence Scale for Children
WM	White matter

BACKGROUND

History: CHD and the brain

The potential negative effects of open-heart surgery, using deep hypothermic circulatory arrest (DHCA) or cardiopulmonary bypass (CPB), on the brain and later neurodevelopmental outcomes have been known for decades (Branthwaite, 1972; Clarkson et al., 1980; Gilman, 1965; Malone et al., 1981; Rossi et al., 1986; Terplan, 1973, 1976; Wells et al., 1983). Based on a survey of six pediatric centers in 1988 and 1989, Ferry (1990) found that all centers reported incidence of neurological symptoms (e.g., seizures, loss of consciousness, choreoathetosis) (Ferry, 1990). McConnell et al. (1990) performed an MRI study of 15 patients before and after open heart surgery with CPB; only 2 of the patients had a normal postoperative MRI scan, compared with 10 in the preoperative period. Although clinicians had been aware of this association between heart surgery and brain injury, it had not yet been systematically studied in a prospective trial.

The first randomized controlled trial investigating these outcomes in CHD patients was the *Boston Circulatory Arrest Study (BCAS)* (Newburger et al., 1993). In the BCAS, neonates and infants born between 1988-1992 with d-Transposition of the Great Arteries (d-TGA) were randomized into two groups based on surgical procedure: repair with a prolonged period of DHCA, or repair using predominantly continuous low-flow CPB. The cohort was a homogeneous group of patients who underwent the arterial switch operation within the first three months of life (most within the first month), and all surgeries occurred at Boston Children's Hospital (BCH). This study design avoided

the difficulties that arise when including patients with different heart defects and therefore varied surgical courses. At one year of age, Psychomotor Development Index (a measure of gross and fine motor function in infants) was lower in the DHCA group; lower scores and neurologic abnormalities were associated with increasing duration of DHCA and with electroencephalographic (EEG) seizure activity (Bellinger et al., 1995). At four years of age, the full d-TGA cohort scored significantly lower than population norms in multiple neuropsychological domains, but differences between treatment groups were limited to worse performance in motor and speech function in the DHCA group (Bellinger et al., 1999). In the next study phase, at eight years, results were similar to those of the four-year assessment (Bellinger et al., 2003). Furthermore, the BCAS investigators showed that the adverse effects of DHCA on neurodevelopment did not appear until DHCA duration exceeded 41 minutes (Wypij et al., 2003).

The latest analysis of neurodevelopmental outcomes in the BCAS cohort at sixteen years of age showed that, while treatment group differences continued to be small, the d-TGA group as a whole had significantly impaired cognitive and behavioral function across multiple domains (Bellinger et al., 2011). In addition, nearly two-thirds of patients received special educational services, the use of psychiatric medications was four times more frequent compared to the referent group, and ADHD diagnosis was significantly higher in the d-TGA group (DeMaso et al., 2014). We also acquired magnetic resonance imaging (MRI) data in the sixteen year-olds, and found differences in white matter microstructure, cortical and subcortical volume, and cortical thickness throughout the brain compared to the control group (Rivkin et al., 2013; Rollins et al.,

2014; Watson et al., 2016). Importantly, several MRI measures were associated with medical variables, such as age at surgery, cooling duration, and length of postsurgical hospital stay, and cognitive outcome scores, including mathematics achievement, inattention/hyperactivity, executive function, and visuospatial skills.

More recent studies have confirmed, in d-TGA and other CHD groups, that such neurodevelopmental deficits persist many years after the initial cardiac surgery (to be discussed in more detail in Neurodevelopmental outcomes). Patients with the most severe forms of CHD *require* surgical intervention in the neonatal period and infancy/early childhood, with single ventricle (SV) patients requiring multiple procedures. With improvements in surgical procedures and postoperative care, the characterization of long-term outcomes in this population has taken focus.

Single ventricle

In the normal heart, the systemic and pulmonary circulations are in series, with each being supported by its own ventricle. In patients with functional SV, the circulations are in parallel, resulting in the mixing of systemic and pulmonary venous blood. This mixing of oxygen-rich and oxygen-poor blood can lead to lower cerebral oxygen saturation (Hoffman et al., 2013; Kurth et al., 2001). The most critically ill patients suffer from a lack of oxygenated blood reaching the body and brain, and will die without surgical intervention. Thus, patients with SV typically undergo a *staged palliation* which consists of one or more (typically a minimum of two) surgeries and culminates in the *Fontan procedure*. In this section, I first describe the epidemiology of

SV defects; I then provide a brief description of the different types of anatomical defects present in our cohort.

Epidemiology

CHD (of any severity) is the most common congenital anomaly, accounting for one-third of all anomalies (Tennant et al., 2010; van der Bom et al., 2011). The birth prevalence of CHD is increasing over time, likely due to reduced mortality and/or improved detection of more minor types. Current estimates show that, since 1995, CHD occurs in approximately 9 per 1,000 live births per year, an increase from less than 1 per 1,000 in the 1930's (van der Linde et al., 2011). SV defects are among the most complex types of CHD and make up nearly 10% of all CHD, in an estimated 4-8 per 10,000 live births (O'Leary, 2002). Among SV defects, hypoplastic left heart syndrome (HLHS) occurs in approximately 41%, tricuspid atresia in approximately 17%, and the remaining 42% are all other types of SV.

Etiology

The causes of CHD in many cases remain unknown, but known associated risk factors include maternal obesity (Madsen et al., 2013), maternal diabetes (Wren et al., 2003), and genetic mutations (Fahed et al., 2013). Genetic causes have been the most extensively studied. In an analysis of 538 CHD trios (the patient and both parents), under 10% were shown to have *de novo* copy number variants (Glessner et al., 2014). In an exome analysis of 1,213 parent-offspring trios (any CHD), 21% had damaging *de novo* mutations, and the investigators identified 21 genes with multiple mutations, including 7 previously implicated in CHD (Homsy et al., 2015). In SV patients only, 13.9% had

pathogenic copy number variants (Carey et al., 2013). In our sample of post-Fontan children and adolescents, 10% had a definite genetic abnormality, and 7.5% had a pathogenic copy number variant (Bellinger et al., 2015). Therefore, genetic testing will not detect CHD in the majority of cases.

Diagnosis and presentation

Diagnosis of SV defects are often made by fetal echocardiography, if indicated clinically by an abnormality on standard ultrasound or in the presence of known CHD risk factors. If the defect goes undetected, then diagnosis is made soon after birth. Prenatal diagnosis is thought to be particularly beneficial in patients with SV, as clinical management can be initiated sooner, and the mother can plan her delivery to take place at an advanced tertiary center. However, outcomes appear to be mixed, with some studies reporting no significant improvement with prenatal diagnosis (in HLHS, tricuspid atresia, and heterotaxy; see Atz et al. (2010); Cohen et al. (2006); Kumar et al. (1999); Wald et al. (2007)) and others reporting lower incidence of brain injury and more favorable pre-surgical status (but with no difference in mortality) (Mahle et al., 2001; Peyvandi et al., 2016; Sivarajan et al., 2009). Presentation varies with the underlying defect, but is nearly always in the neonatal period; symptoms include cyanosis, heart murmur, congestive heart failure, and neonatal shock (O'Leary, 2002).

Survival

Survival (early, interstage, and late) has been improving over time. For patients undergoing the Fontan in the late 1970's to the 1980's (all SV types), early (1-month) survival was between 79% and 84%, and 10-year survival was between 58.1% and 63%

(Driscoll et al., 1992; Fontan et al., 1990). In the large Pediatric Heart Network (PHN) Fontan cohort (n=427), who had their procedure in the late 1990's to early 2000's, survival was 95% at an average of 15 years post-Fontan (Atz et al., 2015). This represents the current best estimate for 10-year survival and longer, which has been shown to be above 90% in other reports as well (Dabal et al., 2014; d'Udekem et al., 2014; Pundi et al., 2015). Survival rates are not equal across the different types of SV; however, the trend of increased survival with time is preserved. In patients with tricuspid atresia diagnosed from 1941-1973, survival to 15 years (without the Fontan procedure) was only 50% (Dick et al., 1975). Survival in this sub-group has similarly increased over time, to approximately 80% at a follow-up of 13-14 years (Mair et al., 2001; Wald et al., 2007). In patients with HLHS, survival beyond infancy was 0% before the introduction of the Norwood procedure (Norwood et al., 1980; Wren and O'Sullivan, 2001). The best current estimates come from the *Single Ventricle Reconstruction Trial (SVRT)*, with 3-year survival at 64% (at the time of this report, only 58% of study subjects had undergone the Fontan) (Newburger et al., 2014). Due to these decreases in perioperative and early postoperative mortality, the prevalence (both of CHD in general and of SV) in adults has been increasing (Marelli et al., 2007).

Co-morbidities and complications

SV patients are in a relatively good state of health several years after the Fontan procedure, but morbidity is not rare and worsens with time. Fontan and colleagues (1990) reported, in 334 patients who underwent the procedure from 1968-1988, an increasing

percentage of patients in New York Heart Association (NYHA) Class III (“poor”) with time after the Fontan; however, even after more than 10 years, this was still less than 10% (Fontan et al., 1990). In a longitudinal study of 363 patients who underwent the Fontan at Boston Children’s Hospital (BCH) from 1973-1991, more than 90% were in “excellent or good” health, and more than 90% were in NYHA Class I or II (“good”), at a median follow-up of 5.4 years (Gentles et al., 1997). In the PHN Fontan cohort, functional health status was lower than controls and United States population norms, but more than 80% were within normal range; similar results were achieved at the 15-year follow-up study (Anderson et al., 2008; Atz et al., 2015; McCrindle et al., 2006).

Although functional health status is good, re-interventions and re-hospitalizations are not rare. Gentles et al. (1997) report that 75 (20.1%) patients underwent a total of 113 late re-operations, and 88 (24.2%) underwent a total of 128 transcatheter procedures. In the PHN cohort, 119 subjects (28%) required additional cardiac surgery, and 242 (57%) had at least one catheter intervention (Atz et al., 2015). At 10 and 15 years post-Fontan, a large series of 406 patients found that a similar rate, one in four, required re-intervention (Hosein et al., 2007). At longer follow-up times (20 years post-Fontan), the majority of patients (66%) will have had an intervention (Ono et al., 2006).

Somatic growth differs between SV patients and healthy children. Patient weight is significantly lower than population norms before Stage II reconstruction and in the early postoperative period and may normalize, whereas height remains low at 15 years of follow-up (Anderson et al., 2008; Atz et al., 2015; Ono et al., 2006; Vogt et al., 2007). Furthermore, shorter stature in the PHN cohort was associated with poorer functional

health status (Cohen et al., 2010). As Vogt et al. (2007) found that patients who had the Fontan at a later age had more impaired growth, it may be desirable to perform the surgery earlier in life so that “catch-up” growth can occur.

Thromboembolic events are a major source of morbidity and mortality, ranging from 3-20%, and can occur at almost any time after the procedure, beginning in the immediate postoperative period (Anderson et al., 2008; Atz et al., 2015; Khairy et al., 2008; Monagle and Karl, 2002; Rosenthal et al., 1995). At longer follow-up, arrhythmias are common, increase in frequency with age, and are thought to be the cause of most cases of sudden death in the post-Fontan SV patient (Khairy et al., 2008; Pundi et al., 2015; Stephenson et al., 2010). Atrial arrhythmias, along with heart failure, represent significant causes of re-hospitalization and increased costs of medical care (Tabtabai et al., 2015).

The liver is particularly affected in Fontan patients (for review, see Rychik et al. (2012)). Liver dysfunction is common and associated with lower cardiac function (Camposilvan et al., 2008). More importantly, hepatic cirrhosis and hepatocellular carcinoma have been reported (Ghaferi and Hutchins, 2005; Kiesewetter et al., 2007). The frequency increases after approximately 20 years follow-up: a retrospective study of all patients who underwent the Fontan at the Mayo Clinic found that freedom from cirrhosis was only 57% at longer follow-up, and the earliest diagnosis of hepatocellular carcinoma was 17 years post-Fontan (Pundi et al., 2016). Protein-losing enteropathy is another common, non-cardiac morbidity in SV patients. Its prevalence is reported to be between 5% and 15% in various cohorts, ranging from 5 to 10 years post-Fontan (Atz et

al., 2015; Feldt et al., 1996; Hirsch et al., 2008; Pundi et al., 2015). This is a major concern, as mortality greatly increases in patients with these complications (Mertens et al., 1998; Pundi et al., 2015). The presence of such serious extracardiac medical conditions underscores the need for long-term, careful follow-up involving a multidisciplinary team in the child with SV.

Types of SV

There are essentially three types of *SV physiology*: 1) obstruction of flow from the ventricle to the aorta; 2) obstruction of flow from the ventricle to the pulmonary artery; and 3) no obstruction of outflow to the body or the lungs. The SV type determines the patient's surgical course (which is discussed in more detail in Staged palliation). Patients may be further categorized based on anatomy:

Hypoplastic left heart syndrome (HLHS) defined by Tchervenkov et al. (2006) as “a spectrum of cardiac malformations with normally aligned great arteries without a common atrioventricular junction, characterized by underdevelopment of the left heart with significant hypoplasia of the left ventricle including atresia, stenosis, or hypoplasia of the aortic or mitral valve, or both valves, and hypoplasia of the ascending aorta and aortic arch” (Tchervenkov et al., 2006, p. 344).

Tricuspid atresia underdevelopment of the tricuspid valve

Double outlet right ventricle (DORV) both the pulmonary artery and aorta arise from the right ventricle

Double inlet left ventricle (DILV) underdeveloped right ventricle along with a transposed pulmonary artery and aorta

Heterotaxy syndrome a non-CHD syndrome in which the heart and visceral organs are arranged abnormally across the body's left-right axis; heart malformations are highly variable in this subgroup

Complex transposition of the great arteries (TGA) the co-occurrence of d-TGA and other heart malformations

Pulmonary atresia with intact ventricular septum (PA/IVS) consists of underdevelopment of the pulmonary valve, along with a lack of ventricular septal defect (VSD) Unbalanced atrioventricular canal the presence of an atrial septal defect, VSD, and malformation of the mitral and tricuspid valves

Mitral atresia underdevelopment of the mitral valve

Fontan surgical course and outcomes

The *Fontan procedure* is the common final operation for all forms of SV. The goal is to separate the systemic and pulmonary circulations. It was first performed in 1968 in a 12 year old patient with tricuspid atresia; the patient had a good prognosis at 30 months follow-up (Fontan and Baudet, 1971). Of the other two patients in the initial report, the second patient had a good prognosis at 10 months post-Fontan, and the third patient died 6 hours after surgery. This procedure is *palliative*, not curative, and patients with a Fontan circulation are at risk for multiple long-term medical problems. First, I describe the common three-stage palliation, followed by a review of the neurodevelopmental outcomes in SV patients post-Fontan.

Staged palliation

As mentioned in Types of SV, there are three types of SV physiology. The initial operation (*Stage I*) usually differs between these subgroups, whereas *Stage II* procedures are similar for all SV patients (Friesen and Forbess, 2002). The goal of the staged palliation is to prepare the patient for having a successful Fontan.

Stage I

The ultimate goal of the Stage I operation is to balance the pulmonary and systemic blood flows, by removing any systemic outflow obstructions and providing a stable source of pulmonary flow. For SV defects of the first type (i.e., obstruction of flow from the ventricle to the aorta), the Stage I operation is typically the Norwood (particularly for hypoplastic left heart syndrome [HLHS]) (Norwood et al., 1980). There are a few different variants of the Norwood. In the “classic” Norwood, a Blalock-Taussig (BT) shunt connects the innominate artery to the pulmonary artery (PA) (Blalock and Taussig, 1945). Alternatively, a shunt is placed connecting the right ventricle to the pulmonary artery (RVPA shunt). Both of these shunts provide forward flow into the PA. Reconstruction of the aortic arch is often performed, as well as ligation of the patent ductus arteriosus (which typically is kept open prior to surgery using prostaglandin E1) (Freed et al., 1981). The Norwood is often performed within the first week of life (Dent et al., 2006; Hehir et al., 2008; Ohye et al., 2010).

Patients with the second (i.e., flow obstruction from the ventricle to PA) or third (i.e., no obstruction of outflow to the body or lungs) type may not need to undergo the Norwood as an initial operation, and their first procedure would be the Glenn (see Stage

II) or even the Fontan (see Stage III) (Fontan and Baudet, 1971; Glenn, 1958). In patients of the third type that do require an initial surgery, it is typically the placement of a PA band, which can be performed as early as the neonatal period (Ramakrishnan et al., 2016).

Stage II

The Stage II procedure is either the *bidirectional Glenn* or the *hemi-Fontan*. The bidirectional Glenn involves a cavopulmonary shunt directing systemic venous flow from the superior vena cava (SVC) to the PA (Hopkins et al., 1985). The hemi-Fontan was introduced to separate the Fontan into a two-stage process to reduce the work performed by the single ventricle (Jacobs et al., 1996). A connection is placed between the right atrial-SVC junction and the PA, and a patch placed in the central portion of the PA. Stage II is typically performed at approximately 6 months of age (Friesen and Forbess, 2002; Jacobs et al., 1996).

Stage III

In all SV patients, Stage III is the Fontan procedure. Its goal is to establish the *Fontan circulation*, consisting of a single ventricle producing all cardiac output, with the systemic and pulmonary circulations in series rather than in parallel. The “classic” Fontan involved a few steps: connection of the SVC to the right PA, an atriopulmonary connection (right atrium to left PA), and closure of the atrial septal defect (if present) (Fontan and Baudet, 1971). De Leval and colleagues (1988) introduced a modification to the Fontan, the *total cavopulmonary connection (TCPC)*, in which both the SVC and inferior vena cava (IVC) are connected to the PA (de Leval et al., 1988) There are two

types of TCPC. For the *intracardiac*, or *lateral tunnel*, TCPC, a baffle is placed in the right atrium. Alternatively, an *extracardiac* TCPC can be performed, in which a conduit connects the IVC to the PA, bypassing the right atrium altogether (Marcelletti et al., 1990). Mortality and medical outcomes are similar for both techniques, although the extracardiac TCPC may reduce postoperative arrhythmias (Azakie et al., 2001; Fiore et al., 2007; Kumar et al., 2003). Another option for the Fontan is *fenestration* of the atrial baffle, which was introduced with the goal of reducing morbidity in patients with ventricular dysfunction or PA stenosis (Bridges et al., 1990). Inclusion of a fenestration has been associated with lower mortality and morbidity (Bridges et al., 1992; Goff et al., 2000; Lemler et al., 2002). The choice for the specific technique used at this stage may depend on the specific SV anatomy and/or the Stage II operation. The Fontan procedure is typically performed between 1.5 and 4 years old.

Neurodevelopmental outcomes

Early postoperative

Assessment of neurodevelopment in the early postoperative period is limited predominantly to motor function and simple mental abilities. A meta-analysis of HLHS patients after the Norwood reported that mean IQ and Bayley-Scales of Infant Development (BSID) scores, while significantly lower than population norms, increased from 1989 to 1999 (Sistino and Bonilha, 2012). At 1 year of age, SV patients consistently show lower BSID scores, with greater impairment in motor function than mental development (Gaynor et al., 2006; Goldberg et al., 2007; Sarajuuri et al., 2009; Tabbutt et al., 2008; Visconti, 2006). This pattern is also present in larger series of

patients at 14 months of age (Gaynor et al., 2015; Newburger et al., 2012; Williams et al., 2013). Additionally, motor development in HLHS infants was significantly worse than other CHD infants. At 2-3 years of age, neurodevelopmental scores remain lower than population norms, particularly in the motor domain (Mussatto et al., 2014; Rogers et al., 1995; Sananes et al., 2012; Sarajuuri et al., 2010). Furthermore, SVRT participants at age 3 years were impaired in terms of behavior, quality of life, and functional health status (Goldberg et al., 2014). In summary, developmental deficits are already evident in many SV patients in the early postoperative period, with motor function showing particularly high degree of impairment.

Pre- and early-school age

Assessment of 4-5 year-old patients who had already undergone the Fontan show deficits in processing speed, visuomotor integration, attention, and impulsivity compared to other CHD patients (i.e., CHD patients with two ventricles who underwent biventricular repair) (Gaynor et al., 2014), although smaller series report low-normal IQ in HLHS and other SV patients (Hoffman et al., 2005; Kern et al., 1998; Sarajuuri et al., 2012; Uzark et al., 1998). Other studies similarly show IQ within the low-normal range for SV patients, in addition to poorer outcomes when compared to other CHD (Forbess et al., 2001, 2002; Goldberg et al., 2000). At nearly 8 years post-Fontan (ages 5-14 years), one in five patients were at least 2 standard deviations below the population mean (expected: 2%); in those with the poorest scores, perceptual reasoning and working memory were more impaired than verbal comprehension and processing speed (Sugimoto et al., 2013). Another group demonstrated significant delays in motor

development in patients 5 years after the Fontan (ages 6-10 years) (Longmuir et al., 2012). In a similarly-aged cohort of SV and other CHD patients, nearly one in three had inattentiveness and hyperactivity scores in the “high-risk” range, and 15% had already been placed in full-time special education classrooms (Shillingford et al., 2008). Similar results were found in a slightly older cohort of HLHS patients (Mahle et al., 2000). Overall, school-age children who have undergone the Fontan continue to perform worse than healthy and non-SV CHD children, and begin to require additional special educational services.

Late childhood and adolescence

Only a handful of studies have followed post-Fontan patients into late childhood and adolescence. Wernovsky et al. (2000) administered standardized testing to children at an average age of 14 years. In more than 100 SV patients who underwent the Fontan in the 1970's and 1980's, IQ and academic achievement were significantly lower than population norms; furthermore, a diagnosis of HLHS was a predictor of lower IQ. Similarly, in a cohort of HLHS children aged 8 to 17 years, operated on in the 1990's, scores on tests of cognition, academic achievement, language function, and executive function all were significantly lower than population norms (Mahle et al., 2006). In the PHN cohort ($N = 537$), assessment at an average age of 12 years revealed attention problems in nearly one-half, vision problems in one-third, and speech problems in one-fourth (McCrinkle 2006). Behavioral problems, anxiety, and depression were also present in 23%, 17%, and 8% of the cohort, respectively. Detailed results of the present cohort (average age: 14 years) is in Neuropsychological outcomes. To summarize, SV

patients continue to have significant problems in cognitive and behavioral function as they near young adulthood. Interventions targeted at strengthening these areas in SV patients should begin even before the child reaches school-age.

Brain and neurologic outcomes

The heart and brain follow a very similar developmental timeline *in utero* (McQuillen and Miller, 2010). In the fetus with congenital heart disease (CHD), abnormal heart development can affect brain development, as the developing brain requires significant metabolic resources, delivered via the cerebrovascular system. I first review the literature on prenatal imaging studies of the fetal brain in the context of CHD, and continue chronologically to the preoperative period, early postoperative period, and finally childhood and adolescence.

Prenatal brain characteristics

Investigation into brain development of the CHD fetus has been performed with MRI and ultrasound (Doppler imaging) as early as 11 weeks gestation. Several studies have focused on body/head measurements. Recently, head volume was assessed in CHD fetuses from 11-14 weeks gestation (Abu-Rustum et al., 2016). Although the sample size was small, head volume was statistically significantly lower in the CHD fetuses, especially those with HLHS. Rosenthal (1996), utilizing only anthropometric measurements at birth, found that HLHS neonates were smaller than controls in all measures (birth weight and length, head circumference and volume), but did not detect differences compared to other CHD types. A nationwide study of CHD patients found significantly smaller head circumference and birth weight in HLHS and other SV defects

(Matthiesen et al., 2016). Similarly, HLHS fetuses were shown to have smaller head sizes, in addition to narrowing of the ascending aorta; interestingly, microcephaly was associated with a more narrow aorta (Shillingford et al., 2007). The finding of a reduction in head size has been replicated by other groups; additionally, there is a significant decrease in both head growth and body weight from the fetal period to birth in HLHS (Berg et al., 2009; Cnota et al., 2013; Donofrio et al., 2003; Hahn et al., 2015; Hinton et al., 2008; Kaltman et al., 2005; Williams et al., 2015).

Doppler imaging in CHD fetuses has been used primarily to measure blood flow patterns. Donofrio et al. (2003) demonstrated that the *brain sparing effect*, a phenomenon in which cerebrovascular resistance is decreased in response to reduction of placental blood flow, does not occur to a high enough degree in HLHS fetuses to restore brain growth to normal levels. Other groups have confirmed this finding of lower resistance in middle cerebral artery (MCA) blood flow, both compared to other CHD types and to controls (Berg et al., 2009; Kaltman et al., 2005). Interestingly, using data from the SVRT and Infant Single Ventricle Trial (ISVT), Hahn et al. (2015) report not only lower MCA resistance throughout gestation (separated into four time periods), but also a greater-than-expected decrease later in gestation (from 30-33 weeks to more than 34 weeks) (Hahn et al., 2015; Szwasz 2012). Notably, lower MCA resistance was associated with higher psychomotor development scores at 14 months of age (Hahn et al., 2015; Williams et al., 2013).

Neuropathological analysis of electively aborted HLHS fetuses (19-22 weeks gestation) revealed widespread white matter (WM) and gray matter (GM) injury in all 11

brains (Hinton et al., 2008). On MRI, gross brain abnormalities are common in CHD: one-fourth of all CHD and one-fifth of HLHS fetuses had an abnormal MRI finding when imaged between 18 and 39 weeks gestation, with a higher frequency of abnormal findings in the third trimester (Brossard-Racine et al., 2014). Fetal brain MRI and ultrasound studies in CHD have consistently shown reduced volumes (total brain, intracranial, cortical and subcortical GM, and total WM) (Andescavage et al., 2015; Clouchoux et al., 2013; Limperopoulos et al., 2010; Sun et al., 2015; Zeng et al., 2015a). Similar to head circumference measurements, brain volumes show a decrease in growth over the third trimester (Clouchoux et al., 2013; Limperopoulos et al., 2010; Zeng et al., 2015a). In addition to volume, Clouchoux et al. (2013) report reductions in cortical gyrification and surface area in HLHS fetuses, and delayed development of primary sulci and cortical depth compared to control fetuses (Clouchoux et al., 2013; Masoller et al., 2016). Furthermore, lower cerebroplacental ratios (the ratio of MCA to umbilical artery flow) were associated with lower GM and WM volumes along with cortical surface area. Brain metabolism is also different in CHD fetuses: lower N-acetyl-aspartate (NAA) to choline ratios, a potential biomarker of brain injury, were seen to progress in later gestation (Limperopoulos et al., 2010; Masoller et al., 2016). Finally, a recent study established the relationship between blood flow and brain growth in CHD fetuses: while the estimated cerebral blood flow was not different from controls, both cerebral oxygen consumption and aortic oxygen saturation were positively correlated with fetal brain weight (Sun et al., 2015). This result suggests that addressing chronic fetal hypoxia may positively affect brain development in the CHD fetus. In support of this, the same group

recently showed that fetal oxygen delivery is increased in response to maternal hyperoxygenation, although they did not investigate potential effects on brain growth (Porayette et al., 2016).

In summary, abnormalities in head and brain size and growth, regional brain macrostructure, metabolism, and vascular resistance are common in CHD fetuses, particularly in those with HLHS. The differences between CHD and control fetuses are detectable even as early as the late first trimester, then diverge and become significantly more frequent in the third trimester. This coincides with the continued growth of thalamocortical axons, and subsequently the first stages of synaptogenesis, in the cortical plate (Huttenlocher, 1990; Huttenlocher and Dabholkar, 1997; Kostovic and Jovanov-Milosevic, 2006). These processes require high levels of oxygen and glucose; thus, perfusion impairments in CHD fetuses may alter brain development beginning in mid-gestation, with a compounding effect over time.

Preoperative brain MRI and pathology studies

In an autopsy study of HLHS infants, nearly one-third had a major or minor central nervous system anomaly, 41% had dysmorphic features (craniofacial, body, or major organ system differences), and one-third had non-neurologic abnormalities (Glauser et al., 1990). In accord with prenatal studies (see previous section), microcephaly and micrencephaly (significantly lower brain weight) were common. Abnormalities on MRI in a cohort of 103 CHD neonates, who also underwent fetal MRI, were higher in frequency on neonatal MRI (one-third compared to one-sixth on fetal

MRI); furthermore, nearly three-quarter of the patients with injury on neonatal MRI did not show signs of injury on fetal MRI (BrossardRacine et al., 2016). This suggests that either fetal MRI does not have the resolution to detect some lesions, and/or the brain injury occurred after the initial scan.

Neonatal MRI studies in CHD have utilized the *Total Maturation Score (TMS)*, a quantitative measurement assessing four aspects of early brain development: myelination, cortical folding, glial cell migration, and germinal matrix distribution (Childs et al., 2001). CHD neonates were found to have delayed brain development: development was estimated to be 1 month behind those of healthy neonates of an equivalent gestational age (Licht et al., 2009). Low TMS has been shown to be associated with a SV defect (especially HLHS) and a higher incidence of preoperative WM injury and periventricular leukomalacia (PVL) (Andropoulos et al., 2010; Goff et al., 2014; Lim et al., 2016). Both globally and regionally, SV neonates have smaller gray matter volumes (frontal and parietal lobes along with cerebellum and brainstem), delayed gyrification, and reduced cortical surface area (Ortinou et al., 2013, 2012). More than two-thirds of CHD neonates have neurobehavioral abnormalities, which are associated with lower subcortical GM and greater cerebrospinal fluid volumes (Owen et al., 2014).

Evidence of brain injury on preoperative MRI is common: WM injury, infarction, or hemorrhage is present in nearly one-half of SV neonates (Andropoulos et al., 2010; Goff et al., 2014; Mahle et al., 2002; Nagaraj et al., 2015; Owen et al., 2014; Sethi et al., 2013). Having a higher brain injury score was associated with lower WM fractional anisotropy (FA) and lower NAA/choline ratios; both hypotension and lower preoperative

oxygen saturation also were associated with more severe brain injury (Dimitropoulos et al., 2013; Mulkey et al., 2014, 2013; Sethi et al., 2013). In a heterogeneous SV cohort, increased ascending aorta diameter was associated with higher FA, providing a potential link between cerebral blood flow and brain development (Sethi et al., 2013). Imaging studies measuring cerebral blood flow (CBF) (using arterial spin labeling, cine phase contrast MRI, and *near infrared spectroscopy (NIRS)*) have reported lower CBF both globally and in the basal ganglia, and that cerebral oxygen delivery is significantly lower in CHD neonates (Dehaes et al., 2015; Lim et al., 2016; Nagaraj et al., 2015).

In summary, study of CHD neonates in the preoperative period continues to show delays in brain development and high incidence of brain injury. This pattern of brain immaturity and injury has drawn comparison to that seen in preterm neonates, and was called “the encephalopathy of congenital heart disease” by Volpe (2014). Brain injury in CHD appears to be due, in part, to the heightened vulnerability of the immature brain to chronic hypoxia-ischemia. As such, interventions targeting the restoration of normal brain development should be initiated as early after birth as possible. As I discuss in the following section, brain injury is often exacerbated after the initial surgery, so postoperative intervention may be too late to be fully effective.

Early postoperative outcomes

The majority of studies in the early postoperative period report an increase in frequency and/or severity of brain injury, compared to the preoperative period. A neuropathologic study of infants who died after surgery discovered that WM injury (PVL or gliosis) was present to some degree in all patients (Kinney et al., 2005). Gray matter

was also affected in two-thirds, especially in the cerebral cortex, thalamus, hippocampus, and brain stem. Large infarcts were found in 18%, and smaller infarcts were in the cerebellar cortex of 30% and thalamus of 28%. The authors concluded that the lesions were primarily hypoxic-ischemic in origin.

Mahle et al. (2002) scanned CHD patients at three timepoints: preoperatively, in the early postoperative period (approximately seven days after surgery), and the late postoperative period (3-6 months after surgery). More than half (7/12) had new or worsened lesions after the Norwood procedure, including frontal and parietal lobe PVL and focal infarct. Interestingly, although one subject had a new infarct and two had cerebral atrophy, all cases with PVL on the early scan showed resolution of PVL on the late scan. This finding was partially replicated by Andropoulos et al. (2010), as only approximately half had (complete or partial) resolution of abnormal MRI findings and one-third had a new finding. Other groups have similarly found PVL in roughly half of SV neonates approximately one week after surgery, although reports of the rates of worsened lesions are conflicting (Andropoulos et al., 2010; Beca et al., 2013; Block et al., 2010; Dent et al., 2006; Dimitropoulos et al., 2013; Galli et al., 2004; Mulkey et al., 2013). In a group of HLHS neonates, postoperative WM injury was associated with a longer time from birth to first surgery, suggesting that allowing the brain to mature more before Stage I may be neuroprotective (Lynch et al., 2014). Finally, Beca et al. (2013) demonstrated resolution of WM injury from one week to 3 months post-surgery; although evidence of brain injury resolved, lower brain maturity at 3 months was associated with lower neurodevelopmental scores at 2 years of age.

At longer follow-up, some of the patients will have undergone Stages I and II procedures. In one study (age at MRI: 16 months), global GM volume was significantly lower than controls, with greater reductions in frontal and temporal lobes (Watanabe et al., 2009). Lower frontal GM volume was also associated with HLHS diagnosis and with preoperative hypoxia. In the same cohort at 3 years of age, global and frontal GM volumes were still significantly lower in the SV infants; in addition, Bayley-Scales of Infant Development (BSID) scores were significantly lower than controls, and associated with smaller brain volumes (Ibuki et al., 2012). Notably, both brain volumes and neurodevelopmental scores normalized in the d-Transposition of the Great Arteries (d-TGA) patient group.

In summary, new and more severe brain injury is frequent after neonatal cardiac surgery, although its appearance on MRI seems to resolve several months later. There are some associations between a more immature brain and smaller regional brain volumes with poorer neurodevelopmental outcomes in the early pre-school age patient. Long-term studies are required to fully understand the effects of SV and neonatal heart surgery on cognitive and behavioral function later in life.

Surgical support and brain injury

There are several potential sources for the increase in brain injury severity that occurs during/after neonatal open-heart surgery. Exposure to anesthesia in CHD has been associated with both new postoperative brain injury and worse cognitive scores at 12 months and 4-5 years of age (but only a minor effect in the latter) (Andropoulos et al.,

2014; Diaz et al., 2016). Although anesthesia/sedation is a reasonable hypothesized source of surgery-related neurologic dysfunction, most research has focused on support strategies: *cardiopulmonary bypass (CPB)* and *deep hypothermic circulatory arrest (DHCA)*.

The use of CPB inherently provokes an inflammatory response in the patient, partly due to the contact of blood with the foreign materials of the extracorporeal circuit (Allan et al., 2010; Stocker et al., 2004; Warren et al., 2009; Westaby, 1987). Studies have found increases in postoperative cytokine levels to be associated with a longer hospital length of stay, indicative of a more complicated recovery (Allan et al., 2010; Mahle et al., 2014). Additional complications related to CPB are emboli and ischemic and reperfusion injury. For many years, CPB was avoided in neonates due to safety concerns, leading to the introduction of DHCA. DHCA minimizes the time required for the patient to be on bypass, thereby avoiding the negative effects of prolonged CPB exposure; it has the additional benefit of reducing the number of cannulas, improving the surgeon's visibility (for historical review, see Jonas (2002)). While use of DHCA has been shown to result in lower levels of inflammation and postoperative edema, WM injury is still a concern (Algra et al., 2014; Tassani et al., 2002).

Ishibashi, Jonas, and colleagues have performed several experiments in animal models to better understand the relationship between CPB, circulatory arrest, and brain injury. In a pig model, regional variability in neuronal damage was dependent on support strategies, mainly due to regional differences in vasculature and metabolism (Ishibashi et al., 2010). Neuronal damage was especially pronounced in subcortical GM and the

cerebellum, and was associated with poorer neurologic recovery. In WM, the same group showed an inverse relationship between maturation and injury, such that pre-oligodendrocytes (cells in an earlier developmental stage) are more vulnerable to CPB-related injury (Ishibashi et al., 2012). Furthermore, inflammation, as measured by microglia numbers, remains high after CPB in the WM (Korotcova et al., 2015). In the mouse, preoperative hypoxia was shown to increase the vulnerability of both oligodendrocyte progenitor cells and more mature oligodendrocytes; hypoxia also altered the response of astrocytes (Agematsu et al., 2016, 2014). Together, these results suggest that addressing the level of *in utero* and preoperative cerebral blood flow may have the potential to improve surgical outcomes in neonates with CHD.

Late childhood and adolescence

Few studies have used brain imaging in SV patients several years after the Fontan procedure. Sarajuuri and colleagues acquired MRI data in SV patients at 5-7 years of age (approximately 2-4 years after the Fontan) (Sarajuuri et al., 2012, 2007). In their first report, 7 of 20 patients had an MRI abnormality; there was a higher percentage of patients who had previously undergone the Norwood procedure with an abnormality. In their second report, they found a higher percentage (73%) of patients with MRI abnormalities; furthermore, patients with more severe lesions had poorer neurodevelopmental outcomes (full-scale IQ, motor function, and adaptive behavior). Other studies of brain MRI in SV patients after the Fontan, carried out in the present cohort, are described in detail in Preliminary studies.

In non-SV CHD, differences in brain structure are still present beyond childhood. Schaer and colleagues report, in a cohort with 22q11.2 deletion syndrome and CHD (age ranging from 6 to 33 years), reduced cortical gyrification and volumes, mainly in medial cortex and temporal and parietal lobes, and reduced hippocampal volumes bilaterally (Fountain et al., 2014; Schaer et al., 2009, 2010). In CHD patients aged 11 to 16 years, there are global and regional reductions in WM and GM volumes, cortical surface area, and subcortical and cerebellar GM volumes (von Rhein et al., 2014). We similarly found volume reductions, alterations in cortical thickness, and WM FA reductions in adolescents with d-TGA (Rivkin et al., 2013; Rollins et al., 2014; Watson et al., 2016).

Graph theory and MRI

A *graph* is a mathematical construct used to represent a real-world network, and consists of a set of *vertices* and *edges* (their connections); the typical notation is $G = (V, E)$. An edge connecting two vertices i and j can be denoted as $\{i, j\}$. Edges can be either unweighted (they either are present or not) or weighted (where the weights are some measure of connection strength), and undirected or directed (for MRI data, all graphs are undirected; i.e., there is no distinction between the edges $\{i, j\}$ and $\{j, i\}$). There are a number of measures that can be calculated for the graph as a whole, for its vertices, and for its edges. A subset of these are measures of: *vertex importance*, related to the number of connections of a given vertex (e.g., degree, strength, betweenness centrality); *segregation* and *integration*, which are graph-level measures that quantify patterns of vertex connections (e.g., modularity, global and local efficiency); *closeness*, both in the topological sense and topographical (three-dimensional) sense (e.g.,

characteristic path length); *asymmetry*, since the brain has separate hemispheres, each of which may have different connectivity patterns; and *robustness*, which represents the stability of a network in the presence of vertex removal, and can be calculated at both the graph- and vertex-levels.

Interest in using graphs to represent the structural and functional connectivity of the brain increased after Watts' & Strogatz's (1998) seminal paper describing *small world* networks (Watts and Strogatz, 1998). Small world networks have high clustering and low characteristic path length, which presumably increases the efficiency of information processing. Furthermore, they showed that disparate networks (biology, social, and physical/structural) possess the small world property. However, it wasn't until after Sporns et al. (2005) proposed the "connectome", or the full structural connectivity matrix of the brain, that studies using human MRI data increased (Sporns et al., 2005). Early work analyzed structural covariance patterns of cortical thickness, structural connectivity using tractography data from diffusion tensor imaging (DTI), and intrinsic functional connectivity using resting-state functional MRI (Achard et al., 2006; Hagmann et al., 2008, 2007; He et al., 2007; Iturria-Medina et al., 2007). In this section, I first review graph theory analysis applied to gray matter (e.g., cortical thickness) data. Next, I discuss its use in studies of white matter (DTI tractography). Finally, I discuss its application to patient groups and the interpretations of graph theoretical measures associated with patient- and medical-related variables.

Gray matter networks

Cortical thickness is a measure reflecting the number of neurons, glial cells, and neuropil in the cerebral cortex. Thickness can be measured at a fine spatial scale across the surface of the brain using standard anatomical MRI sequences (Dale et al., 1999; Fischl and Dale, 2000; Fischl et al., 1999). Analysis of cortical thickness data had typically taken a region of interest (ROI) approach, in which summary measures of thickness were compared across groups. Lerch et al. (2006) were the first to investigate inter-regional covariance, and showed that the covariance map using Broca's area as a seed region resembled the connectivity map generated from DTI tractography. Although structural covariance patterns are not a direct measure of brain connectivity, stronger inter-regional correlations can be considered a surrogate, as these regions may share a similar maturational trajectory due to direct axonal connections or to some mutual influence (Alexander-Bloch et al., 2013a,b; Mechelli et al., 2005). In addition, there may be genetic influences and/or changes with learning and plasticity (for review, see Evans (2013)). Further support comes from a joint structural-functional MRI study demonstrating a high correspondence between intrinsic connectivity and structural covariance networks (Seeley et al., 2009).

The earliest analyses of structural covariance patterns using graph theory focused on healthy control subjects (Chen et al., 2008; He et al., 2007). He et al. (2007) showed that the human structural covariance network possesses the small world property, which is considered to represent a network with an optimal balance of segregation and integration for information processing. Chen et al. (2008) report that the cortical

thickness network possesses the property of *modularity*, and identified six subnetworks that closely corresponded to groups of regions known to participate in different areas of cognitive functioning. Other studies have focused on network development in pediatric cohorts. These demonstrated that network topology changes throughout childhood and adolescence, ultimately reaching the pattern seen in adults (Alexander-Bloch et al., 2013b; Khundrakpam et al., 2013; Nie et al., 2013). Structural covariance networks from ages 5 to 18 years also closely matched a set of intrinsic connectivity networks derived from adult data (Zielinski et al., 2010). Additionally, structural covariance networks had a similar pattern over time compared with functional connectivity and maturational networks in a longitudinal study (Alexander-Bloch et al., 2013b) Furthermore, *hub* regions—regions considered to be most important for the information flow in a network—were shown to appear in the frontal lobes in older age groups, which matches the known late development of the frontal lobes in humans and their importance in executive functions. Moreover, there is moderate agreement between *positive* cortical thickness correlations and both DTI tractography and resting-state functional MRI networks, although there were differences in the location of hub regions and small world parameters between modalities (Gong et al., 2012; Hosseini and Kesler, 2013a). Therefore, while structural covariance networks should not be considered a complete surrogate for tractography networks, they provide important complementary information in the form of possible functionally-related regions that are not directly connected.

White matter networks

Diffusion tensor imaging (DTI) measurements are based on the signal generated by the movement of water molecules. This movement has been found to be *anisotropic* (i.e., dependent on direction) in brain white matter, and more *isotropic* (i.e., equal in all directions) in gray matter and cerebrospinal fluid. The reason for this is due to the cellular microstructure of the surrounding medium: the presence of highly-ordered WM fiber tracts presents an obstacle for movement perpendicular to the long axis of the tract (for review, see Beaulieu (2002)). Tractography utilizes this inherent directionality to estimate the *principal diffusion direction* and infer the orientation of white matter fiber tract bundles. This data is then used to estimate the structural connectivity between regions. Broadly, there are two classes of tractography algorithms: *deterministic* and *probabilistic*. Deterministic tractography starts from a *seed* voxel and follows the principal diffusion direction until certain termination criteria are met (e.g., when the FA of the current voxel is below 0.2) (Mori and van Zijl, 2002). Probabilistic tractography accounts for uncertainty in the measurement of local diffusion parameters and, therefore, local fiber orientations, as opposed to deterministic methods which give a single result (Behrens et al., 2003; Parker et al., 2003). Probabilistic tractography shows better agreement with animal tract tracing data (Knosche et al., 2015). A major limitation of earlier tractography algorithms was the assumption of a single fiber orientation present per voxel, which is only true in approximately one-third of voxels (Jeurissen et al., 2013). Newer algorithms model for the possibility of crossing fibers, improving tracking results (Behrens et al., 2007). While there are limitations to using tractography to infer anatomic

connections in the brain (see Jbabdi and Johansen-Berg (2011) for review), tractography has been shown to have high test-retest reliability (Wang et al., 2012), and can reliably reproduce connections from *in vivo* tracer injections (Azadbakht et al., 2015; Dyrby et al., 2007; Jbabdi et al., 2013; van den Heuvel et al., 2015) and histology (Holl et al., 2011; Seehaus et al., 2013). Additionally, functional connectivity has been reliably predicted from and strongly correlated to structural connectivity (Garces et al., 2016; Greicius et al., 2009; Honey et al., 2009; Skudlarski et al., 2008). However, caution should be exercised when using tractography results as a surrogate measure of anatomical connectivity as there is an inherent trade-off between specificity and sensitivity, with reconstruction of major fiber tracts having the highest reproducibility (Calabrese et al., 2015; Knosche et al., 2015; Thomas et al., 2014). The test-retest reliability of graph measures derived from DTI tractography is good to excellent for global measures and small world parameters (Andreotti et al., 2014; Bastiani et al., 2012; Buchanan et al., 2014; Owen et al., 2013; Vaessen et al., 2010), but the choice of network size (i.e., parcellation) has an effect on global and local measures; however, increasing the spatial resolution while preserving the original boundaries of the atlas shows only a minor effect (Bassett et al., 2011; Zalesky et al., 2010b). Certain vertex-level measures (e.g., high-degree hubs), were consistent across spatial scales.

The structural network of the brain created from tractography data has also been shown to be a small world network, with a structural “core” of highly connected vertices in medial and posterior cortex, greatly overlapping the *default mode network* (Gong et al., 2009; Hagmann et al., 2008, 2007; Iturria-Medina et al., 2008). The discovery of “rich-

club” organization (i.e., a group of regions that are significantly more connected to one another than to the remaining regions) in the human brain was first made using tractography; the rich-club was in good agreement with the structural core reported in Hagmann et al. (2008) (van den Heuvel and Sporns, 2011). The rich-club is similar in both adults and children, and similar to that calculated from functional connectivity data (Grayson et al., 2014). Analysis of tract-tracing data in the cat showed that rich-club regions interconnect distinct functional sub-networks (de Reus and van den Heuvel, 2013b). In summary, graph theory analysis of DTI tractography data has good reproducibility and can be used to identify functionally-relevant networks of brain regions.

Graph theory associated with patient-specific variables

Measures derived from graph theory analyses of brain MRI can differentiate between patient groups and healthy subjects. Using cortical thickness covariance, Alzheimer’s disease patients were shown to have altered small world properties, along with differences in centrality (i.e., vertex importance) in temporal and parietal lobes, brain regions known to be affected by the disease process (He et al., 2008). In multiple sclerosis, the magnitude of white matter lesion load was associated with lower *efficiency* at the global and regional levels (He et al., 2009). Schizophrenic patients demonstrated similar global network properties to controls, but a loss of hub regions in prefrontal cortex and altered connectivity pattern in a network of multimodal brain regions (Bassett et al., 2008). Similar between-group differences have been found in temporal lobe epilepsy (Bernhardt et al., 2011), obsessive compulsive disorder (Kim et al., 2013),

young adults with a history of abuse or neglect (Teicher et al., 2014), and adolescent girls with scoliosis (Wang et al., 2013). Using gray matter volume to construct covariance networks, Yao et al. (2010) showed that the networks of patients with Mild Cognitive Impairment were in an intermediate state between controls and Alzheimer's patients, supporting the theory that Mild Cognitive Impairment is a precursor to developing Alzheimer's disease.

From tractography-based networks, hub regions have been shown to be implicated in multiple brain disorders (Crossley et al., 2014). Hubs were first determined from a set of healthy controls, and a separate meta-analysis was performed to identify the location of lesions that were common across 26 brain disorders investigated. There was a high degree of overlap between the tractography-derived hubs and the lesion maps, suggesting the importance of this graph theory metric. In boys with ADHD, there were regional decreases compared to controls in efficiency that match the symptomatology of ADHD (Cao et al., 2013). Soman et al. (2016) used measures of *segregation* from tractography networks in patients undergoing carotid artery intervention, showing a difference in preoperative MRI data between those who subsequently had cognitive (memory) decline compared to those with no decline (Soman et al., 2016). This information is clinically useful and can help identify patients who would benefit from additional intervention/therapies.

Preliminary studies

In this section, I will discuss the results of our completed analyses in the Fontan cohort (Bellinger et al., 2015). Patients in the Fontan group were recruited from 2010 to 2012 at Boston Children's Hospital (BCH). Inclusion criteria included: age 10-19 years at the time of enrollment; diagnosis of single ventricle; and cardiac surgery including the Fontan procedure, Fontan re-do, or other open heart surgery at least 6 months before testing. Exclusion criteria included: known risk factors for brain disorders (e.g., history of closed head injury with loss of consciousness); any contraindication to acquisition of MRI data (e.g., metal implants); Trisomy 21; adolescents with forms of CHD other than SV defect requiring surgical correction; and cardiac transplantation.

Patient characteristics and surgical history

Demographics for the full sample and stratified by Norwood status are in Table 1.1. P-values for categorical variables were calculated using Fisher's exact test, and for continuous variables using analysis of variance (normally distributed) or Kruskal-Wallis tests (non-normally distributed). The Norwood group had significantly fewer syndromic patients (defined as having either a known genetic diagnosis, a pathogenic variant on array, a variant of unknown significance on array, or syndromic presentation, e.g., dysmorphic features and/or extracardiac birth defects). In the full sample, the majority of patients were male (61%) and white (93%). Almost two-thirds were in NYHA Class 2 (slight limitation of physical activity), and slightly lower than 10% were in Class 3 (marked limitation of physical activity).

Surgical history for the full sample and stratified by Norwood status are in Table 1.2. The Norwood group had the first operation at a significantly younger age (median 5 days vs. 7 days), were more likely to have an open first operation (100% vs. 36%) (because the Norwood is an open operation), had longer DHCA support time (49 vs. 0 minutes) and total support time (125 vs. 0 minutes), had more complications during the first operation (2 vs. 0) and overall (3 vs. 2), and had more open operations (3 vs. 2). In the full sample, patients underwent an average of 3 operations in total and 4 catheterizations. The majority of patients ($N = 123$, 79%) had a bidirectional Glenn as the Stage II procedure, and only 11 (7%) had a hemi-Fontan.

Patients underwent the Fontan between 0.74 and 11.37 years of age (IQR = 1.97-3.37). The distribution of ages at Fontan procedure is shown in Figure 1.1. The year the Fontan procedure was performed in was between 1992 and 2011 (IQR = 1997-2002). The distribution of the years in which the Fontan procedure was performed is shown in Figure 1.2. The time from the Fontan procedure to study enrollment was 11.52 years. A table of the type of Fontan procedure performed is shown in Table 1.3. Nearly all subjects ($n = 138$, 88%) underwent a lateral tunnel fenestrated Fontan. There were no differences in type of Fontan procedure based on Norwood status ($p = 0.13$; calculated using Fisher's exact test). The Norwood and non-Norwood groups did not differ in terms of the age they underwent the Fontan, the year of Fontan procedure, or the time from Fontan procedure to study enrollment.

The specific SV diagnoses in our cohort include: hypoplastic left heart syndrome (HLHS), tricuspid atresia, double outlet right ventricle (DORV), double inlet left ventricle (DILV), heterotaxy, complex TGA, pulmonary atresia with intact ventricular septum (PA/IVS), unbalanced atrioventricular (AV) canal, and mitral atresia. The number of patients in each diagnostic group and percent of the total cohort are shown in Table 1.4. The predominance of HLHS and tricuspid atresia patients parallels what has been observed in other studies (O’Leary, 2002). A plot of age at Fontan stratified by diagnostic group is shown in Figure 1.3. The groups are in increasing order (from left-to-right) of the median age at Fontan.

Neuropsychological outcomes

A full report of differences in neuropsychological outcomes is presented in Bellinger et al. (2015). Study subjects were administered a series of neuropsychological tests, in addition to parent-, self-, and teacher-completed questionnaires. Scores on most tests were significantly lower in the Fontan group compared to population norms or to the control group. In analyses comparing Norwood and non-Norwood subgroups, the Norwood group scored significantly worse in most areas than the non-Norwood group, including general intelligence, reading and math achievement, executive function, visuospatial function, and social cognition. Risk factors for poorer scores included: longer total support and DHCA times; more operations, operative complications, catheterizations, and catheterization complications; younger gestational age (GA) at birth; open first operation; and history of seizures. Gross abnormalities on brain MRI were found in 66% of Fontan subjects (compared to only 6% of control subjects). Evidence of

stroke was particularly high, present in 13% of the cohort. Patients with diffuse MRI abnormalities had more operative complications, and patients with evidence of focal infarction or atrophy had worse executive function, attention, and social cognition. Finally, nearly one-fourth had been diagnosed with attention deficit hyperactivity disorder (ADHD), and more than one-third with a learning disability. These results highlight the extensive cognitive and behavioral deficits in SV patients, and suggest a possible association with brain structure.

Gray matter differences

We have analyzed subcortical and cortical gray matter volumes and thicknesses between the Fontan and control groups (Watson et al., manuscript under review). These differences are shown in Figure 1.4. In the top portion, each gyrus was combined across hemispheres. In the bottom portion, a vertex-wise surface-based analysis of cortical thickness was performed; the red-yellow areas indicate vertices in which cortical thickness was significantly lower in the Fontan group, based on a linear model adjusting for age at MRI, sex, and scanner field strength (FDR-adjusted $p < 0.025$). Cortical volumes were significantly lower in the Fontan group in temporal, parietal, and occipital regions, and subcortical volumes were smaller in the thalamus, putamen, pallidum, hippocampus, and amygdala. There were extensive thickness decreases bilaterally in all major lobes of the brain, particularly the frontal and parietal lobes. In the Fontan group, we found lower cortical thickness in various regions to be significantly associated with older age at first operation, more catheterizations and catheterization complications, and shorter total support time. Similarly, lower volumes in various regions were associated

with more operations (open and total) and operative complications, and more catheterizations and catheterization complications.

In a related study, we investigated differences in gray matter volumes and thicknesses between Fontan patients with and without ADHD. (Hammerness et al., manuscript in preparation) Patients were diagnosed with two methods: the Schedule for Affective Disorders and Schizophrenia for School-Aged Children –Present and Lifetime Version (Kaufman et al., 1997), and the Conners' ADHD/DSM-IV Scales (CADS-P) (Conners, 2004). Compared to non-ADHD Fontan patients, those who met criteria for ADHD had significantly lower volumes in dorsolateral and ventrolateral prefrontal cortices, anterior cingulate, striatum, and parietal regions. In addition, the central and mid-posterior segments of the corpus callosum were significantly smaller in the ADHD subgroup. While no difference was found between the groups in cortical thickness, the regionally-reduced volumes corresponded to cortical regions known to participate in networks active in attentiveness and executive functions.

White matter differences

We have also analyzed white matter (WM) microstructure using diffusion tensor imaging (DTI) data (Watson et al., manuscript in preparation). DTI measures were calculated using the diffusion tensor and registered into standard space using Tract-Based Spatial Statistics (Smith et al., 2006). Subsequently, we calculated the average of each measure in twenty WM fiber tracts (obtained from a standard atlas) and compared between groups (Wakana et al., 2007). Fractional anisotropy (FA) and axial diffusivity (AD) were lower in the Fontan group in nearly all fiber tracts tested, bilaterally and in

deep subcortical and cerebellar WM. Radial diffusivity (RD) was higher in the Fontan group in a handful of tracts. There were only a few differences in WM microstructure based on Norwood status. Voxel-wise analysis of FA and AD resulted in similar findings (see Figure 1.5 and Figure 1.6). In the Fontan group, lower FA was associated with more surgical complications, younger age, and longer total support time (all for the first operation), with history of a stroke or neurologic event, and with more total operations.

Summary

In summary, our analyses of the present cohort of post-Fontan children and adolescents have revealed that they have deficits in multiple domains of cognition and behavior and extensive areas of altered brain structure. Furthermore, the MRI data show multiple associations with factors pertaining to the patients' surgical courses. These findings are important and may inform clinicians and surgeons when considering treatment and intervention plans for their patients. The work reported in this dissertation takes the logical next step, using a network-based approach to better characterize the associations between brain structure/connectivity and cognition and behavior in SV children and adolescents who have undergone the Fontan procedure.

	Total (N = 156)	Non-Norwood (N = 93)	Norwood (N = 63)	P-value
Birth weight, kg	3.29 ± 0.63	3.21 ± 0.66	3.39 ± 0.57	0.12
Gestational age, wk	38.92 ± 2.24	38.75 ± 2.38	39.16 ± 2.00	0.38
Sex, F	61 (39)	40 (43)	21 (33)	0.25
<i>Race</i>				0.15
Asian	4 (3)	4 (4)	0 (0)	
Black	7 (4)	3 (3)	4 (6)	
White	145 (93)	86 (92)	59 (94)	
<i>NYHA class</i>				0.19
1	45 (28.85)	29 (31.18)	16 (25.40)	
2	98 (62.82)	59 (63.44)	39 (61.90)	
3	13 (8.33)	5 (5.38)	8 (12.70)	
Social class at 16 yr of age†	53 (41 – 60)	55 (43 – 61)	48 (38 – 58)	0.07
Non-syndromic	91 (58)	47 (51)	44 (70)	0.021

Table 1.1: **Subject demographics, full cohort (N = 156)**. Values are N (%), mean ± SD, or median (range). F: female; NYHA: New York Heart Association; kg: kilograms; wk: weeks; yr: years

† Score on the Hollingshead Four Factor Index of Social Status; higher scores indicate higher social class
P-values were calculated by Fisher's exact test for categorical variables and Wilcoxon rank sum test for continuous variables.

	Total (N = 156)	Non-Norwood (N = 93)	Norwood (N = 63)	P-value
Age at 1 st op, d	6 (3 – 21)	7 (3 – 87)	5 (3 – 8)	0.01
Closed 1 st op	64 (41)	64 (69)	0 (0)	<0.0001
DHCA time 1 st op, min	0 (0 – 46)	0 (0 – 0)	49 (33 – 58)	<0.0001
# of complications 1 st op	1 (0 – 2)	0 (0 – 1)	2 (1 – 3)	<0.0001
Total # of ops	3 (3 – 3)	3 (2 – 3)	3 (3 – 3)	0.10
Total # of open ops	3 (2 – 3)	2 (2 – 2)	3 (3 – 3)	<0.0001
Total # of surgical complications	2 (1 – 5)	2 (1 – 4)	3 (2 – 6)	<0.0001
Total # of cath	4 (3 – 5)	4 (3 – 5)	4 (3 – 4)	0.11
Total # of cath complications	1 (0 – 1)	1 (0 – 1)	0 (0 – 1)	0.77
Age at Fontan, yr	2.93 ± 1.52	3.14 ± 1.77	2.62 ± 0.99	0.11
Year of Fontan	2000 (1997 – 2002)	2000 (1997 – 2002)	2000 (1998 – 2002)	0.53
Time since Fontan, yr	11.52 ± 3.11	11.56 ± 3.24	11.48 ± 2.93	0.82

Table 1.2: **Surgical history data, full cohort (N = 156)**. Values are N (%), mean ± SD, or median (range). op: operation; d: days; DHCA: deep hypothermic circulatory arrest; min: minutes; cath: catheterization. P-values were calculated by Fisher's exact test for categorical variables and Wilcoxon rank sum test for continuous variables.

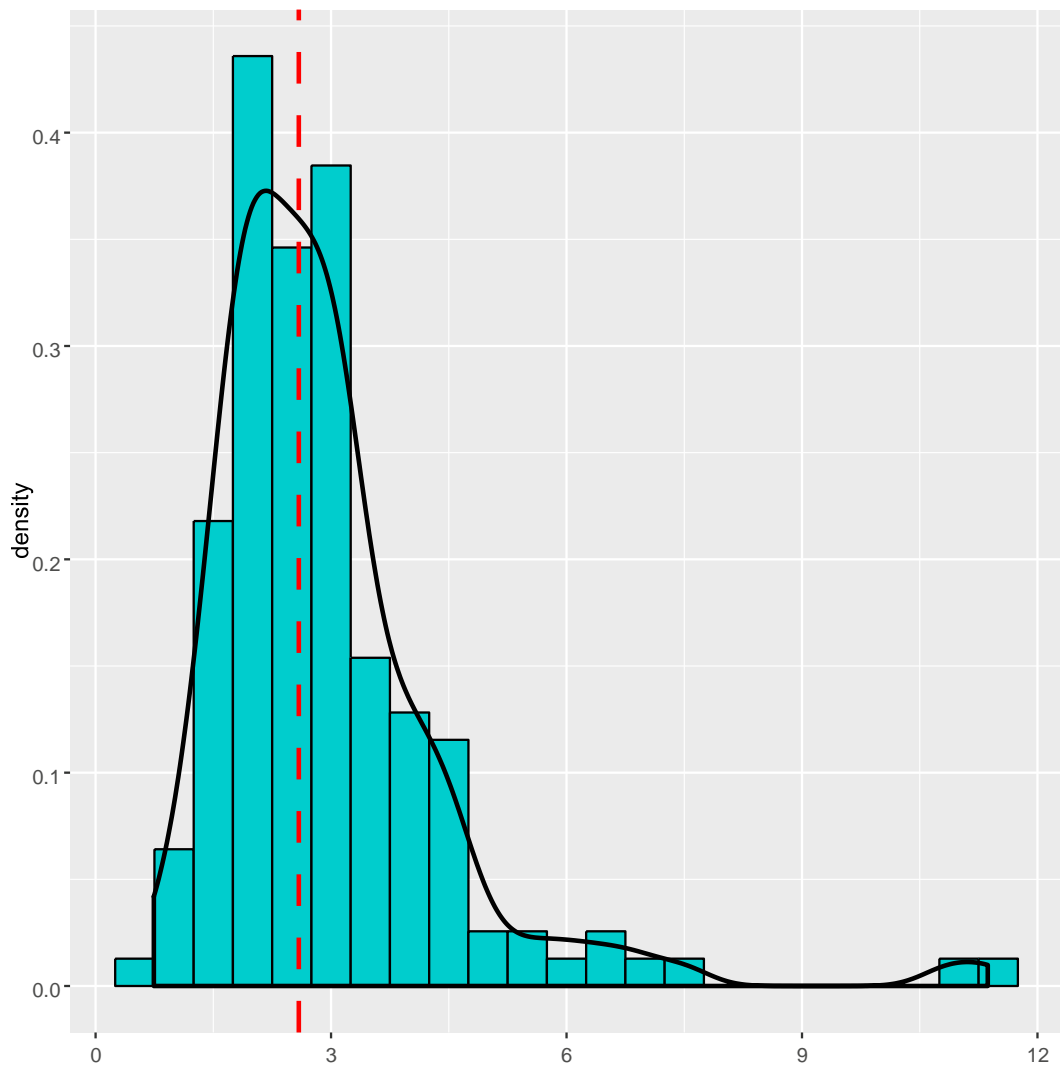


Figure 1.1: **Age at Fontan.** Histogram of the age (in years) at which the patients underwent the Fontan procedure. The vertical dashed red line indicates the median age for the entire group (2.58 years). The black line represents the kernel density estimate of the distribution.

	Total (N = 156)	Non-Norwood (N = 93)	Norwood (N = 63)
Extracardiac, fenestrated	10 (6)	9 (10)	1 (2)
Extracardiac, non-fenestrated	6 (4)	4 (4)	2 (3)
Lateral tunnel, fenestrated	138 (89)	78 (85)	60 (95)
Lateral tunnel, non-fenestrated	1 (1)	1 (1)	0 (0)

Table 1.3: **Type of Fontan procedure, full cohort (N=156)**. Values are N (%). Data were not available for one patient.

Diagnosis	N	%
HLHS	41	26.28
Tricuspid atresia	30	19.23
DORV	19	12.18
DILV	18	11.54
Heterotaxy	17	10.90
Complex TGA	12	7.69
PA/IVS	10	6.41
Unbalanced AV canal	4	2.56
Other	3	1.92
Mitral atresia	2	1.28

Table 1.4: **Anatomic diagnosis, full cohort (n=156)**. N: number per diagnosis; HLHS: hypoplastic left heart syndrome; DORV: double outlet right ventricle; DILV: double inlet left ventricle; TGA: transposition of the great arteries; PA/IVS: pulmonary atresia with intact ventricular septum; AV: atrioventricular.

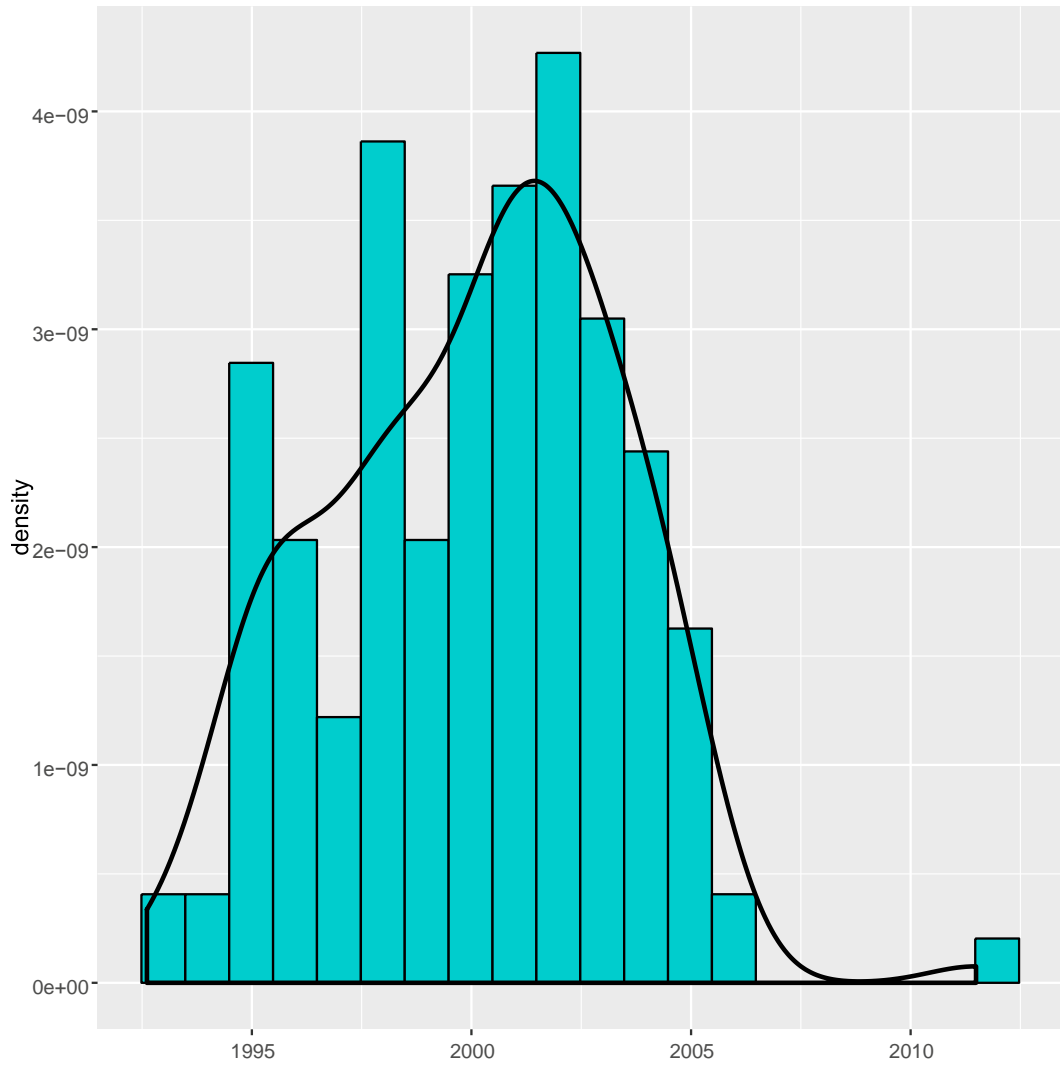


Figure 1.2: **Year of Fontan procedure.** Histogram of the year in which patients underwent the Fontan procedure. The black line represents the kernel density estimate of the distribution.

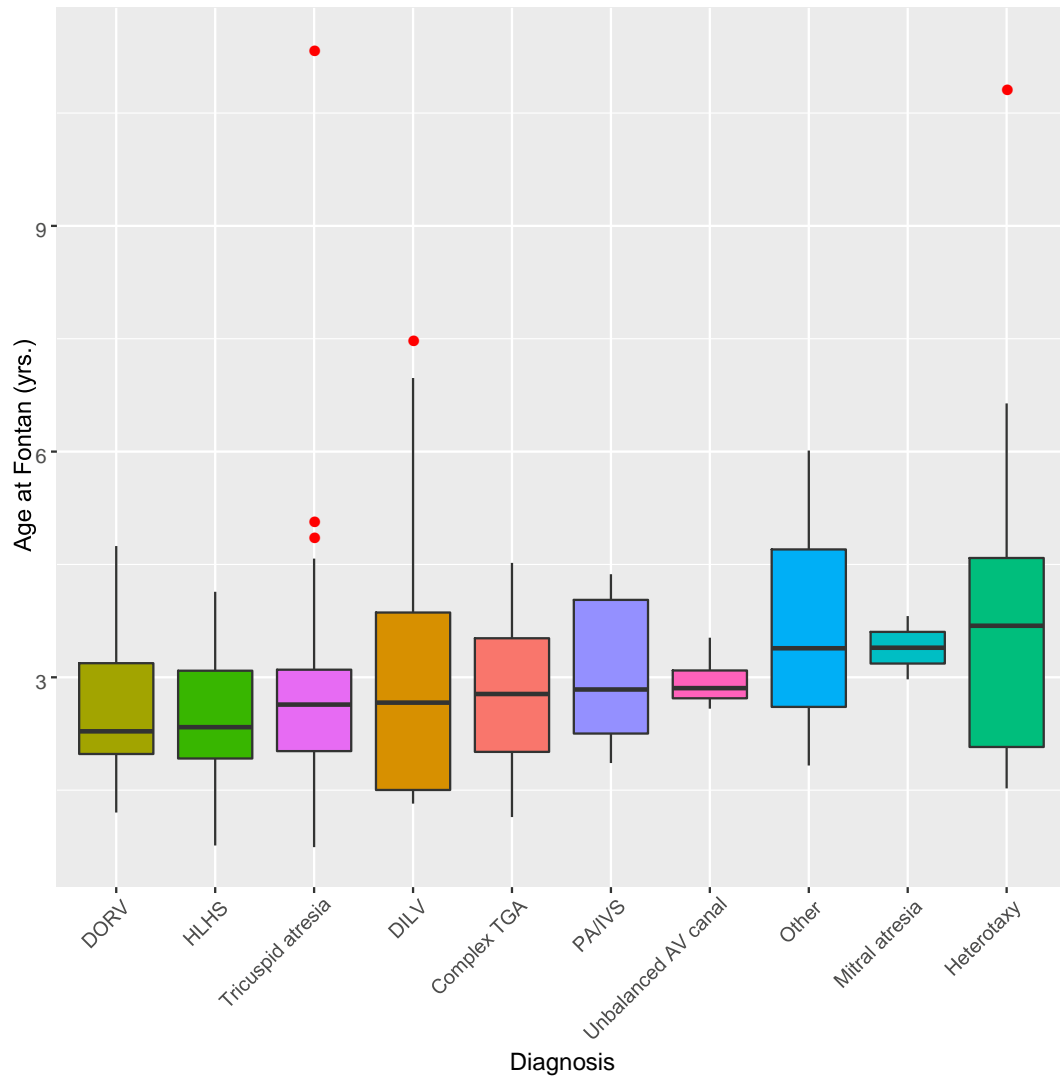


Figure 1.3: **Age at Fontan by diagnosis.** Boxplot of the age (in years) at which the patients underwent the Fontan procedure; each box represents a different subgroup, stratified by diagnosis. Outliers are those values beyond $1.5 \times IQR$ (interquartile range), and are represented by red closed circles. The bars are ordered by increasing median "Age at Fontan" of each subgroup (from left to right).

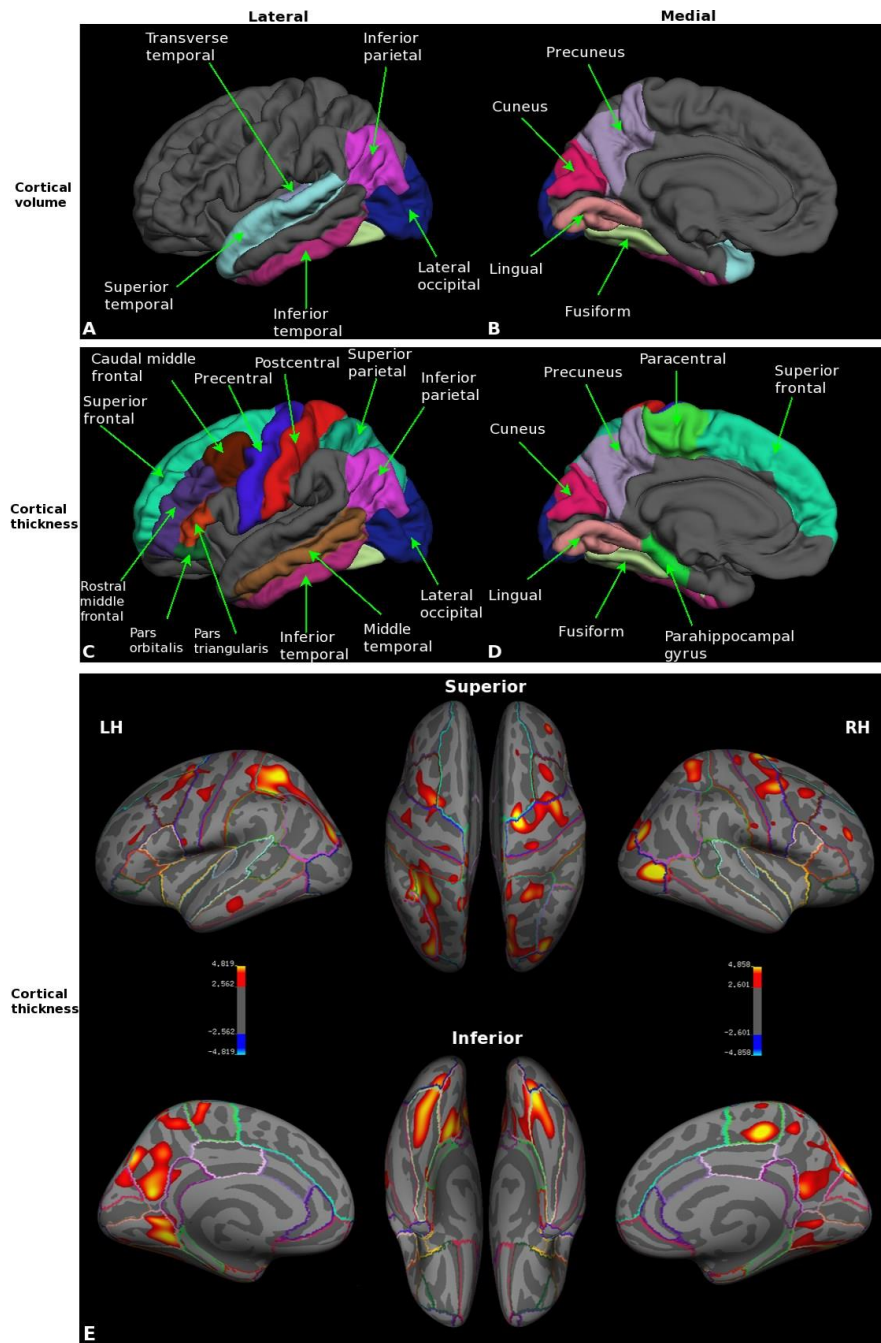


Figure 1.4: **Differences in cortical volume and thickness between Fontan and control subjects.** (A-D) Volumetric measures were averaged across hemispheres. Cortical volume differences along the lateral (A) and medial (B) aspects of the brain. Cortical thickness differences along the lateral (C) and medial (D) aspects of the brain. (E) Vertex-wise cortical thickness differences in which the Fontan group has thinner cortex than the control group.

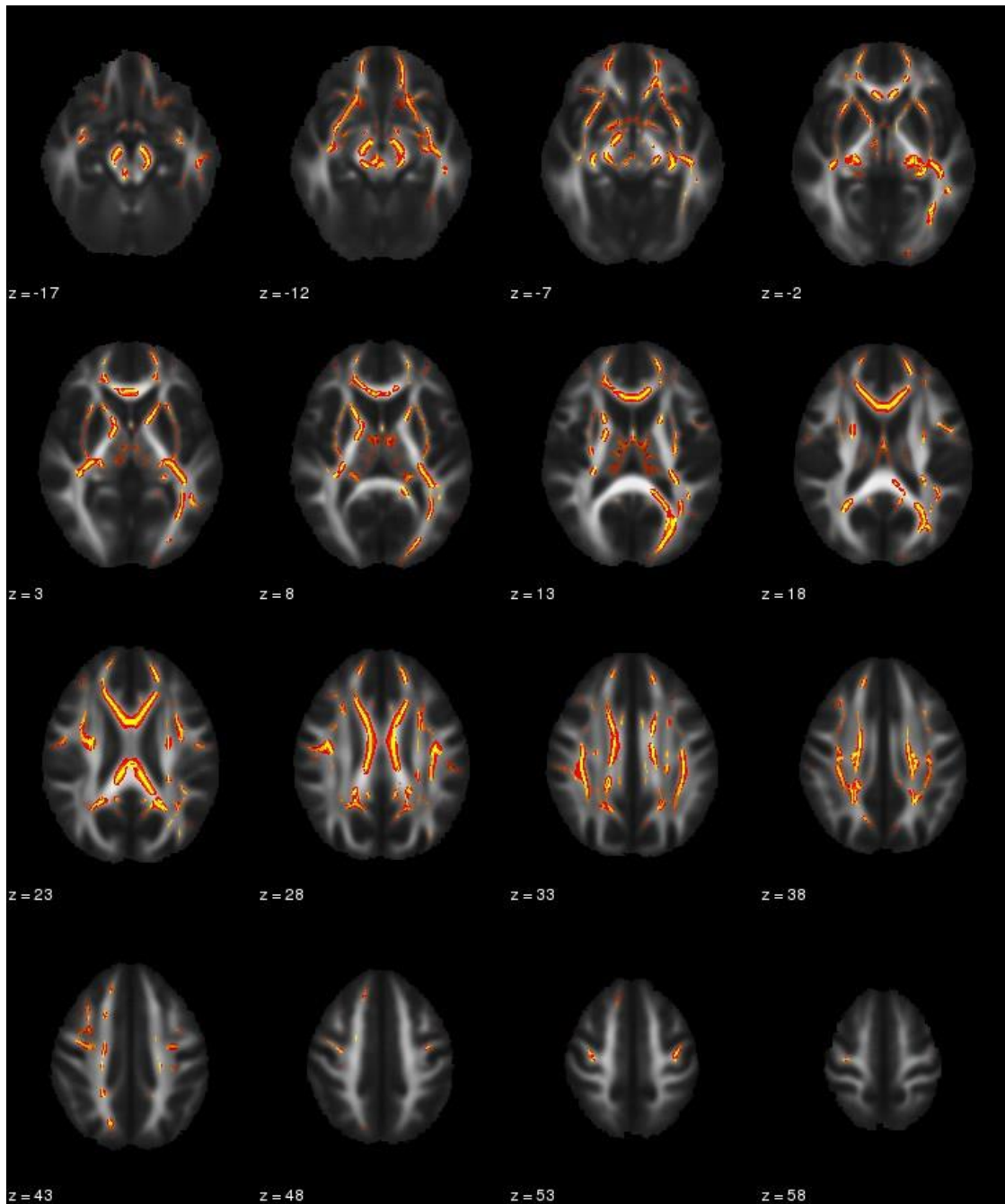


Figure 1.5: **Differences in fractional anisotropy (FA) between Fontan and control subjects.** The red-yellow color indicates voxels in which FA was significantly lower in the Fontan group. The left hemisphere of the brain is in the left half of the figure. The axial slices go from inferior to superior from the top-left to bottom-right.

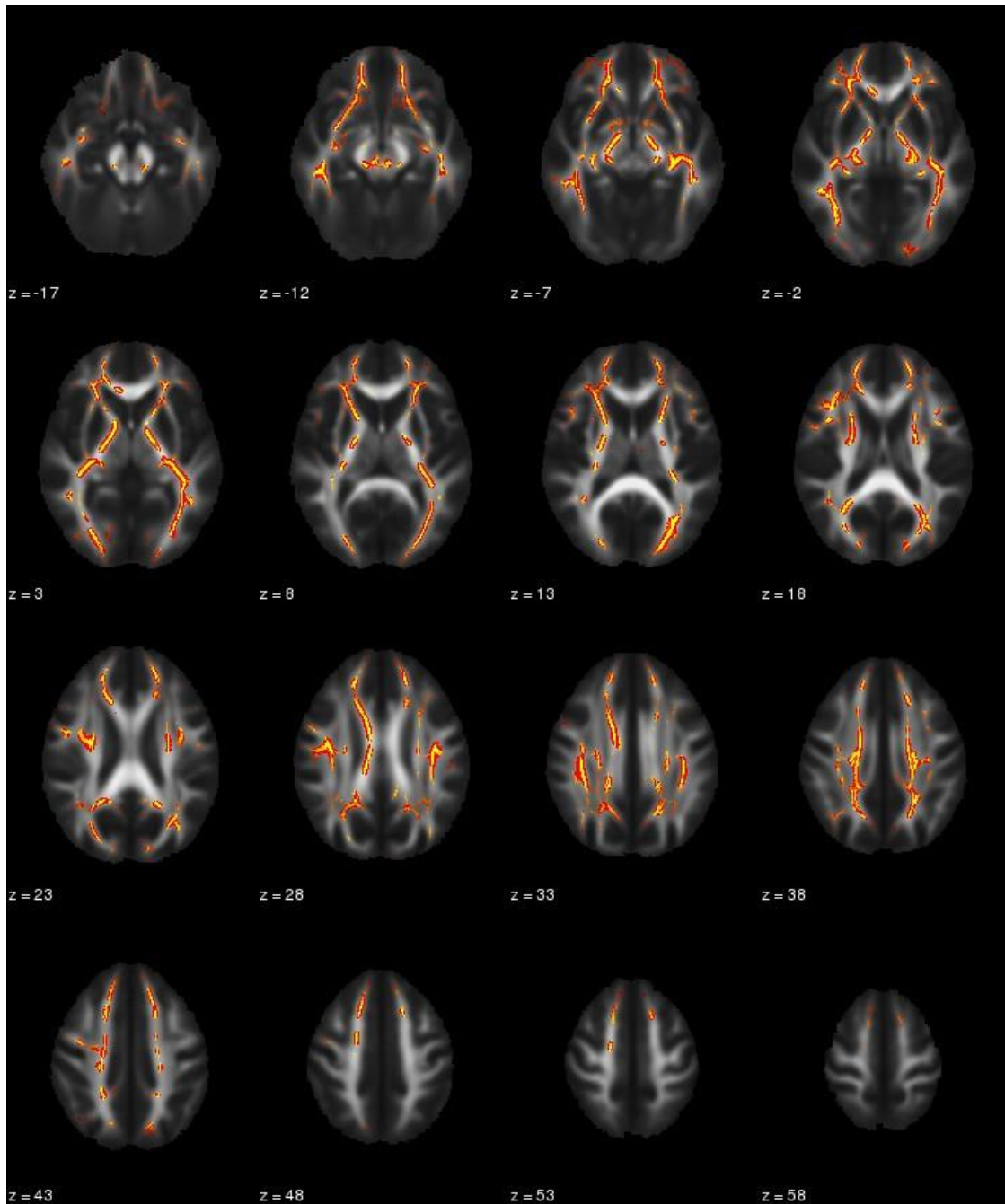


Figure 1.6: **Differences in axial diffusivity (AD) between Fontan and control subjects.** The red-yellow color indicates voxels in which AD was significantly lower in the Fontan group. The left hemisphere of the brain is in the left half of the figure. The axial slices go from inferior to superior from the top-left to bottom-right.

GRAPH THEORY ANALYSIS OF GRAY MATTER NETWORKS IN POST-FONTAN CHILDREN AND ADOLESCENTS

Introduction

Congenital heart disease (CHD) occurs in approximately 9 per 1,000 live births per year worldwide, representing a significant public health issue (van der Linde et al., 2011). Single ventricle (SV) defects, which are among the most severe types of CHD, make up nearly 10% of patients with CHD (O’Leary, 2002). SV, and particularly hypoplastic left heart syndrome (HLHS), is associated with high mortality and morbidity; coupled with a steadily increasing survival for several decades, this has led to a large increase in SV patients reaching adulthood (Anderson et al., 2015; Rogers et al., 2012). Long-term patient management has shifted to focus on neurodevelopmental outcomes; studies in children and adolescents with SV have revealed cognitive deficits and behavioral problems to be generally more pronounced compared to other CHD (Bellinger et al., 2015, 2011; Gaynor et al., 2014; McCrindle et al., 2006). Currently, no studies have investigated changes in structural brain connectivity that may underlie these deficits.

The brain in SV patients begins to show structural changes and abnormalities in the late first trimester, with differences increasing from mid-gestation to birth (Abu-Rustum et al., 2016; Brossard-Racine et al., 2014; Clouchoux et al., 2013; Hinton et al., 2008; Licht et al., 2009; Limperopoulos et al., 2010; Zeng et al., 2015a). Furthermore, autopsy and magnetic resonance imaging (MRI) studies demonstrate signs of brain injury and abnormal cerebral hemodynamics in the neonatal period, before the patient

undergoes any open heart procedures (Glauser et al., 1990; Goff et al., 2014; Nagaraj et al., 2015; Ortinou et al., 2013, 2012; von Rhein et al., 2015). Preoperative brain injury tends to be exacerbated after the initial surgery, both in terms of frequency and severity (Beca et al., 2013; Dent et al., 2006; Lynch et al., 2014). While white matter (WM) injury is a frequent occurrence, gray matter (GM) differences are present as well, including infarcts, cerebral atrophy, and lower total brain, frontal, and temporal lobe volumes (Ibuki et al., 2012; Kinney et al., 2005; Watanabe et al., 2009). The surgical course for SV patients is usually a *staged palliation* approach, with Stage I in the neonatal period (if necessary depending on the underlying cardiac anatomy), a Stage II procedure in the first year of life, and ending with the Fontan procedure from 1.5 to 4 years of age (Feinstein et al., 2012; Fontan and Baudet, 1971; Norwood et al., 1980). Undergoing multiple surgeries may exert a compounded effect on brain injury and/or neurodevelopmental disruption. In older children and adolescents with SV, we reported a high incidence of gross anatomic brain abnormalities on MRI, along with lower cortical and subcortical volumes and thicknesses, and altered white matter microstructure throughout the brain (Bellinger et al., 2015) (Watson et al., manuscript under review). Furthermore, patients who had the Norwood procedure as their Stage I operation had poorer neurodevelopmental outcomes and lower brain volumes compared to the non-Norwood patients. Given widespread differences in both GM and WM as compared to controls, it is likely that there are differences in the global organization (connectivity) of the brain in post-Fontan SV patients; however, there has not been any investigation of this type in this patient group.

Correlations in regional cortical thickness have been used to construct structural covariance networks from brain MRI data both in healthy subjects and clinical/disease groups (Alexander-Bloch et al., 2013b; Bernhardt et al., 2011; Chen et al., 2008; He et al., 2008, 2007, 2009). Regions with high structural covariance are presumed to share a maturational trajectory due to direct axonal connections, to be similarly affected by learning or plasticity, or to have some mutual genetic or physiological influence (suggesting an indirect connection) (Alexander-Bloch et al., 2013b; Evans, 2013). Diffusion tensor imaging (DTI) tractography is a method that more directly estimates brain structural connectivity. In healthy subjects, there is a moderate agreement between networks constructed from *positive* cortical thickness covariance and networks from DTI tractography data (Gong et al., 2009). Furthermore, structural covariance networks in pediatric subjects show overlap with known functional connectivity networks obtained in adult data (Zielinski et al., 2010). The “small-world” property—considered to represent an optimal balance between functional integration and segregation and found in network analyses of different species and methodologies—in addition to modularity/community structure—representative of functional segregation—are present in cortical thickness networks, similarities shared with tractography and functional connectivity networks (Achard et al., 2006; Chen et al., 2013, 2008; He et al., 2007; Iturria-Medina et al., 2008; Sporns et al., 2004; Tononi et al., 1998). These features are present as early as 1 month of age and persist throughout development (Fan et al., 2011; Khundrakpam et al., 2013). Analysis of structural covariance networks can also detect organizational brain differences in patient groups compared to healthy subjects, including Alzheimer’s

disease, Parkinson's disease, and epilepsy (Bernhardt et al., 2011; He et al., 2008; Pereira et al., 2015). These studies found connectivity alterations in brain regions that match the pathology of the respective patient group.

Here, we use a graph theoretical approach to analyze brain networks based on cortical thickness covariance to compare brain structural connectivity in children and adolescents with SV who have undergone the Fontan procedure with that of typically developing control subjects. We also investigate potential differences between subgroups of the SV patients, including those whose Stage I operation was the Norwood procedure, whether or not the initial operation was in the neonatal period, and whether the initial operation was open or not (shunt).

Methods

Subjects

Adolescents in the Fontan group were recruited from 2010 to 2012 at BCH. Inclusion criteria included: age 10-19 years at the time of enrollment; diagnosis of single ventricle; and cardiac surgery including the Fontan procedure, Fontan re-do, or other open heart surgery at least 6 months before testing. Exclusion criteria included: known risk factors for brain disorders (e.g. history of closed head injury with loss of consciousness); any contraindication to acquisition of MRI data (e.g. metal implants); Trisomy 21; adolescents with forms of CHD other than single ventricle defect requiring surgical correction; and cardiac transplantation. The criteria used to recruit healthy control subjects were adapted from those of the NIH MRI study of normal brain

development (Almli et al., 2007; Evans, 2006). This study was approved by the BCH Institutional Review Board and adhered to institutional guidelines. Parents provided informed consent, and adolescents provided assent.

MRI acquisition

Subjects were scanned on either a GE 3 Tesla (T) or 1.5T system (General Electric, Milwaukee, WI) with an eight-channel head coil at Beth Israel Deaconess Medical Center. The volumetric series for each subject was acquired using a Magnetization-Prepared Rapid Acquisition Gradient Echo (MP-RAGE) sequence with parameters: TR/TE/TI = 7.004ms/2.856ms/650ms, flip angle = 8°, acquisition matrix = 256 x 256, FOV = 256mm, slice thickness = 1mm, with resultant voxel size = 1 x 1 x 1 mm³. All images were inspected by a radiologist to assure data quality and detect structural abnormalities (e.g. tumors, stroke, etc.).

Cortical thickness calculation

Images were processed using *Freesurfer v5.3* (A.A. Martinos Center for Biomedical Imaging, Massachusetts General Hospital). Image processing details are described elsewhere (Dale et al., 1999; Fischl and Dale, 2000; Fischl et al., 1999). Briefly, MRI images are first partitioned into white matter, gray matter, and cerebrospinal fluid. The outer pial surface of the brain is calculated, as is the surface comprising the white matter/gray matter junction. Cortical thickness is obtained by taking the distance between these two surfaces at every vertex. Finally, the cortical surface is parcellated into distinct units based on gyral and sulcal anatomy (Fischl et al., 2004) The *Desikan-Killiany-Tourville (DKT)*. atlas, which contains 31 regions per hemisphere, was used for the

parcellation (Klein and Tourville, 2012). Mean cortical thickness was obtained for all regions for each subject.

Network construction

All statistics were performed in R version 3.3.0 (2016-05-03), using functions in the packages igraph v1.1.0 and brainGraph (Csardi and Nepusz, 2006; Kolaczyk and Csardi, 2014; R Core Team, 2015). First, a general linear model (GLM) was specified for each brain region, with mean regional cortical thickness as the outcome variable and age, sex, and scanner field strength (1.5T or 3T) as covariates. Next, Pearson correlation coefficients were calculated for the model residuals between all regions, creating a single adjacency matrix of size 62 x 62 for each group.

The adjacency matrix of each group was binarized by thresholding and removing any matrix entry with a correlation coefficient lower than the threshold. Negative correlations were not considered, as these likely do not represent real anatomic connections in the brain (Gong et al., 2012). To ensure equal network sizes for both groups, the thresholds were chosen to result in a specific *density* (the ratio of the number of edges present in the network to the total number of edges possible). Network density ρ is represented mathematically as $\rho = \frac{2m}{n(n-1)}$ where m is the number of edges and n is the number of vertices (in this study, $n = 62$). A range of densities from 0.07-0.40 (step size = 0.01) was investigated. The networks created from these matrices were undirected, unweighted, and simple (i.e. no loops).

Network metrics

Vertex- (i.e., region-) and graph-level metrics were calculated for both groups at each density. For visualization purposes, a density of 30% was chosen; this was the lowest density for which, in both groups, at least 95% of vertices were connected. This density is within the range used in other studies (Bernhardt et al., 2011; He et al., 2008).

Vertex importance

Vertex *degree* (the number of connections of a vertex), *betweenness centrality* (the number of shortest paths a vertex lies on), and *nodal efficiency* were used as measures of vertex importance. Furthermore, a vertex was considered to be a *hub* if its betweenness centrality was at least one standard deviation greater than the mean across vertices (for a given density) (Bernhardt et al., 2011; Hosseini and Kesler, 2013b; Tijms et al., 2013; Wang et al., 2013). The degree k_i of vertex i is calculated as

$$k_i = \sum_{j=1}^n A_{ij}$$

where n is the number of vertices in the graph and A_{ij} is the graph's adjacency matrix.

Betweenness centrality $c_B(v)$ of vertex v is

$$c_B(v) = \sum_{s \neq t \neq v \in V} \frac{\sigma(s, t | v)}{\sigma(s, t)}$$

where $\sigma(s, t | v)$ is the number of shortest paths from s to t and passing through v , $\sigma(s, t) = \sum_v \sigma(s, t | v)$, and V is the vertex set of the graph (Kolaczyk, 2009). The nodal efficiency $E_{nodal}(i)$ of vertex i is

$$E_{nodal}(i) = \frac{1}{n-1} \sum_{j \in V} \frac{1}{L_{ij}}$$

where L_{ij} is the shortest path length between vertices i and j (Achard and Bullmore, 2007).

Network segregation and integration

Network *segregation* was assessed with three metrics. *Modularity* measures the strength of a given network partition. Higher modularity indicates that vertices belonging to the same network community (i.e., module) are more connected to each other than they are to vertices of a different community. The Louvain algorithm was used to partition the networks into communities and compute the modularity (Blondel et al., 2008; Clauset et al., 2004). The modularity Q is

$$Q = \frac{1}{2m} \sum_{ij} \left(A_{ij} - \frac{k_i k_j}{2m} \right) \delta(c_i, c_j)$$

where m is the number of edges in the graph, k_i is the degree of vertex i , c_i is the “class” of vertex i , and δ is the Kronecker delta function (Newman, 2010). *Degree assortativity* is a related metric that measures the strength with which vertices of similar degree connect to one another; higher assortativity indicates that high-degree vertices are more likely to connect to other high-degree vertices compared to low-degree vertices. The degree assortativity r is

$$r = \frac{\sum_{ij} (A_{ij} - k_i k_j / 2m) k_i k_j}{\sum_{ij} (k_i \delta_{ij} - k_i k_j / 2m) k_i k_j}$$

where δ_{ij} is the Kronecker delta function (equaling 1 if vertices i and j are connected and have the same degree, and 0 otherwise) (Newman, 2010). We also introduce *lobe assortativity*, which measures the number of inter-lobar connections relative to intra-lobar connections. This is equivalent to calculating the modularity of the network if it were *a priori* partitioned into the lobes of the brain (i.e., frontal, parietal, temporal, occipital, insula, and cingulate). Higher values of lobe assortativity are present in networks with relatively fewer inter-lobar connections. The assortativity coefficient r for categorical variables is

$$r = \frac{\sum_i e_{ii} - \sum_j a_i b_i}{1 - \sum_i a_i b_i}$$

where e_{ij} is the fraction of edges between vertices of category i and vertices of category j , $a_i = \sum_j e_{ij}$, and $b_j = \sum_i e_{ij}$ (Newman, 2003).

Networks possessing the small-world property are considered to have an optimal balance between segregation and integration (Watts and Strogatz, 1998). Small-world parameters *clustering coefficient* (C ; the tendency of a vertex's neighbors to be connected to one another) and *characteristic path length* (L ; the average of shortest path lengths between all vertices) were calculated, along with the average of each parameter from 1,000 random graphs (denoted C_{rand} and L_{rand} , respectively) for each group and at each density. Random graphs were generated by randomly rewiring the edges in the group-specific graphs for 10,000 iterations, keeping constant the observed graph's density and degree sequence (Maslov and Sneppen, 2002; Viger and Latapy, 2015). The *small-world index* σ is then calculated as the ratio of the normalized C to the normalized

L (calculated as $\gamma = C/C_{rand}$ and $\lambda = L/L_{rand}$, respectively), and a network is considered to possess the “small-world” property if $\sigma > 1$ (Humphries and Gurney, 2008).

Mathematically,

$$\sigma = \frac{C / C_{rand}}{L / L_{rand}} = \frac{\gamma}{\lambda}$$

Since the gray matter networks in this study are generated from correlations, these networks will tend to have a higher-than-expected level of clustering (Hosseini and Kesler, 2013b; Zalesky et al., 2012). As a result, the random graphs generated by a simple rewiring procedure may not be entirely appropriate, as they will tend to have very low clustering by design (Newman, 2010). Thus, as an alternative we generated, for each density and each group, 100 random networks while controlling for global clustering using a Markov Chain process (Bansal et al., 2009). We then calculated an alternate small-world index, ω , using the equation from Telesford et al. (2011):

$$\omega = \frac{L_{rand}}{L} - \frac{C}{C_{latt}}$$

Here, C_{latt} is the mean clustering coefficient of a set of equivalent *lattices*; the graphs generated from the Markov Chain process are used to calculate this value. L_{rand} is the mean characteristic path length from the set of randomly rewired graphs (described in the previous paragraph). A network is considered to be a “small-world” network if $-0.5 \leq \omega \leq 0.5$; networks with ω closer to -1 are more similar to a lattice, and networks with ω closer to 1 are more similar to a random network.

Network closeness

Edge distances were calculated as the Euclidean distance in Montreal Neurological Institute (MNI) coordinates (in mm) between centroids of pairs of connected regions (Alexander-Bloch et al., 2013b; Bassett et al., 2008; He et al., 2007). *Vertex distances* were calculated as the mean distance of all edges connecting a given vertex to all other vertices (Alexander-Bloch et al., 2013c). Similarly, the characteristic path length L serves as a measure of the global closeness of a network.

Asymmetry

A measure of asymmetry, the *asymmetry index (AI)*, was calculated as the difference in the number of left and right hemisphere intra-hemispheric connections, divided by the average number of intra-hemispheric connections of both hemispheres, i.e.

$$AI = 2 \times \frac{m_{lh} - m_{rh}}{m_{lh} + m_{rh}}$$

If $AI < 0$, this indicates that the network has more intra-hemispheric connections in the right compared to the left hemisphere. The range of AI is $[-2, 2]$; the limits are achieved only if all edges are in one hemisphere. In addition to the global AI, an AI was calculated for each vertex.

Network robustness

Network *robustness* was assessed using *targeted attack* and *random failure* analyses, in addition to the calculation of global and vertex *vulnerability* (Albert et al., 2000; Bernhardt et al., 2011; He et al., 2008; Iturria-Medina et al., 2008; Romero-Garcia et al., 2012; Wang et al., 2013). In a *targeted attack* analysis, vertices are sorted in

descending order by betweenness centrality. The size of the largest connected component (the number of vertices that are reachable from any other vertex) is computed, and then the vertex with the highest betweenness is removed. After removal of that vertex and its connections, the size of the largest connected component is computed for the new network. These steps are repeated until all vertices have been removed. In a *random failure* analysis, vertices are removed in random order, and the size of the largest connected component is recorded after each removal. This was repeated 1,000 times, and the average over all iterations was used as the final result. Both targeted attack and random failure analyses were also performed with edge removals, using the same procedure (except edges were sorted in descending order of *edge betweenness*).

Vulnerability is dependent on the *global efficiency* E_{glob} ,

$$E_{glob} = \frac{1}{n(n-1)} \sum_{i \neq j} \frac{1}{d_{ij}}$$

where n is the number of vertices and d_{ij} is the shortest path length between vertices i and j . Vulnerability V_i is then calculated for each vertex i as

$$V_i = 1 - \frac{E_{glob}(i)}{E_{glob}}$$

where $E_{glob}(i)$ is the global efficiency of the network after removing vertex i . Global vulnerability V_G is the maximum across all vertices; i.e., $V_G = \max_i V_i$. Higher values indicate that the network is less stable in the presence of vertex removal.

Statistics

For demographic variables, P-values were calculated by Fisher's exact test for categorical variables and Wilcoxon rank sum test for continuous variables. Permutation testing was performed to assess group differences in global network measures (i.e., number of hubs, modularity, assortativity, clustering coefficient, characteristic path length, edge asymmetry, global and local efficiency, and vulnerability). Each subject was randomly assigned to one of two groups (of the same size as the Fontan and control groups), and then we followed the procedure for network construction described above. This resulted in two networks for which we calculated the between-group difference in global network measures. This was repeated for 10,000 permutations at each density. Furthermore, for both global and vertex measures (nodal efficiency, betweenness centrality, degree), subjects were randomly assigned to a group (as described above), and significance was assessed across all densities by calculating the area under the curve (AUC) for each group and vertex and taking the difference (Hosseini et al., 2012). We performed 10,000 permutations for global measures and 5,000 for vertex measures. Permutation P-values were calculated as the proportion of times the randomized set of between-group differences was greater than (for number of hubs, clustering coefficient, global and local efficiency, and vertex measures) or less than (for modularity, assortativity, characteristic path length, and asymmetry) the observed between-group difference of control and Fontan subjects. For global measures, we did not adjust P-values for multiple comparisons; for vertex measures, the false discovery rate (FDR) was used to adjust P-values across vertices (Genovese et al., 2002). Group differences in edge

distance and in mean vertex distance of hub regions were assessed using a two-sample Wilcoxon rank-sum test at each density, with P-values controlling for the FDR at a significance level of 0.05.

Results

Subjects

A total of 111 Fontan subjects were included in the analysis, after the removal of 6 due to the presence of a large stroke. A total of 45 control subjects were included in the analysis. Subject demographics and education history are summarized in Table 2.1. A significantly greater proportion of Fontan subjects than controls were scanned at 1.5T (41.03% vs. 10.26%, $p = 0.01$). NYHA class was significantly higher (i.e., more limitation in ordinary physical activity) in the Fontan group than controls (1 vs. 2, $p < 0.0001$). Regarding education history, the Fontan group had significantly greater numbers for all variables (tutoring, grade retention, early intervention, occupational therapy, physical therapy, special education, psychotherapy and counseling, and any special services; all $p < 0.05$).

Network hubs

Hub regions for the Control group are shown in Figure 2.1 and for the Fontan group in Figure 2.2. These are regions that were classified as hubs in at least half of the 44 densities tested. There were 8 hubs in the control group and 5 hubs in the Fontan group. Hubs in the control group were more likely to be in the frontal lobe and in the right hemisphere, whereas hubs in the Fontan group were present roughly equally in both hemispheres and across lobes. For these regions, a plot of the densities at which they

were determined to be hubs is shown in Figure 2.3. The only region present in both groups is the right superior frontal gyrus (rSFG); in the Fontan group, it is no longer a hub at higher densities.

Network segregation

Figures 2.4 and 2.5 show the adjacency matrices for both the Fontan and control groups at a density of 30%. Each color represents one of the major lobes of the brain; matrix entries that are gray indicate inter-lobar connections, and all others indicate intra-lobar connections. Qualitatively, the Fontan group has more fronto-frontal and fronto-parietal connections than the control group, and the control group has more posterior/cingulate connections.

Small world

Figure 2.6 (top) shows the small-world parameter σ plotted across densities for both groups. A network is considered to be a “small-world” network if this value is greater than 1. For the control group, $\sigma > 1$ from densities of $\approx 20\%$ to 35% ; for the Fontan group, $\sigma < 1$ from $\approx 27\%$ and higher.

Figure 2.6 (bottom) shows the small-world parameter ω across densities for both groups. At every density, both groups’ networks are in the small world range, with the control group being closer to a lattice than the Fontan group for most densities.

Network closeness

Average edge distance (in millimeters) was higher in the Fontan group for several higher densities ($p < 0.05$ for densities 0.39, 0.4, 0.41, 0.42, 0.43, 0.46, 0.47, 0.48, 0.49, 0.5). When considering the average edge distance for hub regions, although lower in the

Fontan group for nearly all densities, the between-group difference did not reach statistical significance.

Permutation analysis

Figure 2.7 shows global network measures plotted against graph density for both subject groups. Asterisks indicate densities for which the particular global measure is significantly different between groups, calculated from 10,000 permutations. At all densities, asymmetry is significantly lower in the control group ($p < 0.05$, adjusted for multiple comparisons using a FDR across all densities). The difference across densities (AUC) was also significant in the same direction. This indicates that there are significantly more right-hemispheric connections relative to left-hemispheric connections in the control group than in the Fontan group.

Vertex differences

Figure 2.8 shows the vertices in which nodal efficiency was significantly different between groups, as determined by permutation testing ($p < 0.05$). Red vertices are those in which nodal efficiency was greater in the control group than in the Fontan group, and blue vertices are those in which nodal efficiency is lower in the control group than in the Fontan group. Table 2.2 lists the regions of significant difference, the observed group difference, and the permutation P-values.

Figure 2.9 shows the vertices in which betweenness centrality was significantly different between groups, as determined by permutation testing ($p < 0.05$). Red vertices are those in which betweenness centrality was greater in the control group than in the Fontan group, and blue vertices are those in which betweenness centrality was lower in

the control group than in the Fontan group. Table 2.3 lists the regions of significant difference, the observed group difference, and the permutation P-values.

Robustness

Figure 2.10 shows the results from the robustness analysis. For both the random vertex and random edge removals, networks from both groups were relatively resilient to removal of edges or vertices in a random order (top-left and top-right panels). Furthermore, both groups were resilient to targeted removal of edges (from highest to lowest edge betweenness; lower-left panel). Both groups were relatively less resilient to targeted removal of vertices (from highest to lowest betweenness centrality; lower-right panel). There were no between-group differences in global vulnerability at any density.

	Total (N = 156)	Control (N = 45)	Fontan (N = 111)	P-value
Age at MRI, yr	14.96 ± 2.87	15.48 ± 2.44	14.75 ± 3.01	0.19
Scanner, 1.5T	80 (51)	16 (36)	64 (58)	0.01
Intracranial volume, L	1.33 ± 0.25	1.38 ± 0.21	1.31 ± 0.26	0.11
Sex, F	65 (42)	19 (42)	46 (41)	1.0
NYHA class	2 (1 – 2)	1 (1 – 1)	2 (1 – 2)	<0.0001
Social class at 16 yr of age†	50.32 ± 12.85	54.11 ± 8.88	48.81 ± 13.86	0.07
Birth weight, kg	3.29 ± 0.65	3.47 ± 0.58	3.23 ± 0.66	0.06
Gestational age, wk	38.98 ± 2.21	39.67 ± 1.20	38.71 ± 2.45	0.06
Race (white)	143 (92)	38 (84)	105 (95)	0.05
Received tutoring	72 (46)	13 (29)	59 (53)	0.008
Held back in school	26 (17)	0 (0)	26 (23)	<0.0001
Early intervention	64 (41)	2 (4)	62 (56)	<0.0001
Occupational therapy	60 (38)	0 (0)	60 (54)	<0.0001
Physical therapy	61 (39)	7 (16)	54 (49)	0.0001
Special education	38 (24)	0 (0)	38 (34)	<0.0001
Psychotherapy and counseling	51 (33)	7 (16)	44 (40)	0.004
Any special services	118 (76)	24 (53)	94 (85)	<0.0001

Table 2.1: **Subject demographics and education history.** Values are N (%), mean SD, or median (range). P-values were calculated by Fisher's exact test for categorical variables and Wilcoxon rank sum test for continuous variables. yr: years; T: tesla; L: liters; F: female; NYHA: New York Heart Association; kg: kilograms; wk: weeks. †Score on the Hollingshead Four Factor Index of Social Status; higher scores indicate higher social class.

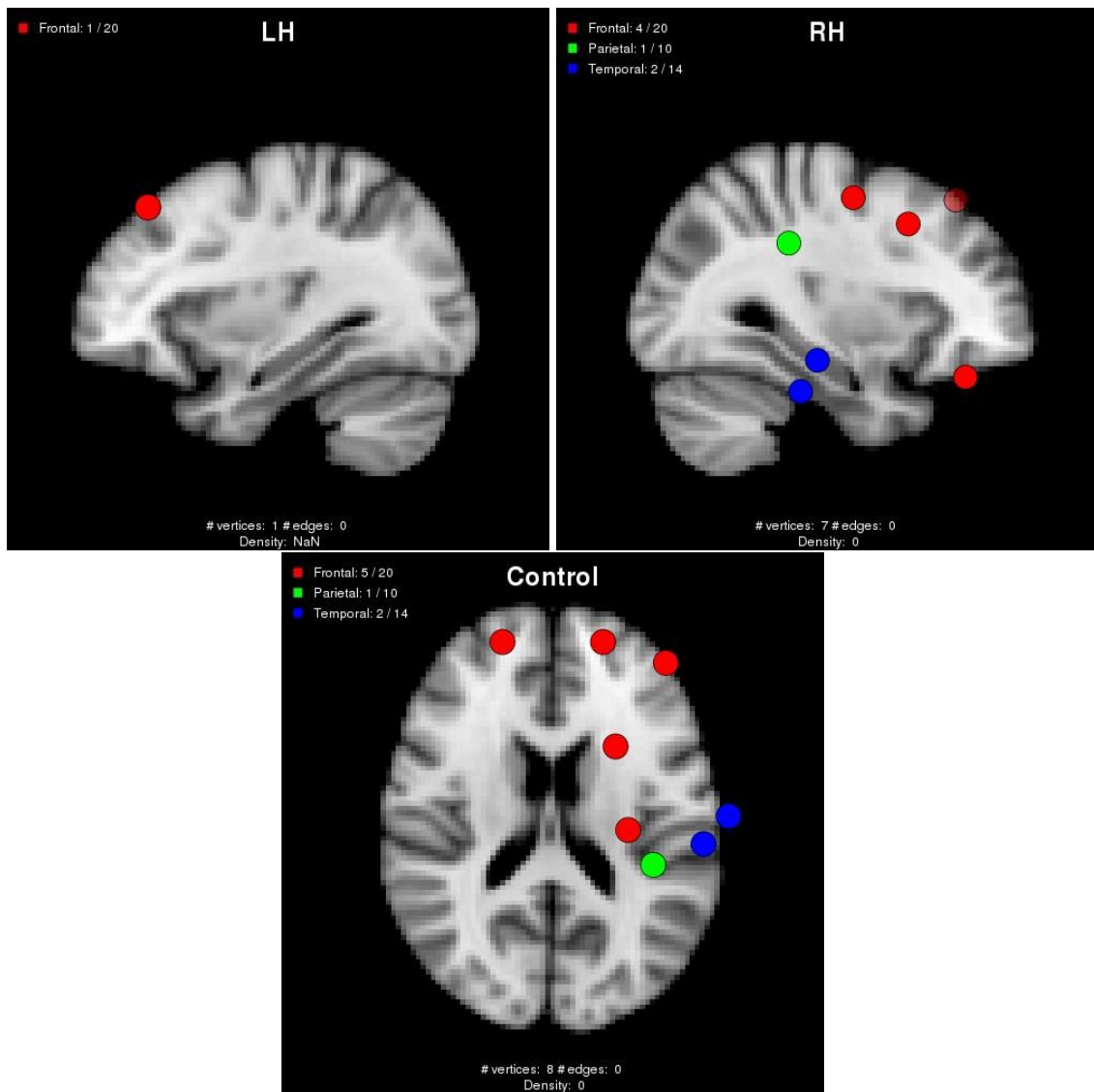


Figure 2.1: **Hub regions in the Control group.** Vertex colors signify lobe membership (red: frontal; green: parietal; blue: temporal; magenta: occipital)

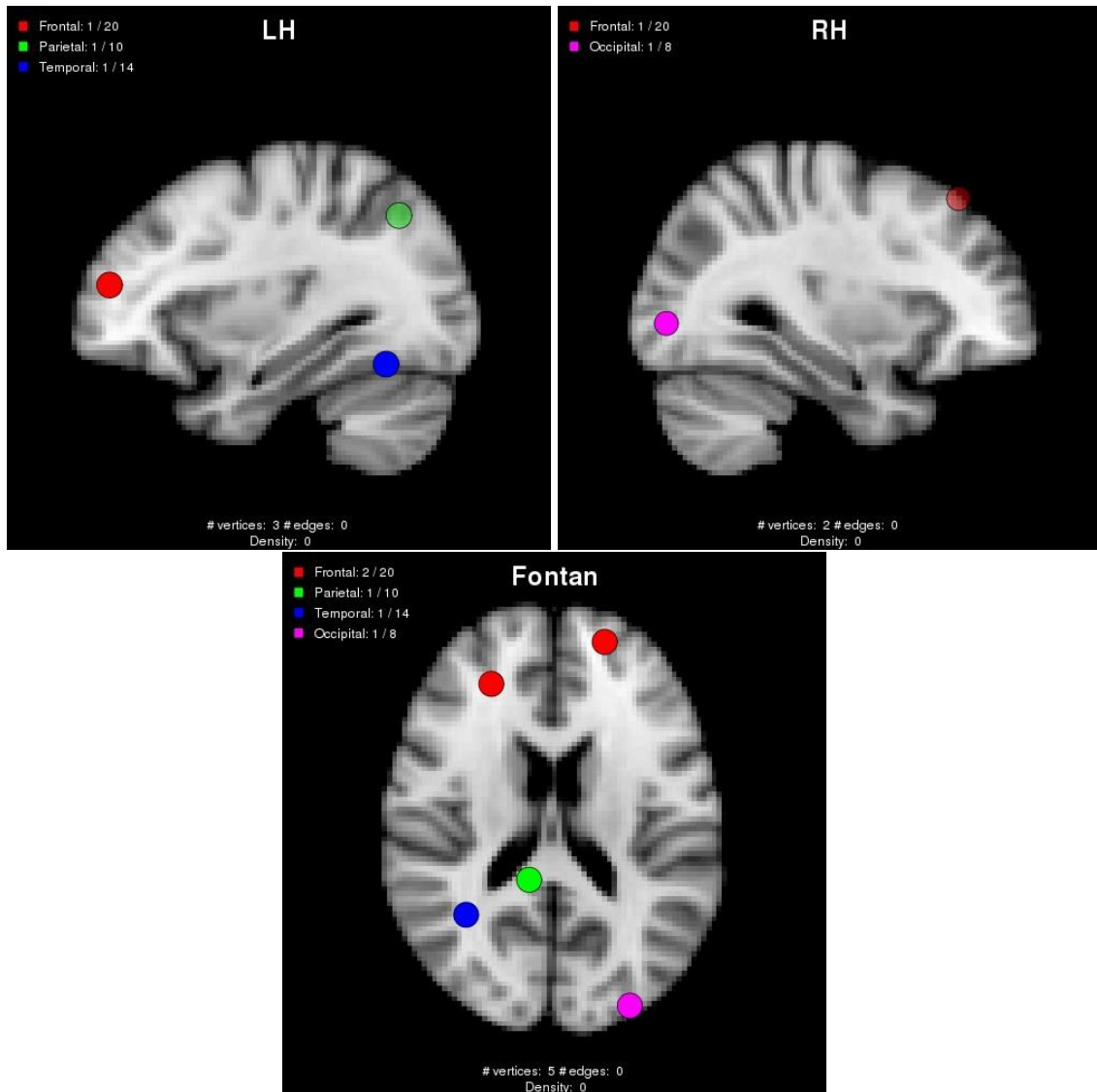


Figure 2.2: **Hub regions in the Fontan group.** Vertex colors signify lobe membership (red: frontal; green: parietal; blue: temporal; magenta: occipital)

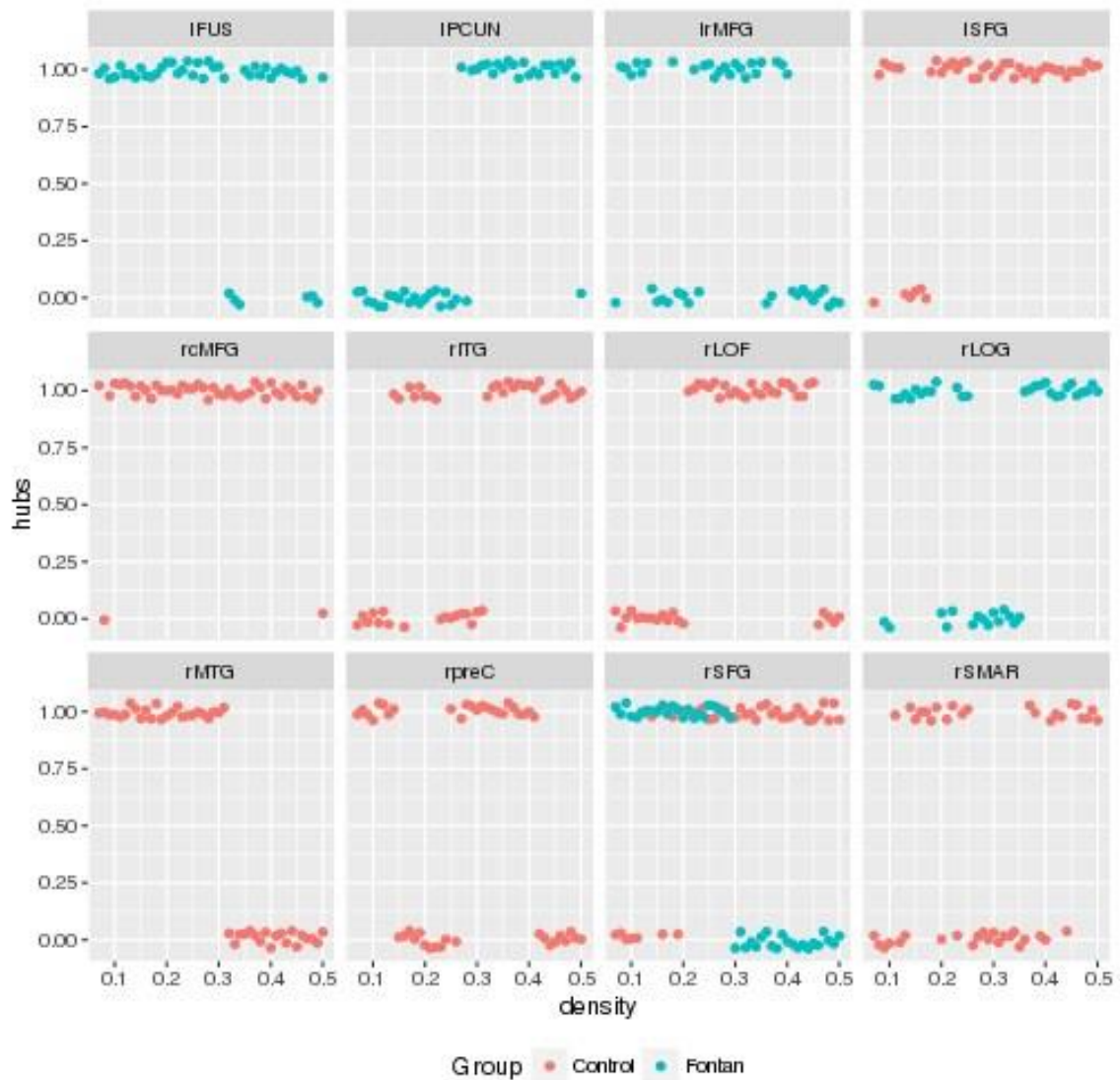


Figure 2.3: **Hub regions across densities.** Points take a value of 1 if the region was determined to be a hub at the specific density, and a 0 otherwise. Each facet of the plot is for a different brain region. Cyan points are the Fontan group and red points are the control group.

l: left; r: right; FUS: fusiform; PCUN: precuneus; rMFG: rostral middle frontal; SFG: superior frontal; cMFG: caudal middle frontal; ITG: inferior frontal; LOF: lateral orbitofrontal; LOG: lateral occipital; MTG: middle temporal; preC: precentral; SFG: superior frontal;

SMAR: supramarginal



Figure 2.4: **Adjacency matrix for the Control group at a density of 30%.** Non-gray boxes represent intra-lobar connections, and gray boxes are inter-lobar connections. Regions (from top-to-bottom and left-to-right) first are ordered by lobe, then by hemisphere (left hemisphere first), and then alphabetically by region abbreviation.

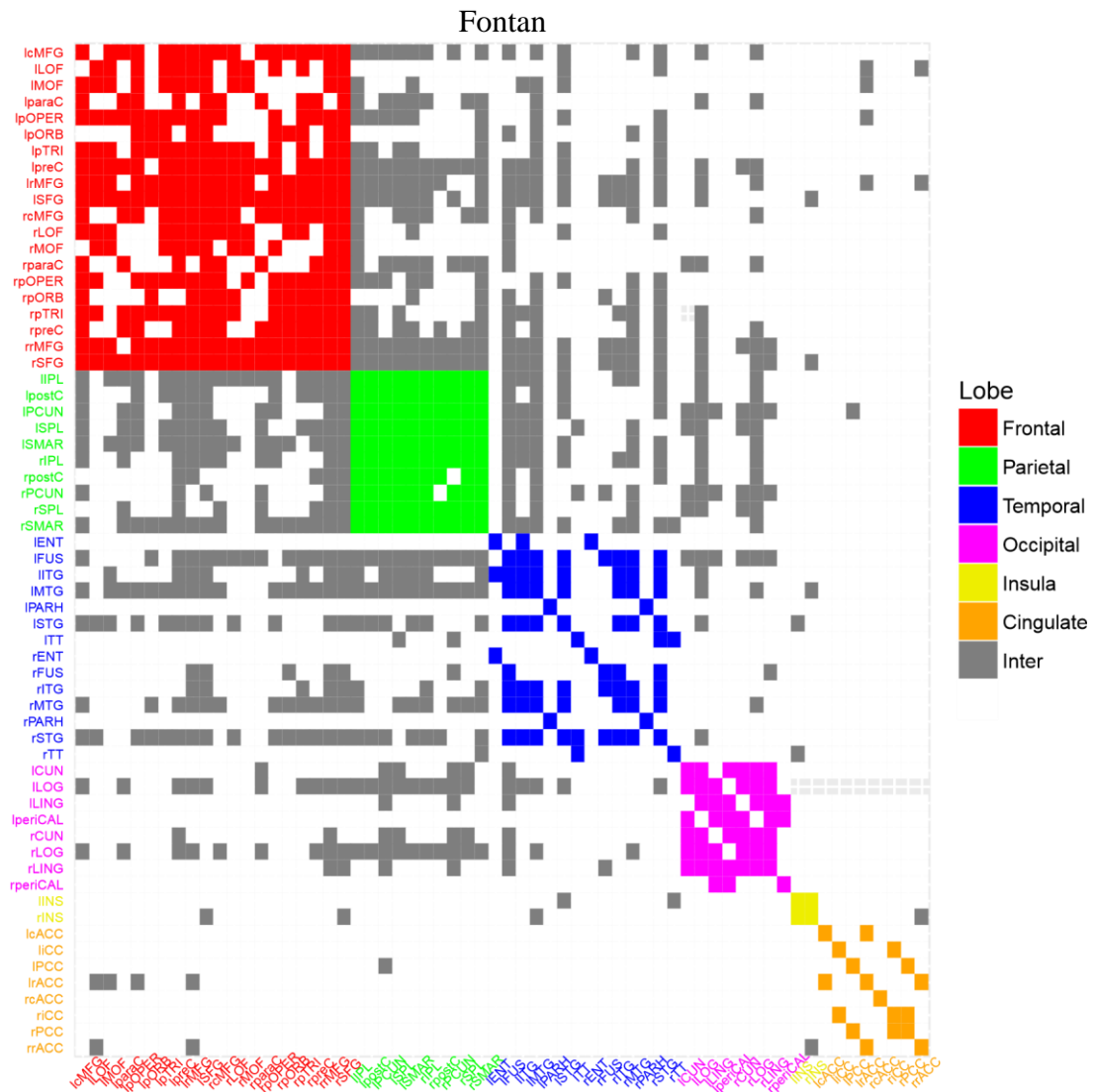


Figure 2.5: **Adjacency matrix for the Fontan group at a density of 30%.** Non-gray boxes represent intra-lobar connections, and gray boxes are inter-lobar connections. Regions (from top-to-bottom and left-to-right) first are ordered by lobe, then by hemisphere (left hemisphere first), and then alphabetically by region abbreviation.

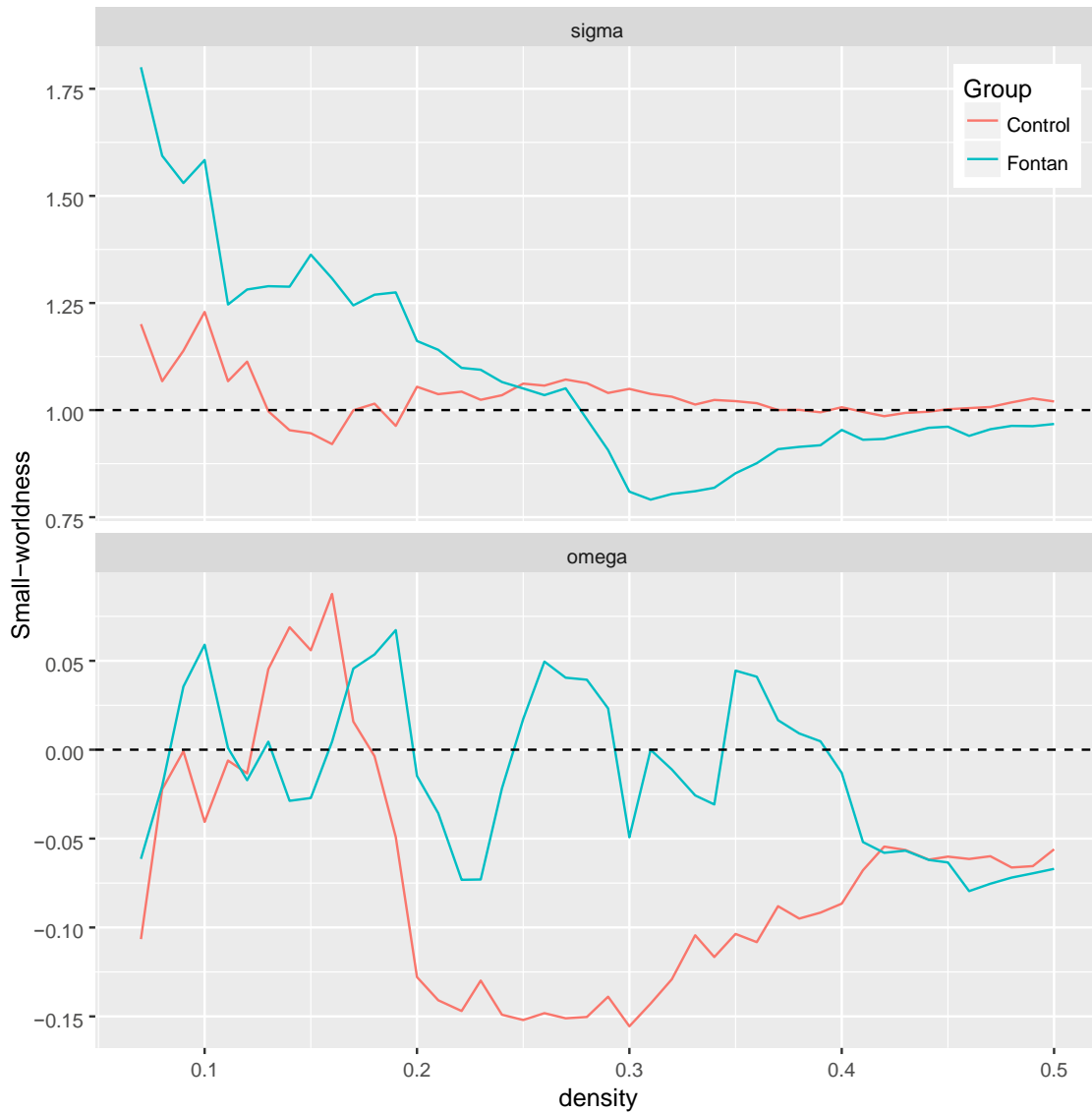


Figure 2.6: **Small-world indices.** (top) The classic small-world index, σ ; the dashed horizontal line at $y = 1$ is included to show the minimum value for a network to be considered “small-world” (Watts and Strogatz, 1998) (bottom) The small-world index ω introduced by Telesford et al. (2011); the dashed horizontal line at $y = 0$ indicates the value at which the network displays a balance between clustering coefficient and characteristic path length.

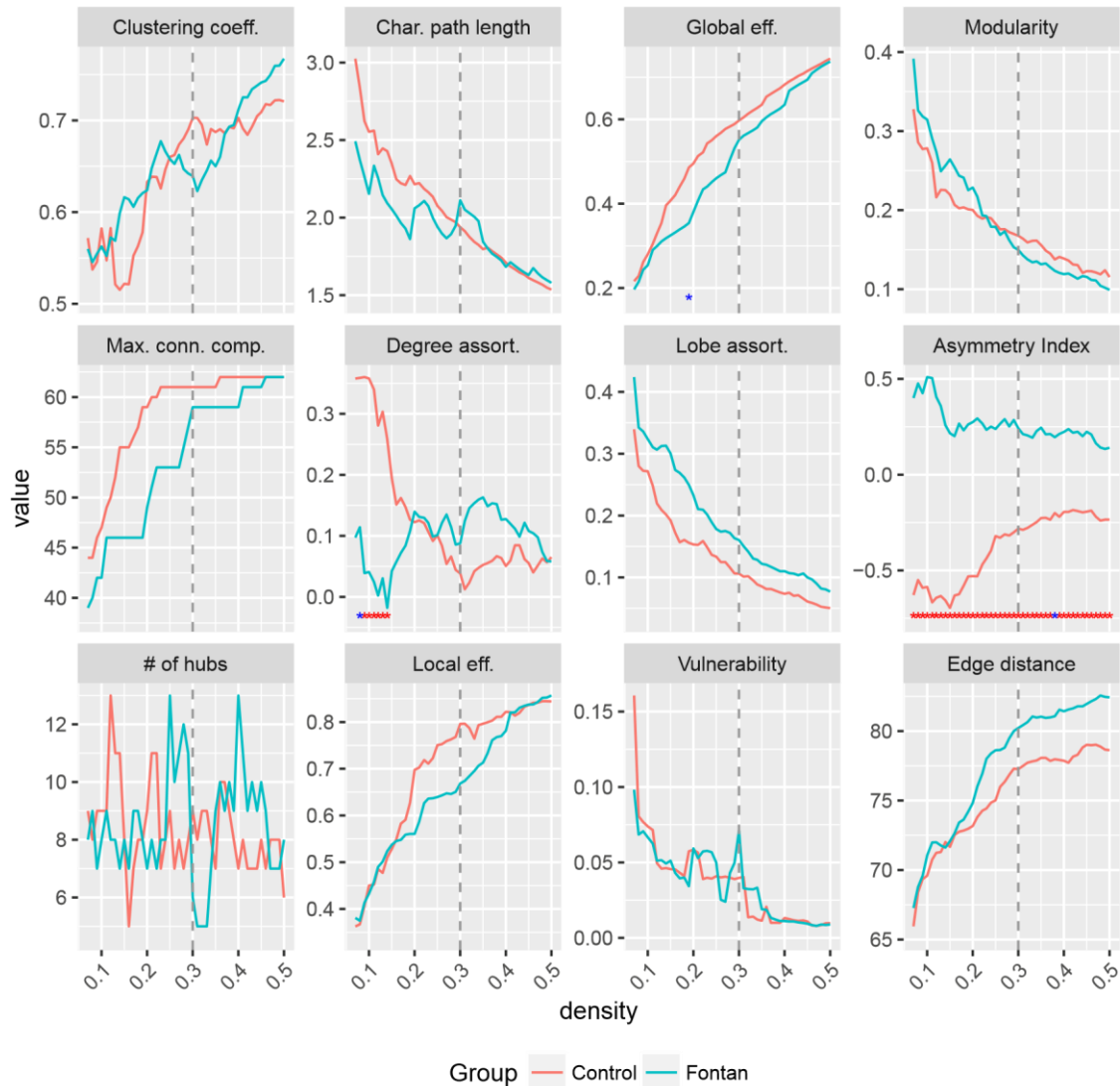


Figure 2.7: **Global network measures against density.** The dashed vertical line indicates a density of 30%. Red asterisks indicate a significant ($p < 0.05$) group difference as determined by permutation analysis ($N = 10,000$). Blue asterisks indicate a "trend" ($p < 0.1$).

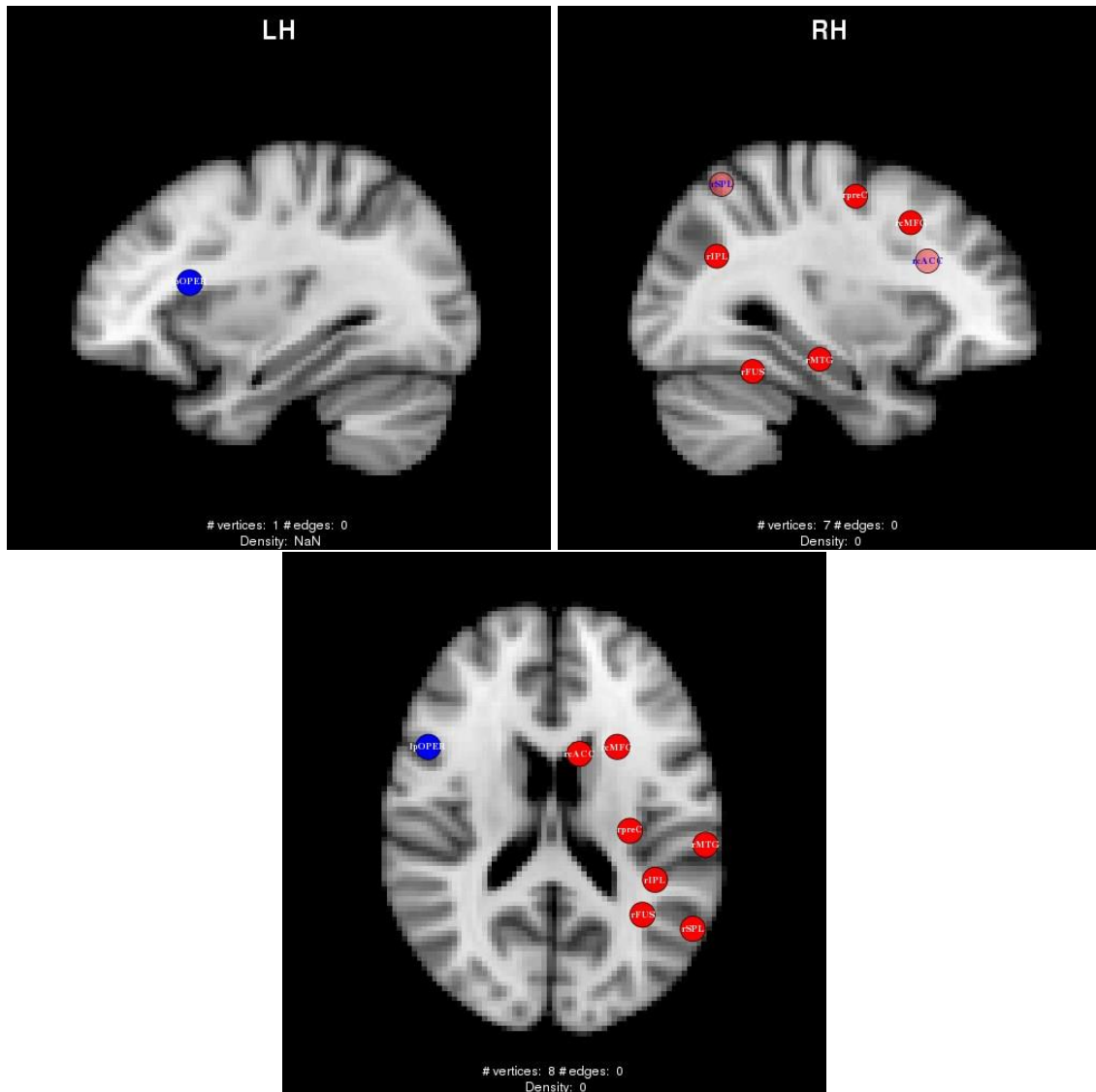


Figure 2.8: **Vertices with significant between-group differences in nodal efficiency.** Significance was determined by permutation testing ($N = 5,000$). Blue vertices are those in which nodal efficiency is greater in the Fontan group compared to the control group, and red vertices are those in which nodal efficiency is greater in the control group than the Fontan group.

Region	Group diff	P-value
L pars opercularis	-0.12	0.02
R caudal anterior cingulate	0.18	0.04
R caudal middle frontal gyrus	0.05	0.02
R fusiform	0.08	0.04
R inferior parietal lobule	0.05	0.03
R middle temporal gyrus	0.05	0.01
R precentral	0.06	0.02
R superior parietal lobule	0.06	0.02

Table 2.2: **Group differences in nodal efficiency.** List of vertices for which vertex nodal efficiency was significantly different ($p < 0.05$) between groups. Group differences greater than 0 indicate higher values in the control group compared to the Fontan group. L: left; R: right

Region	Group diff	P-value
L entorhinal	20.77	0.01
L pericalcarine	25.76	0.01
R caudal middle frontal gyrus	34.49	0.006
R lateral orbitofrontal	27.06	0.02
R middle temporal gyrus	28.06	0.03
R precentral	30.82	0.01

Table 2.3: **Group differences in betweenness centrality.** List of vertices for which vertex betweenness centrality was significantly different ($p < 0.05$) between groups. Group differences greater than 0 indicate higher values in the control group compared to the Fontan group. L: left; R: right

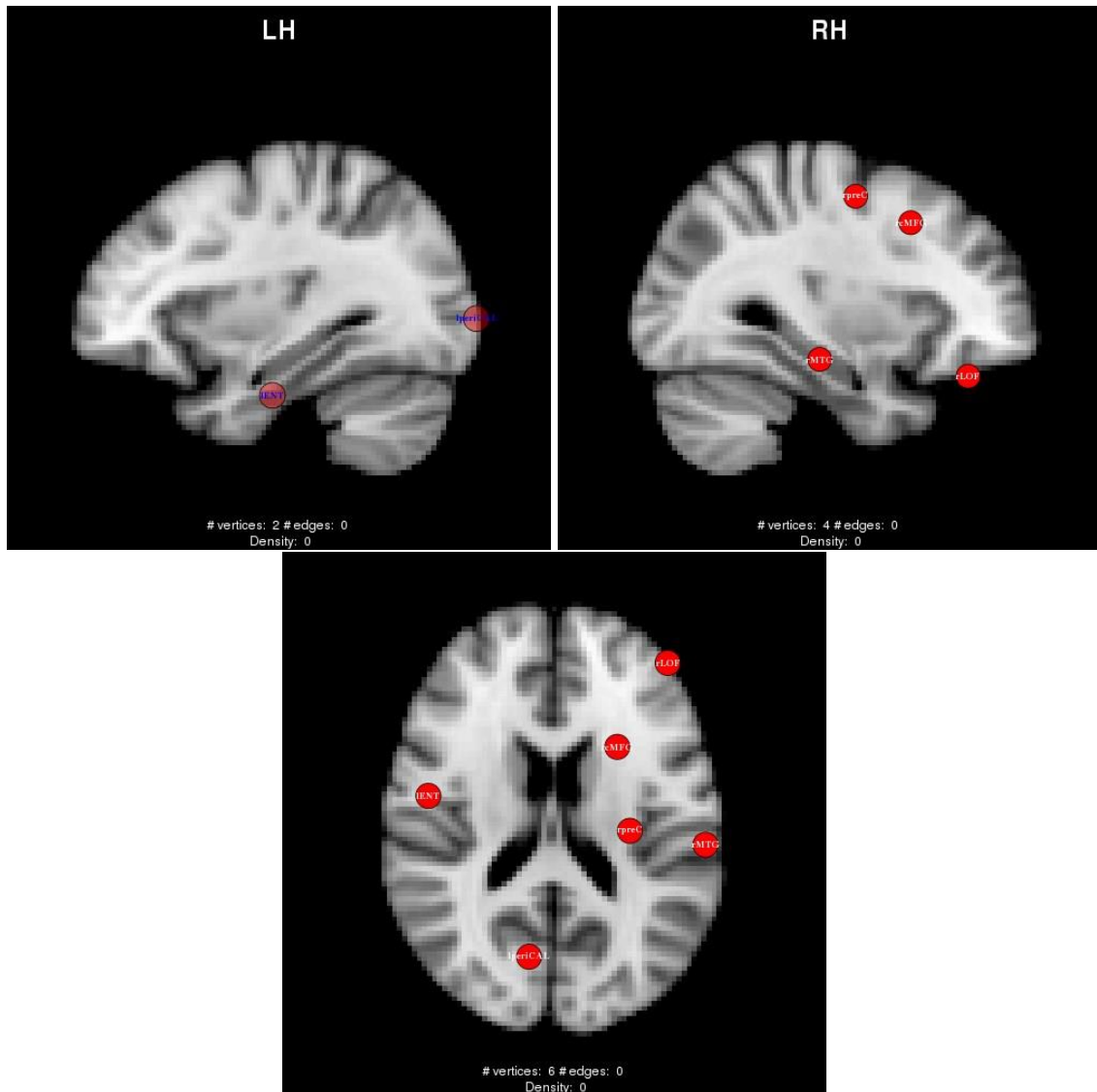


Figure 2.9: **Vertices with significant between-group differences in betweenness centrality.** Significance was determined by permutation testing ($N = 5,000$). Blue vertices are those in which betweenness centrality is greater in the Fontan group compared to the control group, and red vertices are those in which betweenness centrality is greater in the control group than the Fontan group.

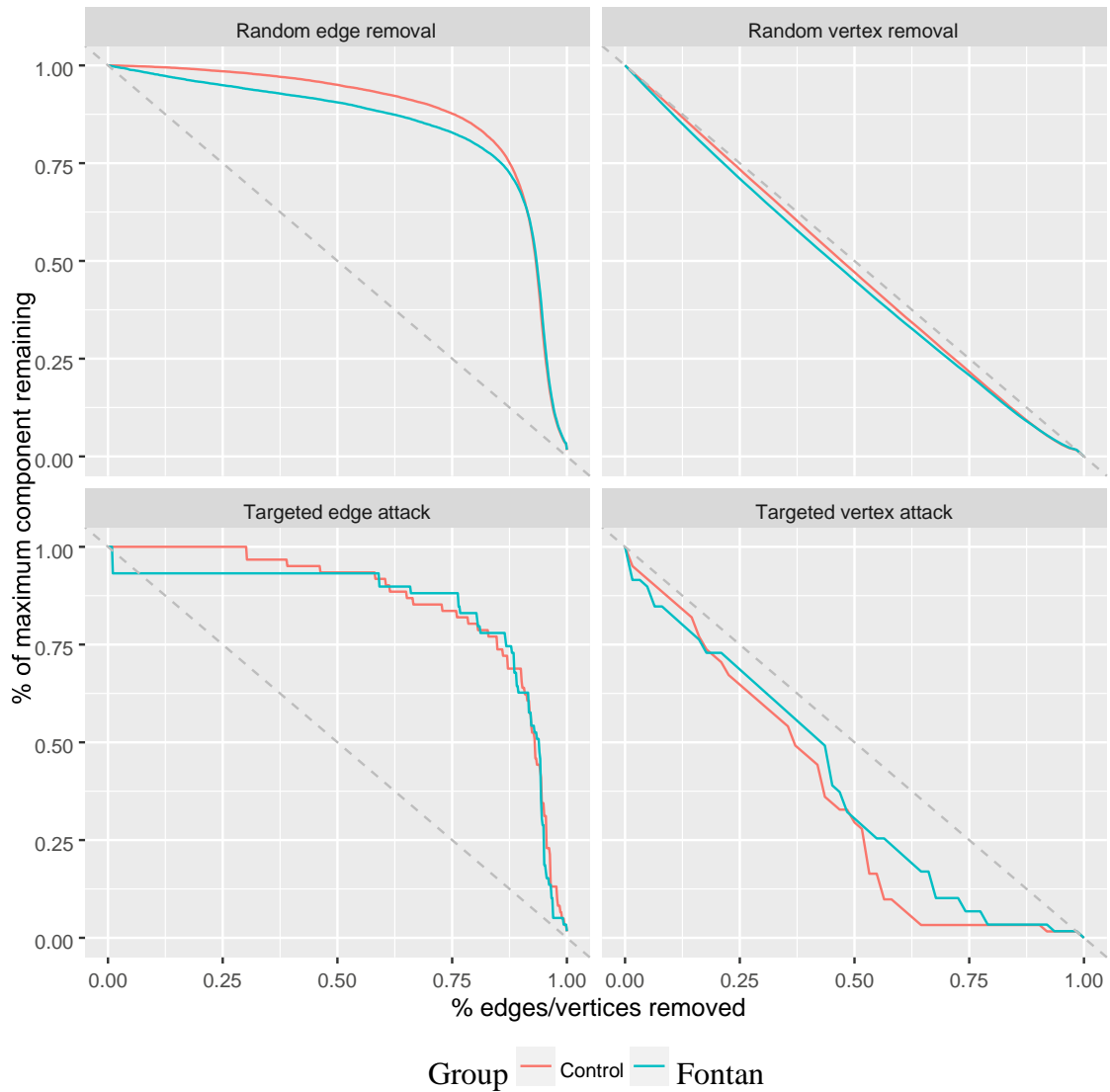


Figure 2.10: **Robustness analysis.** Each plot depicts the percentage of the largest connected component, relative to the observed maximum for each group, as a function of the percentage of edges or vertices removed. (top-left) Random edge removal. (top-right) Random vertex removal. (bottom-left) Targeted edge attack. (bottom-right) Targeted vertex attack.

Subgroup analysis

Norwood status

First, the Fontan group was separated into patients who had undergone the Norwood operation and those who had not. Based on permutation testing (5,000 permutations), there were no group differences in the AUC for any global graph measures. Group differences in nodal efficiency are shown in Figure 2.11. Red vertices are those in which nodal efficiency was greater in the non-Norwood group than in the Norwood group, and blue vertices are those with the opposite relation. Table 2.4 lists the vertices, the observed group difference, and the permutation P-values. Group differences in vertex degree were nearly identical to those of nodal efficiency (data not shown). Group differences in betweenness centrality are shown in Figure 2.12. Red vertices are those in which betweenness centrality was greater in the non-Norwood group than in the Norwood group, and blue vertices are those with the opposite relation. Table 2.5 lists the vertices, the observed group difference, and the permutation P-values.

Type of first operation

The Fontan group was also separated into patients who had a closed first operation and those who had an open first operation. Based on permutation testing (5,000 permutations), there were differences in the AUC for two global graph measures. Modularity was higher in the “Open” group at a trend level ($p = 0.06$). Global clustering coefficient was lower in the “Open” group, also at a trend level ($p = 0.07$). Group differences in nodal efficiency are shown in Figure 2.13. Red vertices are those in which

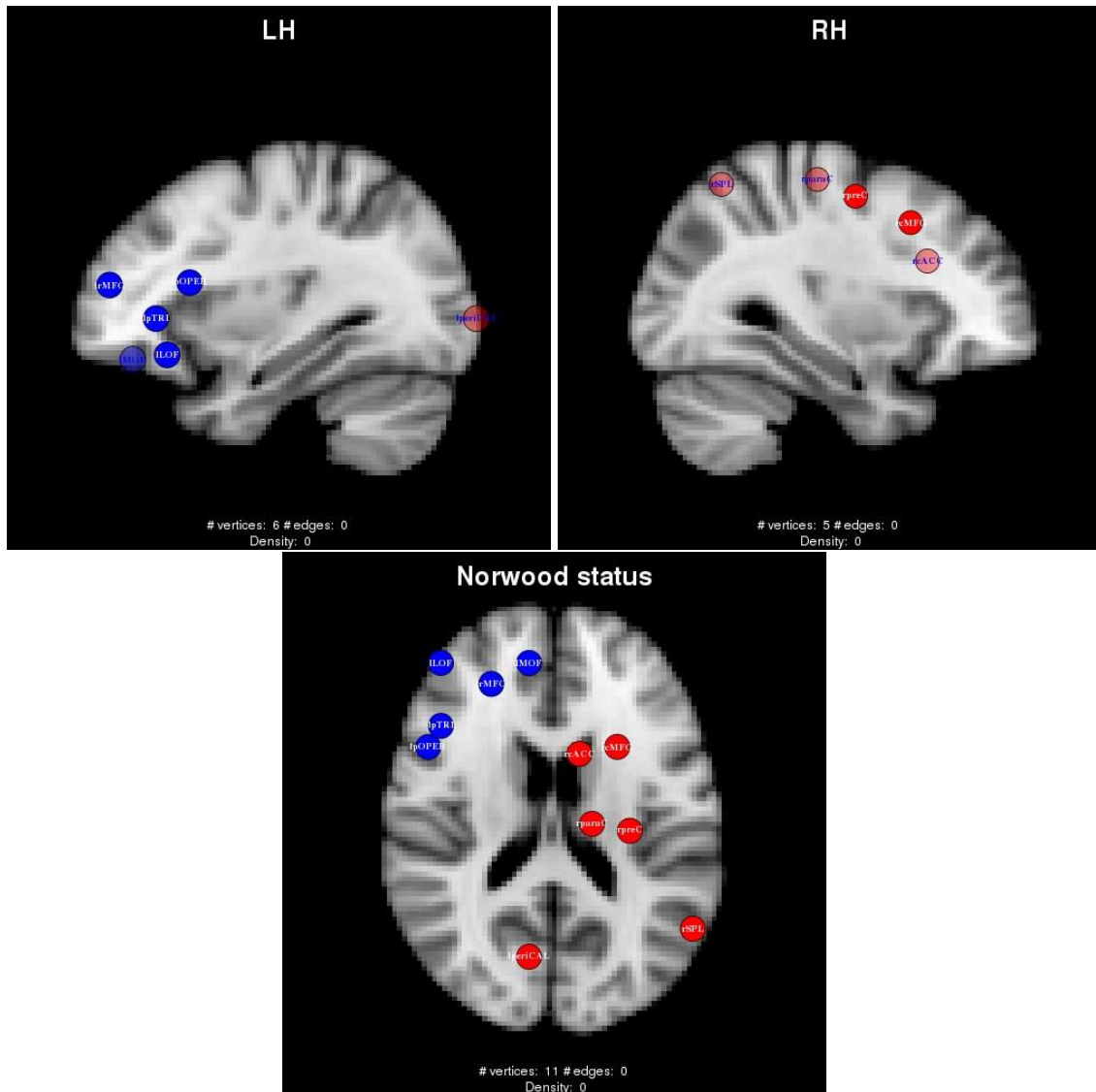


Figure 2.11: **Vertices with significant between-group differences in nodal efficiency, Norwood status.** Significance was determined by permutation testing ($N = 5,000$). Blue vertices are those in which nodal efficiency is greater in the Norwood group compared to the non-Norwood group, and red vertices are those in which nodal efficiency is greater in the non-Norwood group than the Norwood group.

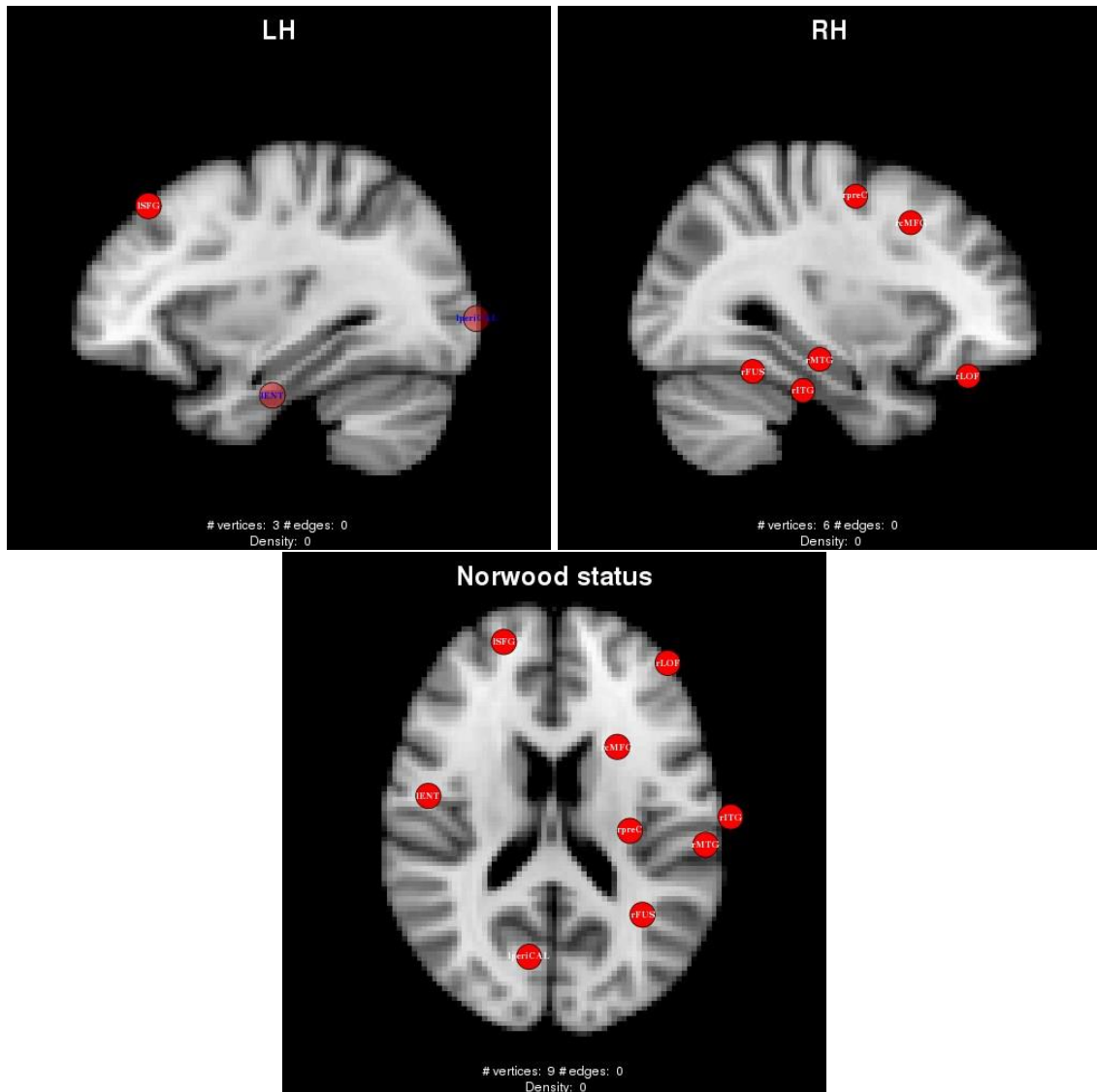


Figure 2.12: **Vertices with significant between-group differences in betweenness centrality, Norwood status.** Significance was determined by permutation testing ($N = 5,000$). Blue vertices are those in which betweenness centrality is greater in the Norwood group compared to the non-Norwood group, and red vertices are those in which betweenness centrality is greater in the non-Norwood group than the Norwood group.

Region	Group diff	P-value
L lateral orbitofrontal	-0.11	0.003
L medial orbitofrontal	-0.15	0.006
L pars opercularis	-0.14	< 0.001
L pars triangularis	-0.08	0.03
L pericalcarine	0.14	0.03
L rostral middle frontal gyrus	-0.06	0.01
R caudal anterior cingulate	0.18	0.04
R caudal middle frontal gyrus	0.06	0.03
R paracentral	0.08	0.03
R precentral	0.07	0.03
R superior parietal lobule	0.06	0.03

Table 2.4: **Group differences in nodal efficiency, Norwood status.** List of vertices for which vertex nodal efficiency was significantly different ($p < 0.05$) between groups. Group differences greater than 0 indicate higher values in the non-Norwood group compared to the Norwood group. L: left; R: right

nodal efficiency was greater in the “Closed” group than in the “Open” group, and blue vertices are those with the opposite relation. Table 2.6 lists the vertices, the observed group difference, and the permutation P-values. Group differences in betweenness centrality are shown in Figure 2.14. Red vertices are those in which betweenness centrality was greater in the “Closed” group than in the “Open” group, and blue vertices are those with the opposite relation. Table 2.7 lists the vertices, the observed group difference, and the permutation P-values.

Age at first operation

Finally, the Fontan group was separated into patients who had their first operation as neonates and those who had their first operation after the neonatal period. Based on

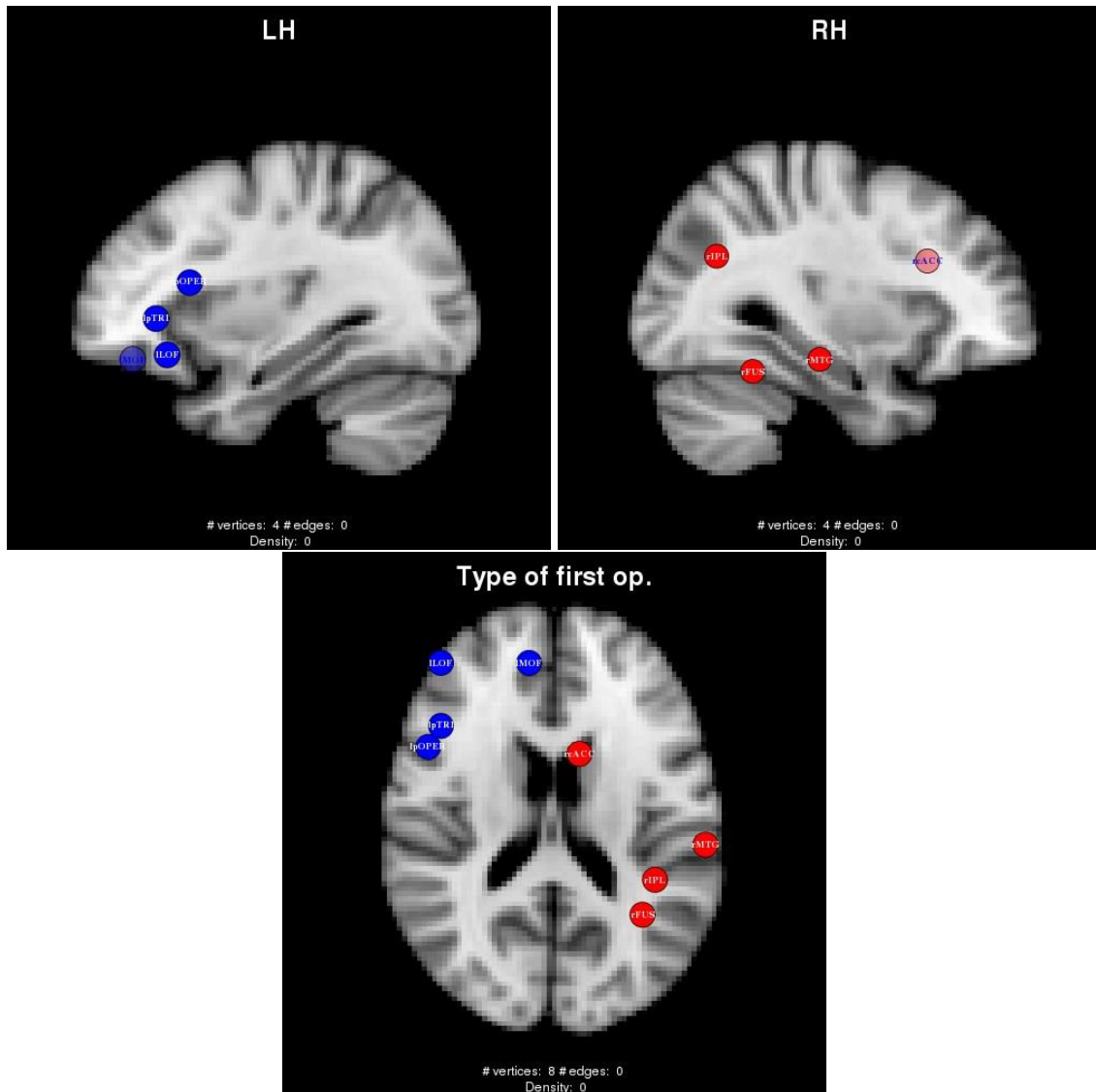


Figure 2.13: **Vertices with significant between-group differences in nodal efficiency, type of first operation.** Significance was determined by permutation testing ($N = 5,000$). Blue vertices are those in which nodal efficiency is greater in the Open group compared to the Closed group, and red vertices are those in which nodal efficiency is greater in the Closed group than the Open group.

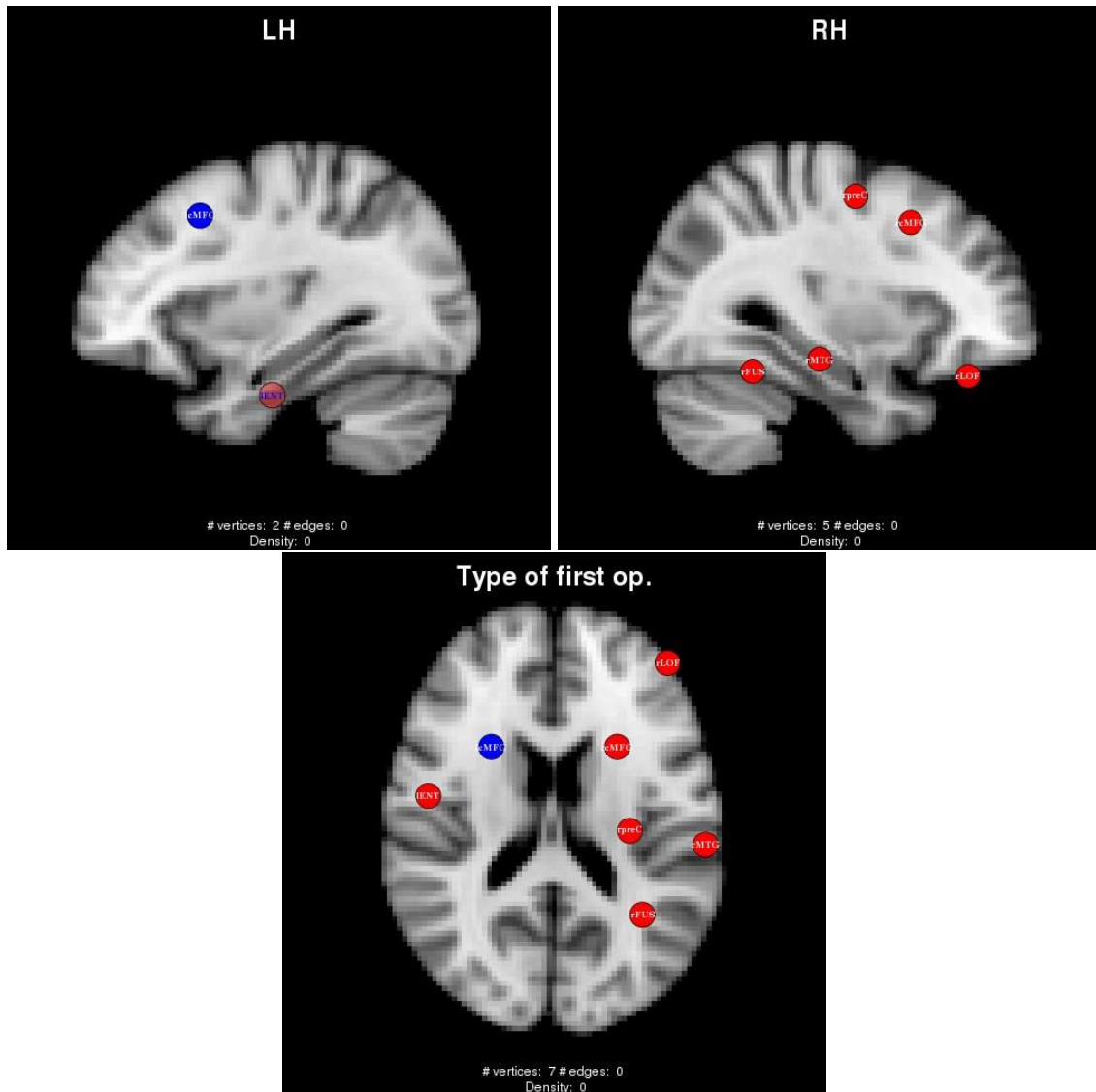


Figure 2.14: **Vertices with significant between-group differences in betweenness centrality, type of first operation.** Significance was determined by permutation testing ($N = 5,000$). Blue vertices are those in which betweenness centrality is greater in the Open group compared to the Closed group, and red vertices are those in which betweenness centrality is greater in the Closed group than the Open group.

Region	Group diff	P-value
L entorhinal	22.07	0.004
L pericalcarine	30.93	0.003
L superior frontal gyrus	28.26	0.04
R caudal middle frontal gyrus	36.12	< 0.001
R fusiform	20.58	0.02
R inferior temporal gyrus	21.57	0.04
R lateral orbitofrontal	27.24	0.008
R middle temporal gyrus	27.71	0.02
R precentral	31.86	0.004

Table 2.5: **Group differences in betweenness centrality, Norwood status.** List of vertices for which vertex betweenness centrality was significantly different ($p < 0.05$) between groups. Group differences greater than 0 indicate higher values in the non-Norwood group compared to the Norwood group. L: left; R: right

permutation testing (5,000 permutations), there were no group differences in the AUC for any global graph measures. Group differences in nodal efficiency are shown in Figure 2.15. Red vertices are those in which nodal efficiency was greater in the non-neonate group than in the neonate group, and blue vertices are those with the opposite relation. Table 2.8 lists the vertices, the observed group difference, and the permutation P-values. Group differences in betweenness centrality are shown in Figure 2.16. Red vertices are those in which betweenness centrality was greater in the non-neonate group than in the neonate group, and blue vertices are those with the opposite relation. Table 2.9 lists the vertices, the observed group difference, and the permutation P-values.

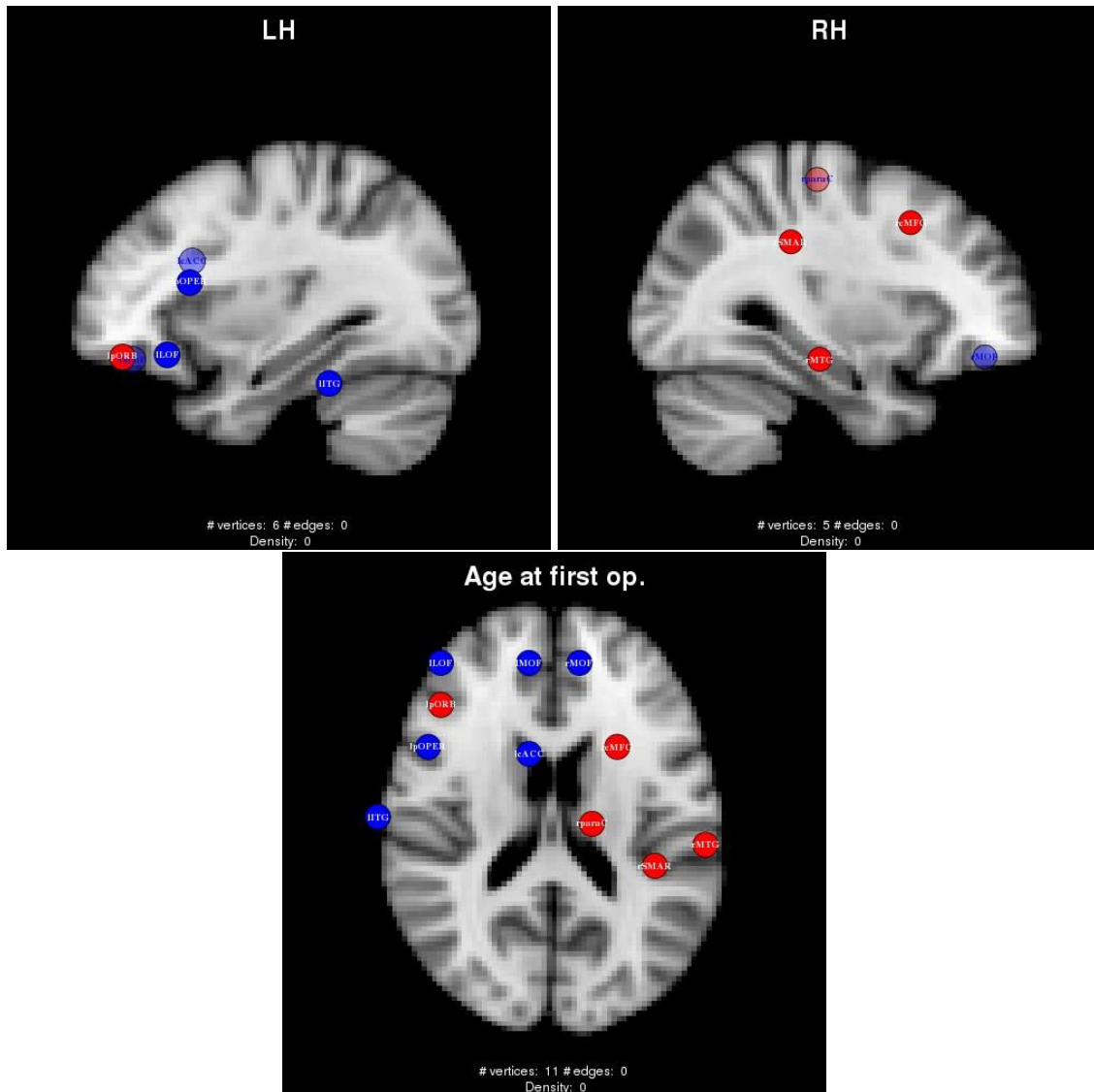


Figure 2.15: **Vertices with significant between-group differences in nodal efficiency, age at first operation.** Significance was determined by permutation testing ($N = 5,000$). Blue vertices are those in which nodal efficiency is greater in the Neonate group compared to the non-Neonate group, and red vertices are those in which nodal efficiency is greater in the non-Neonate group than the Neonate group.

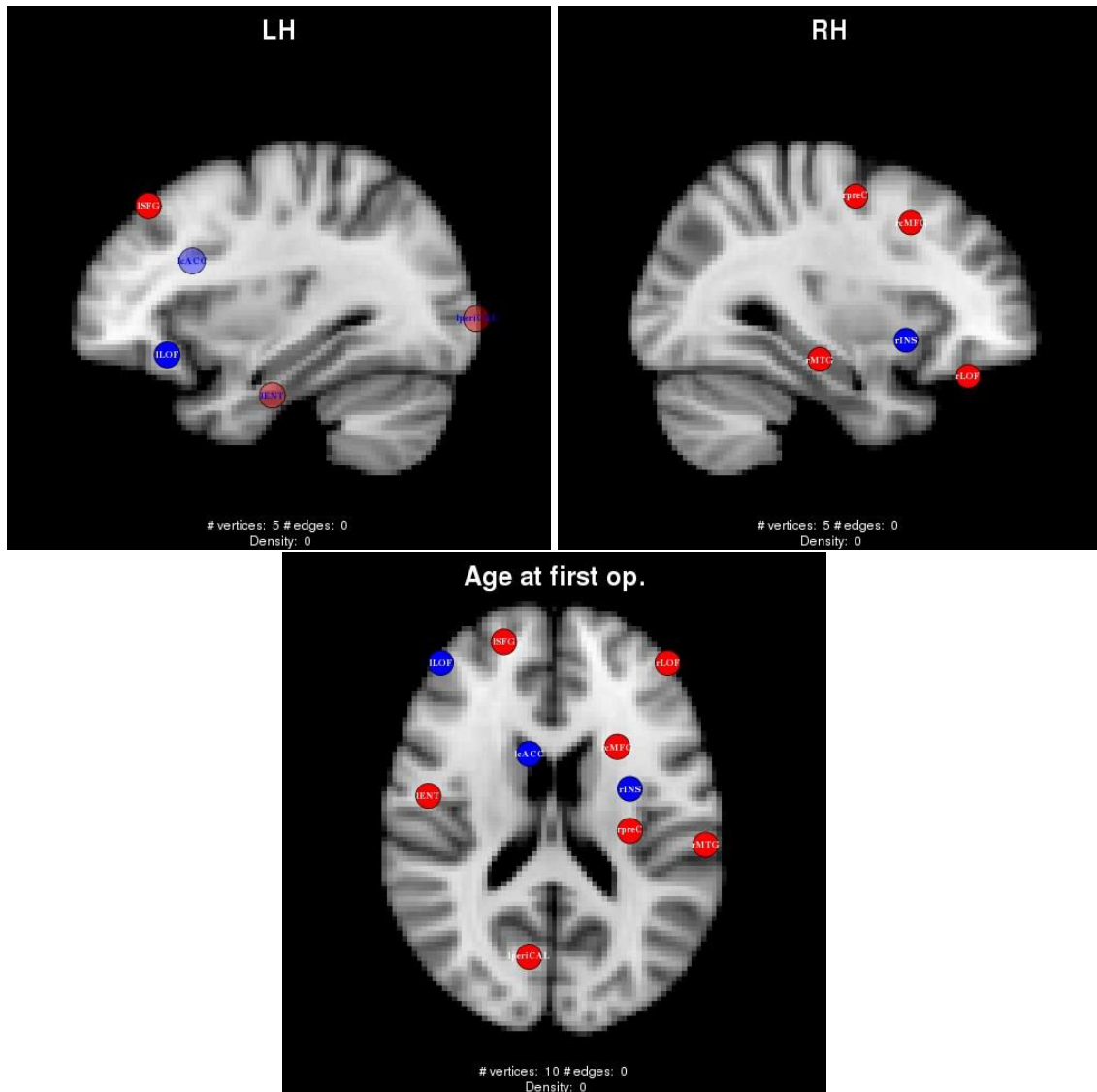


Figure 2.16: **Vertices with significant between-group differences in betweenness centrality, age at first operation.** Significance was determined by permutation testing ($N = 5,000$). Blue vertices are those in which betweenness centrality is greater in the Neonate group compared to the non-Neonate group, and red vertices are those in which betweenness centrality is greater in the non-Neonate group than the Neonate group.

Region	Group diff	P-value
L lateral orbitofrontal	-0.06	0.03
L medial orbitofrontal	-0.10	0.01
L pars opercularis	-0.11	0.002
L pars triangularis	-0.07	0.02
R caudal anterior cingulate	0.13	0.03
R fusiform	0.07	0.04
R inferior parietal lobule	0.04	0.04
R middle temporal gyrus	0.05	0.01

Table 2.6: **Group differences in nodal efficiency, type of first operation.** List of vertices for which vertex nodal efficiency was significantly different ($p < 0.05$) between groups. Group differences greater than 0 indicate higher values in the Closed group compared to the Open group. L: left; R: right

Region	Group diff	P-value
L caudal middle frontal gyrus	-13.48	0.04
L entorhinal	11.98	0.03
R caudal middle frontal gyrus	28.55	< 0.001
R fusiform	18.26	0.02
R lateral orbitofrontal	23.57	0.005
R middle temporal gyrus	22.85	0.02
R precentral	20.71	0.01

Table 2.7: **Group differences in betweenness centrality, type of first operation.** List of vertices for which vertex betweenness centrality was significantly different ($p < 0.05$) between groups. Group differences greater than 0 indicate higher values in the Closed group compared to the Open group. L: left; R: right

Region	Group diff	P-value
L caudal anterior cingulate	-0.15	0.008
L inferior temporal gyrus	-0.09	0.003
L lateral orbitofrontal	-0.13	< 0.001
L medial orbitofrontal	-0.14	0.003
L pars opercularis	-0.12	0.005
L pars orbitalis	0.12	0.02
R caudal middle frontal gyrus	0.14	< 0.001
R medial orbitofrontal	-0.10	0.03
R middle temporal gyrus	0.06	0.008
R paracentral	0.08	0.02
R supramarginal gyrus	0.04	0.04

Table 2.8: **Group differences in nodal efficiency, age at first operation.** List of vertices for which vertex nodal efficiency was significantly different ($p < 0.05$) between groups. Group differences greater than 0 indicate higher values in the non-Neonate group compared to the neonate group. L: left; R: right

Region	Group diff	P-value
L caudal anterior cingulate	-27.21	0.02
L entorhinal	13.86	0.03
L lateral orbitofrontal	-29.24	0.02
L pericalcarine	27.83	0.004
L superior frontal gyrus	26.12	0.03
R caudal middle frontal gyrus	32.26	0.004
R lateral orbitofrontal	24.11	0.02
R middle temporal gyrus	30.27	0.02
R precentral	20.26	0.04
R insula	-32.49	0.01

Table 2.9: **Group differences in betweenness centrality, age at first operation.** List of vertices for which vertex betweenness centrality was significantly different ($p < 0.05$) between groups. Group differences greater than 0 indicate higher values in the non-Neonate group compared to the neonate group. L: left; R: right

Discussion

This is the first study of brain gray matter (GM) networks based on cortical thickness covariance in post-Fontan children and adolescents with single ventricle (SV) heart defects. We report differences in several aspects of brain network organization in the Fontan group compared to a control group. Globally, the control network had a significant rightward asymmetry in connectivity pattern. At the vertex (i.e., regional) level, several regions were consistently determined to be *hubs* in the control group, with a different pattern of regions classified as hubs in the Fontan group. Furthermore, several regions in the right hemisphere had higher efficiency in the control group, and in both hemispheres several regions had higher betweenness centrality. Within the Fontan group, patients who had their first operation as neonates showed several regions of reduced vertex degree, nodal efficiency, and betweenness centrality, compared to patients with initial surgery as non-neonates. Also, Fontan patients with an open first operation showed differences in the same vertex measures compared to patients with a closed first operation. Similarly, patients who did not have a Norwood procedure had higher betweenness in several regions, and a mixture of higher or lower nodal efficiency compared to patients who did have a Norwood procedure. These results suggest that having an initial surgery in the neonatal period and undergoing the Norwood are associated with altered brain development even into adolescence. However, our study is not designed to determine causality, calling for careful interpretation of these results.

Although this is the first investigation of GM covariance networks in pre-teenage and adolescent children with SV, we have previously carried out similar analyses in

adolescents with d-transposition of the great arteries (d-TGA) (Watson et al., manuscript under review). In that patient group, we also found a significant rightward asymmetry in addition to different hub distribution between groups. Network hubs are by definition important (in a network context) as they represent those regions that lie on a large proportion of shortest paths between pairs of other region. Based on a meta-analysis of white matter (WM) connectivity data, hubs have been shown to be involved in a multitude of brain disorders such that lesions are more likely to affect hub regions (Crossley et al., 2014). While SV is not characterized specifically by such gross pathology (compared to, for example, Alzheimer's disease), it is possible that the altered hub distributions we see in SV patients is representative of altered brain structure at the microscopic level. Cortical thickness asymmetry is common across development, with more rightward asymmetry seen frontally and leftward asymmetry seen in posterior regions (Zhou et al., 2013). A longitudinal study of healthy and ADHD children and adolescents showed that the frontal rightward asymmetry was disrupted in the ADHD group (Shaw et al., 2009). The Fontan group has a high proportion of children diagnosed with ADHD, and the observed lack of asymmetry, coupled with Shaw et al.'s (2009) finding of a lack of increased right frontal thickness, point to an association between right hemispheric cortical thickness and ADHD. Our results add to a growing body of work indicating that the structural brain differences seen *in utero* and in the neonatal period do not necessarily normalize as patients near the end of development and persist in a broad distribution.

Longstanding differences in brain GM seen in adolescence may derive from *in utero* experience (Volpe, 2014). Using MRI and cranial ultrasound as early as 18 weeks gestation, CHD fetuses—including those with hypoplastic left heart syndrome (HLHS)—were consistently shown to have smaller head circumference (Hinton et al., 2008; Williams et al., 2015), increased prevalence of brain abnormalities (Brossard-Racine et al., 2014; Mlczoch et al., 2013), lower total brain volumes (Clouchoux et al., 2013; Limperopoulos et al., 2010; Sun et al., 2015), and white matter abnormalities (Brossard-Racine et al., 2014; Hinton et al., 2008). Growth rates in head circumference (Williams et al., 2015), cerebral total, gray, and white matter volumes (Clouchoux et al., 2013; Licht et al., 2009; Zeng et al., 2015b), and brain metabolic biomarkers (Limperopoulos et al., 2010) are slower for CHD fetuses relative to controls. Importantly, Sun et al. (2015) found that brain size at 36 weeks gestation correlates positively with both ascending aortic oxygen saturation and cerebral oxygen volume, suggesting that chronic hypoxia *in utero* is a major contributor to these developmental brain differences (Sun et al., 2015).

Brain abnormalities present in preoperative studies are often exacerbated after neonatal heart surgery, particularly WM injury (Andropoulos et al., 2010; Beca et al., 2013; Dent et al., 2006; Mahle et al., 2002). Indeed, infants with CHD have brain immaturity similar to that of preterm infants: the WM injury that often manifests in preterm infants, periventricular leukomalacia (PVL), has also been reported in CHD infants and suspected to be caused by hypoxic-ischemic damage (Galli et al., 2004; Volpe, 2009). Although PVL is specific to WM, it can trigger consequent neuronal death

and disruption of thalamocortical connectivity (Inder et al., 1999; Leviton and Gressens, 2007; McQuillen and Ferriero, 2005). Young adults born premature have demonstrated altered GM covariance in frontal, temporal, and parietal lobes, along with lower clustering coefficient compared to term-born young adults (Scheinost et al., 2015). Taken together, the GM differences we show in children and adolescents with SV could be related to *in utero* and perinatal/perioperative WM injury with consequent GM disruption through Wallerian degeneration and its effects on developing cortical circuits (Volpe, 2014).

Analysis of subgroups within the Fontan cohort revealed lower graph measures in the Norwood subgroup, in the subgroup who had an “open” first operation, and in the subgroup who had the first operation in the neonatal period. The Norwood operation was initially introduced to palliate HLHS (Norwood et al., 1980), a patient group often associated with poorer neurodevelopmental outcomes, more delayed brain development, and a higher incidence of perioperative WM injury (Andropoulos et al., 2010; Wernovsky et al., 2000). As nearly two-thirds of our Norwood subgroup were diagnosed with HLHS, our findings would suggest that brain development in HLHS patients continues to differ from other SV types even into adolescence. Time to surgery has been shown to be a factor in HLHS neonates, such that a later surgery was associated with increased frequency or worsened postoperative PVL (Lynch et al., 2014). This finding is opposite to ours; however, Lynch et al. (2014) studied only HLHS neonates (no other SV subtypes), and the range of age at first surgery was only one to seven days (compared to

our stratification into neonates and non-neonates). Further investigation is required to explore the effects of surgical timing on long-term development.

This study has some limitations. We were unable to scan all subjects on a 3T MRI due to the lack of safety data for some of the implanted cardiac coils. As a result, a higher percentage of Fontan patients were scanned on a 1.5T MRI compared to controls; therefore, we adjusted for this factor in our statistical analyses (Han et al., 2006; Pardoe et al., 2008; Stonnington et al., 2008). Although age at MRI was not different between groups, the age range of all subjects was relatively wide (10 to 19 years). Brain development continues throughout this period, even into the third decade (Giedd, 2004). Although we included subject age as a covariate in our analyses, it is possible that there is a nonlinear relationship that we did not capture. Third, the date of Fontan procedure spanned many years, the majority from 1995-2003, and was not performed at the same center for all patients. While this does not limit our findings in terms of tertiary care center or surgeon, there may be increased associated variability not captured. Although the patient group comprises only those with a diagnosis of SV who underwent the Fontan procedure, there were multiple diagnoses (e.g., HLHS, tricuspid atresia, double outlet right ventricle, heterotaxy, etc.) with differing number of patients in each sub-group. As such, our results may not directly apply to any one SV anatomic group. Finally, this article only reports the results of networks created from cortical thickness covariance, which can only be considered an indirect and incomplete measure of brain structural connectivity. Other analyses of this cohort will use DTI tractography to assess connectivity based on white matter structure.

Conclusions

In conclusion, children and adolescents with SV heart defects who have undergone the Fontan procedure continue to show differences in brain structure, here measured by cortical thickness covariance networks. Within the Fontan group, there are global and regional differences in connectivity associated with the initial procedure and the time in early life at which this procedure is performed. These results highlight the importance of early-life brain development, and future analyses will assess the relationship between brain network structure and cognitive and behavioral function.

GRAPH THEORY ANALYSIS OF WHITE MATTER NETWORKS IN POST-FONTAN CHILDREN AND ADOLESCENTS

Introduction

Single ventricle (SV) heart defects are among the most severe types of congenital heart disease (CHD) (Hoffman and Kaplan, 2002; Moons et al., 2005). Since the introduction of the Fontan procedure in the 1970's and the Norwood procedure in the 1980's, post-surgical survival of SV patients has been increasing over time, even for more complex forms such as hypoplastic left heart syndrome (HLHS) (Coats et al., 2014; Fontan and Baudet, 1971; Khairy et al., 2010; Norwood et al., 1980; O'Leary, 2002; Oster et al., 2013; Raissadati et al., 2015). This decrease in early mortality has resulted in an aging CHD population, allowing for more extensive study of SV patients beyond early childhood (Marelli et al., 2007). Many studies of SV patients have focused on neurodevelopmental and health status, reporting deficits in many areas of cognition, along with a high rate of learning disability and behavioral problems; these issues continue to be present into adolescence (Bellinger et al., 2015; Longmuir et al., 2012; Mahle et al., 2000; Shillingford et al., 2008; Sugimoto et al., 2013; Wernovsky et al., 2000).

Delayed brain development and white matter (WM) injury are common in SV patients and are detectable as early as the fetal period (Clouchoux et al., 2013; Glauser et al., 1990; Goff et al., 2014; Hinton et al., 2008; Kaltman et al., 2005; Licht et al., 2009; Limperopoulos et al., 2010). Brain structure in SV patients tends to differ from those in

other types of CHD and may arise from the different hemodynamic profile associated with having a SV defect (Berg et al., 2009; Hahn et al., 2015; Ibuki et al., 2012; Lynch et al., 2014; Rosenthal, 1996; Sethi et al., 2013). The brain injury seen in autopsy and fetal imaging studies can persist after surgery, and many patients show signs of new and more extensive WM injury in the postoperative period compared to the preoperative period (Andropoulos et al., 2010; Block et al., 2010; Dent et al., 2006; Dimitropoulos et al., 2013; Mahle et al., 2002). Neuroimaging study of SV patients beyond infancy has been rare, but shows brain abnormalities in many at ages ranging from 3 to 8 years (Goldberg et al., 2000; Sarajuuri et al., 2012, 2007). In the current cohort of post-Fontan patients (undergoing MRI between 10 and 19 years of age), we showed an increased prevalence of gross anatomic brain abnormalities, in addition to multiple areas of reduced cortical thickness and cortical and subcortical gray matter volume spanning all major lobes of the brain (Watson et al., manuscript under review). Furthermore, WM microstructure, measured with diffusion tensor imaging (DTI), is altered and shows a pattern suggestive of early hypoxic-ischemic injury (Watson et al., manuscript in preparation). This same cohort also demonstrated impairment in multiple areas of neurodevelopment, results which have been found in other SV cohorts (Bellinger et al., 2015). Although there is an abundance of neurodevelopmental data in post-Fontan children and adolescents, no study has performed detailed analysis of brain WM connectivity.

DTI tractography is an *in vivo*, non-invasive method of mapping WM structural connectivity in the human brain (Hagmann et al., 2008, 2007; Iturria-Medina et al., 2008).

Taking a graph theoretical approach treats the brain as a *network*, and allows for investigation of global and regional topology (Rubinov and Sporns, 2010). Exploring the structural brain network moves beyond traditional analyses of brain regions as isolated units, and can be particularly useful in brain disorders thought to arise from reductions in connectivity, such as schizophrenia, Alzheimer's disease, 22q11.2 deletion syndrome, and depression (Bohlken et al., 2016; Crossley et al., 2014; Qin et al., 2014; Vasa et al., 2016). In adolescents with d-transposition of the great arteries (d-TGA), we previously showed alterations in integration and segregation of the patient group's network, and that these topological changes mediated cognitive function in domains that CHD patients are known to have deficits in (Panigrahy et al., 2015). Although informative, the d-TGA group was homogeneous in regards to age at surgery and type of heart defect. Consequently, the findings in children with d-TGA are not necessarily applicable to a more varied CHD patient group.

We acquired DTI data to complement our prior analysis of gray matter networks and to compare features of WM structural connectivity between post-Fontan SV patients with healthy control children and adolescents. Second, we examined associations between perioperative and medical history characteristics and measures of network integration, segregation, and efficiency. In particular, we made further group comparisons by dividing the Fontan subjects into patients who underwent the Norwood procedure as their first operation and those who did not, patients who were neonates

during their first operation, and explored the effect of operative complications on the WM network.

Methods

Subjects

Details of subject recruitment and inclusion/exclusion criteria are presented in Chapter 2 (“Graph theory analysis of gray matter networks in post-Fontan children and adolescents”).

MRI acquisition

Subjects were scanned on either a GE 3 Tesla (T) or 1.5T system (General Electric, Milwaukee, WI) with an eight-channel head coil at Beth Israel Deaconess Medical Center. The DTI sequence was acquired using single-shot spin-echo echo planar imaging with parameters: TR/TE = 15000/84 ms, flip angle = 90°, acquisition matrix = 96 x 96, FOV = 240mm, slice thickness = 2.5mm, with resultant voxel size = 2.5 x 2.5 x 2.5 mm³. A single non-diffusion weighted volume was acquired ($b = 0$ s / mm²), and 25 diffusion-weighted volumes ($b = 1,000$ s / mm²).

DTI preprocessing and tractography

All DTI image processing was performed with *FSL v5.0.6* and the *FSL Diffusion Toolbox (FDT)* (Smith et al., 2004). All of the following steps were applied to each subject. First, eddy-current correction was performed to correct for image distortions and head motion. Next, the diffusion tensor was calculated at every voxel using the tool *dtifit*. Distributions of diffusion parameters were calculated at every voxel using the tool

bedpostx with default parameters (Behrens et al., 2007, 2003; Jbabdi et al., 2007). Finally, probabilistic tractography was performed with the tool *probtrackx2*. Fiber tracking was initiated from 76 regions of the *DKT* atlas (62 cortical and 14 subcortical regions) (Klein and Tourville, 2012). For each voxel, 5,000 samples were drawn from the probability distribution of the principle fiber direction; each step in the process was 0.5 mm, and tracking stopped after a maximum of 2,000 steps. All other parameters used were default parameters.

Network construction

All statistics were performed in R version 3.3.0 (2016-05-03), using functions in the packages *igraph* v1.1.0 and *brainGraph* (Csardi and Nepusz, 2006; Kolaczyk and Csardi, 2014; R Core Team, 2015). For each subject, a connectivity matrix A was obtained from the probabilistic tractography procedure described above. The matrices for all subjects were combined into a multidimensional array, such that each element $A(i, j, k)$ equals the number of *streamlines* (i.e., fibers that connect two regions) between regions of interest (ROIs) i and j for subject k . A series of operations were performed on these matrices to remove spurious connections.

First, streamline counts were adjusted for ROI size (as pairs of larger brain regions will tend towards higher streamline counts by virtue of being a larger target) by dividing each matrix entry by the average volume of the ROI pairs, i.e.,

$$A_{norm}(i, j, k) = \frac{A(i, j, k)}{5000 \times 0.5 (V_i(k) + V_j(k))}$$

where $A(i, j, k)$ is the original streamline count, $V_i(k)$ and $V_j(k)$ are the volumes of ROI's i and j , and 5,000 is the number of samples per voxel (from the tractography algorithm) (Gong et al., 2009; Hagmann et al., 2008). Next, a range of thresholds x from 0.001 - 0.105 (step size of 0.01) were applied at the individual level to remove the lowest streamline counts (i.e., entries less than that threshold were changed to 0). These values were chosen empirically and resulted in a range of densities similar to the literature (range: 3.3 - 24.7 %) (Gong et al., 2009; Hagmann et al., 2008). This resulted in a set of 11 connectivity matrices $A_{thr}(k)$ per subject k . Mathematically,

$$A_{thr}(i, j, k) = \begin{cases} A_{norm}(i, j, k), & A_{norm}(i, j, k) \geq x \forall x \\ 0, & A_{norm}(i, j, k) < x \forall x \end{cases}$$

A second threshold was applied, again at the individual subject level but using information from the entire group, by keeping only those entries which were present in at least 50% of subjects per group (similar results were obtained when using the entire sample; data not shown). This was applied separately for each group. Mathematically,

$$A_{final}(i, j, k) = \begin{cases} A_{thr}(i, j, k), & \sum_k I(A_{thr}(i, j, k)) \geq 0.5 \times N_k \\ 0, & \sum_k I(A_{thr}(i, j, k)) < 0.5 \times N_k \end{cases}$$

where I is an indicator function which equals 1 if its argument is greater than 0, and equals 0 otherwise; and N_k is the group size of subject k . This group threshold (50%) is within the optimal range determined by a previous report, and was chosen to balance the number of false positive and false negative structural connections (de Reus and van den Heuvel, 2013a). Finally, group-averaged connectivity matrices were calculated by taking

the mean across subjects for each group and each threshold. In sum, there are 15 connectivity matrices per subject, in addition to the 30 group-averaged connection matrices. Edge weights for all matrices are streamline counts normalized by average ROI-pair volumes.

Group differences in global- and vertex-level measures

Group differences in global measures were assessed by Wilcoxon rank sum tests across thresholds. P-values were adjusted using the false discovery rate (FDR), and differences were considered significant if $p_{FDR} < 0.05$.

Group differences in vertex-level measures were assessed by specifying a general linear model (GLM) at each vertex, in which the response variable was the vertex measure of interest, and predictors were age, sex, scanner (1.5T or 3T), and group membership. Next, permutation testing was performed in a procedure similar to that used in the randomise tool from FSL (Nichols and Holmes, 2002). The set of subject graphs was permuted such that each subject was randomly assigned to one of the two subject groups, creating two groups with sample sizes matching the original data. The maximum t-statistic for the *group* predictor variable (calculated from the GLM) across vertices was recorded; 10,000 permutations were performed. The permutation P-value was calculated directly as the number of times the maximum t-statistic in the permutation set exceeded the observed maximum t-statistic, divided by the number of permutations, i.e.,

$$p_{perm} = \frac{1 + \sum_i t_{perm}(i) \geq t_{obs}}{1 + N}$$

where $t_{perm}(i)$ is the i -th t-statistic from the permutation distribution, t_{obs} is the observed maximum t-statistic, and N is the number of permutations (here, $N = 10,000$) (Phipson and Smyth, 2010). Vertex differences were considered significant if $p_{perm} < 0.05$. This procedure provides control over the family-wise error rate (see Nichols and Holmes (2002)).

The *strength* s_i of vertex i is the sum of the edge weights of all adjacent edges to that vertex:

$$s_i = \sum_j A_{ij} W_{ij}$$

where W_{ij} is the matrix of edge weights. The *shortest path length* l_i of vertex i is

$$l_i = \frac{1}{n-1} \sum_{j \neq i} d_{ij}$$

where n is the number of vertices in the graph and d_{ij} is the length of a geodesic path between vertices i and j (Newman, 2010). Nodal efficiency is defined in Chapter 2.

Network-based statistic

To determine group differences in overall connectivity, the *network-based statistic (NBS)* method was employed (Zalesky et al., 2010a). This method allows for familywise error control of network data that is analogous to cluster-based thresholding in the functional MRI literature. To calculate the NBS, first a GLM adjusting for age at MRI, sex, and scanner field strength was specified for each element of the $N \times N$ connectivity matrix (i.e., the matrices thresholded by ROI size). A matrix of t-statistics

associated with the *Group* predictor was thresholded by an initial P-value threshold (here, $p < 0.001$). A graph was then created from this matrix, and the largest connected component recorded. Next, the data were permuted 10,000 times, in which each subject was randomly assigned to one of two groups (of equal size as the original Fontan and control groups). The same GLM was again specified at every matrix entry, a t-statistic matrix calculated and thresholded (again by $p < 0.001$), and the largest connected component was recorded for each permutation. The null distribution of largest connected component sizes was used to calculate a P-value associated with the connected components of the observed data (as the proportion of times the permutation component sizes exceeded the observed size).

Demographic and medical history variables

Demographic variables included socioeconomic status (measured by the Hollingshead Four-Factor Index of Socioeconomic Status) (Hollingshead et al., 1975), birth weight, gestational age (GA) at birth, and race. Surgical history variables related to the first operation were investigated as potential predictor variables in general linear model (GLM) analyses. These included: Norwood status (“Norwood” or “non-Norwood”), age at first operation (“neonate” or “non-neonate”), type of first operation (“open” or “closed”), number of complications during the first operation, and DHCA and total support time (in minutes). Medical history variables included: history of any seizures, and history of any neurologic event (stroke, seizure, choreoathetosis, and meningitis). In between-group comparisons of demographic variables, P-values were

calculated by Fisher's exact test for categorical variables and Wilcoxon rank sum test for continuous variables, with significance at a level of $p < 0.05$. In the GLM analyses of between-group differences in global- and vertex-level graph measures, age at MRI, sex, and MRI field strength were included as covariates. Associations were considered significant if $p < 0.01$.

Results

Subjects

A total of 112 Fontan subjects and 44 control subjects were included in the analysis. The number of subjects with unacceptable data due to motion artifact did not differ between groups (18/129 in the Fontan group, and 4/48 in the control group; Fisher's exact test P-value = 0.44). Subject demographics and education history are summarized in Table 3.1. Fontan subjects were significantly more likely than controls to be scanned at 1.5T ($p = 0.007$), social class was significantly lower in the Fontan group than controls ($p = 0.04$), and NYHA class was significantly greater (i.e., more limitation in ordinary physical activity) in the Fontan group than controls ($p < 0.0001$). For education history, the Fontan group had significantly greater numbers for all variables (tutoring, grade retention, early intervention, occupational therapy, physical therapy, special education, psychotherapy and counseling, and any special services; all $p < 0.01$).

Global graph measures

The control group had significantly higher network density at each threshold, both at the single-subject and group levels. Figure 3.1 shows several graph-level

measures plotted against threshold. The control group had significantly higher strength, global efficiency (weighted and unweighted), and local efficiency (weighted and unweighted) than the Fontan group at most or all thresholds. The Fontan group had significantly higher characteristic path length and modularity (weighted and unweighted) at most or all thresholds.

Vertex-level differences

Figure 3.2 shows a graph containing only vertices with significantly higher *strength* in the control group compared to the Fontan group ($p < 0.05$, based on permutation testing). Vertex and edge color are based on lobe membership. There were no vertices in which strength was significantly higher in the Fontan group. A table listing the average group difference in vertex strength, the parameter estimate (β), standard error of the parameter estimate, t-statistic, and P-value for all vertices is shown in Table 3.2.

Similarly, Figure 3.3 shows a graph containing only vertices with significantly higher *weighted nodal efficiency* in the control group compared to the Fontan group ($p < 0.05$). There were no vertices in which weighted nodal efficiency was higher in the Fontan group. The tables of group differences, parameter estimates, standard errors, t-statistics, and associated P-values are in Table 3.3 (left hemisphere) and Table 3.4 (right hemisphere).

Figure 3.4 shows a graph containing only vertices with significantly lower *weighted shortest path length* in the control group compared to the Fontan group ($p < 0.05$). There were no vertices in which weighted shortest path length was lower in the

Fontan group. The tables of group differences, parameter estimates, standard errors, t-statistics, and associated P-values are in Table 3.5 (left hemisphere) and Table 3.6 (right hemisphere).

Associations with first operation

Nodal efficiency

Table 3.7 shows the operative variables that were significantly associated with weighted nodal efficiency in the Fontan group. For *type* of first operation, a negative parameter estimate (β) indicates that weighted nodal efficiency was lower in patients with an open first operation compared to those with a closed first operation. For *Norwood*, a negative estimate indicates that weighted nodal efficiency was lower in patients who underwent the Norwood procedure compared to those who did not. The remaining operative variables are numeric, so a negative association indicates a decrease in weighted nodal efficiency with an increase in, for example, number of complications during the initial operation. The most robust findings were associated with Norwood stratification and number of operative complications. The Norwood subgroup had significantly lower weighted nodal efficiency for several brain regions, all located in temporal areas, and predominantly in the left hemisphere (all $p < 0.01$). Figure 3.5 also shows the vertices with a significant association, overlaid on brain slices; red vertices are associated with number of complications in the first operation, blue vertices are associated with Norwood, and green vertices with both.

Local efficiency

Table 3.8 shows the operative variables that were significantly associated with weighted local efficiency in the Fontan group. For *Norwood*, a negative parameter estimate (β) indicates that weighted local efficiency was lower in patients who underwent the Norwood procedure compared to those who had not. And for operative complications, a negative association indicates a decrease in weighted local efficiency with increasing number of complications during the initial operation. Norwood patients had lower weighted local efficiency in the superior temporal gyrus bilaterally. An increasing number of operative complications was associated with lower weighted local efficiency in regions of the right frontal lobe. Figure 3.6 also shows the vertices with a significant association; red vertices are associated with number of complications in the first operation, and blue vertices are associated with Norwood.

Strength

Table 3.9 shows the operative variables that were significantly associated with vertex strength in the Fontan group. For *type* of first operation, a negative parameter estimate (β) indicates that strength was lower in patients with an open first operation compared to those with a closed first operation. For *age* at first operation, a negative parameter estimate indicates that strength was lower in patients who were neonates at first operation compared to those who were older. The remaining operative variables are numeric, so a negative association indicates a decrease in strength with an increase in, for example, DHCA time (in minutes) during the initial operation. None of the operative variables were significantly associated with strength in more than one region, but all

significant associations were located in the temporal lobes (specifically, fusiform and transverse temporal gyri) and insula.

Network-based statistic

Calculation of the network-based statistic revealed 4 connected components with a total of 30 vertices in which the connectivity strength was significantly higher in the control group compared to the Fontan group ($p < 0.05$ for all components). Axial and sagittal views of the vertices and edges in these components is in Figure 3.7. Vertex and edge colors are based on component membership from largest to smallest: red (13 vertices and 13 edges), green (8 vertices and 8 edges), blue (6 vertices and 5 edges), and magenta (3 vertices and 2 edges). These components spanned both hemispheres, and most of the regions involved were in the frontal lobes and subcortical gray matter. The largest (red) component was solely in the left hemisphere, including regions of frontal and temporal lobe, insula, cingulate gyrus, and subcortical gray matter.

	Total (N = 156)	Control (N = 44)	Fontan (N = 112)	P-value
Age at MRI, yr	14.96 ± 2.85	15.59 ± 2.42	14.71 ± 2.98	0.10
Scanner, 1.5T	84 (54)	16 (36)	68 (61)	0.007
Sex, F	65 (42)	19 (43)	46 (41)	0.86
NYHA class	2 (1 – 2)	1 (1 – 1)	2 (1 – 2)	<0.0001
Social class at 16 yr of age†	49.91 ± 12.55	54.26 ± 8.13	48.24 ± 13.54	0.04
Birth weight, kg	3.32 ± 0.62	3.44 ± 0.56	3.28 ± 0.64	0.27
Gestational age, wk	39.08 ± 2.07	39.56 ± 1.18	38.90 ± 2.29	0.26
Race (white)	144 (92)	39 (89)	105 (94)	0.32
Received tutoring	74 (47)	14 (32)	60 (54)	0.02
Held back in school	26 (17)	0 (0)	26 (23)	<0.0001
Early intervention	63 (40)	2 (5)	61 (54)	<0.0001
Occupational therapy	57 (37)	0 (0)	57 (51)	<0.0001
Physical therapy	59 (38)	7 (16)	52 (46)	0.0004
Special education	37 (24)	0 (0)	37 (33)	<0.0001
Psychotherapy and counseling	53 (34)	7 (16)	46 (41)	0.003
Any special services	120 (77)	25 (57)	95 (85)	0.0005

Table 3.1: **Subject demographics and education history.** Values are N (%), mean SD, or median (range). P-values were calculated by Fisher's exact test for categorical variables and Wilcoxon rank sum test for continuous variables. yr: years; T: tesla; L: liters; F: female; NYHA: New York Heart Association; kg: kilograms; wk: weeks. †Score on the Hollingshead Four Factor Index of Social Status; higher scores indicate higher social class

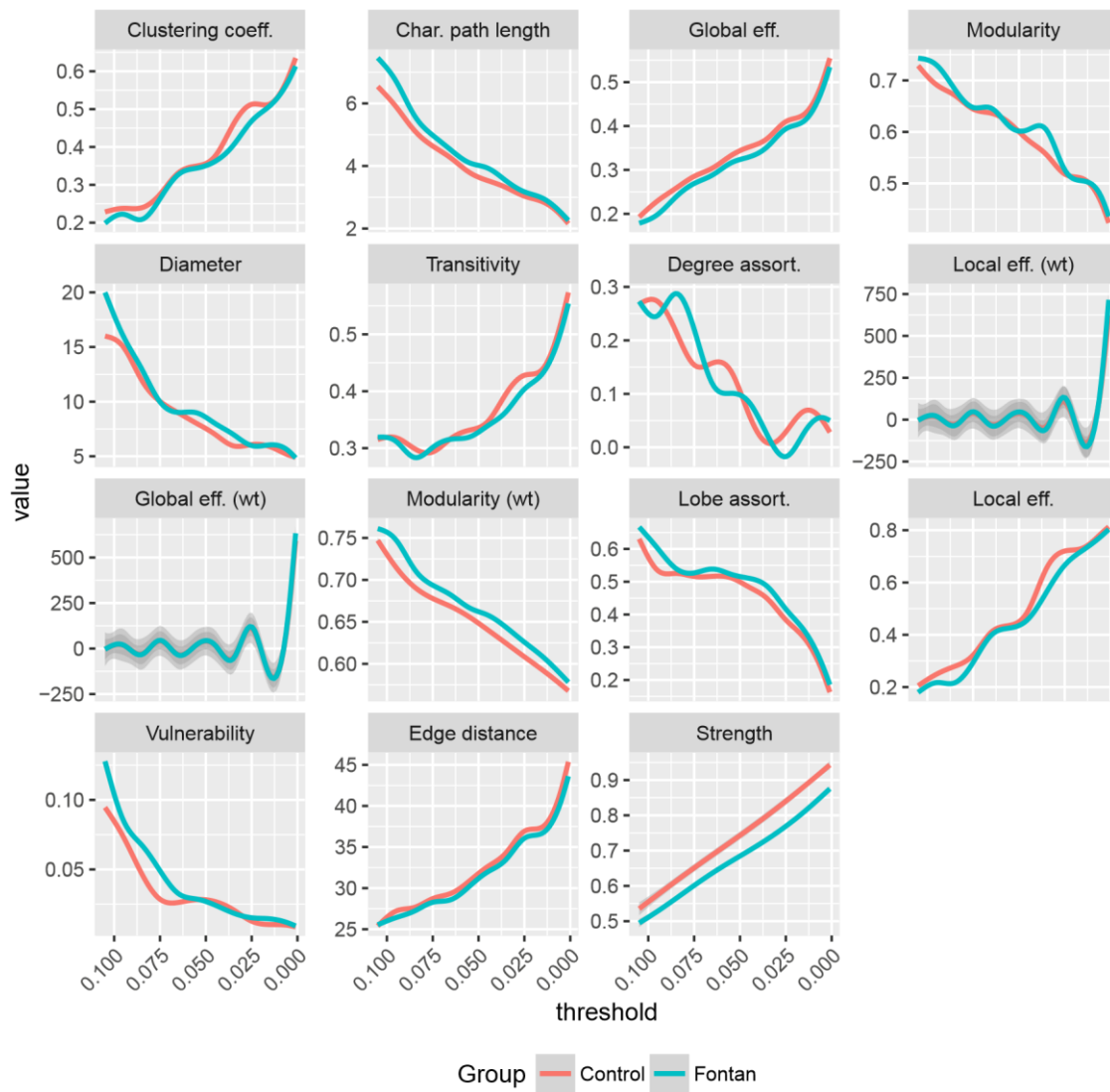


Figure 3.1: **Global network measures across thresholds.** The shaded regions represent the 95% confidence regions obtained via predictions from a generalized additive model. wt: weighted (indicating that the given measure is calculated using edge weights)

Region	Group diff.	β	Std. error	T	P-value
L fusiform	0.17	-0.13	0.02	-7.18	<0.001
L insula	0.19	-0.11	0.03	-4.14	0.001
L superior frontal gyrus	0.10	-0.07	0.01	-6.37	<0.001
L thalamus	0.20	-0.17	0.03	-5.74	<0.001
L caudal anterior cingulate	0.10	-0.07	0.02	-4.63	<0.001
L pars opercularis	0.10	-0.08	0.02	-4.59	<0.001
L rostral middle frontal gyrus	0.17	-0.14	0.02	-7.66	<0.001
R caudate	0.15	-0.12	0.02	-4.99	<0.001
R fusiform	0.12	-0.08	0.01	-5.36	<0.001
R middle temporal gyrus	0.06	-0.05	0.01	-5.95	<0.001
R posterior cingulate cortex	0.07	-0.06	0.02	-3.31	0.03
R precuneus	0.15	-0.13	0.02	-5.27	<0.001
R superior frontal gyrus	0.10	-0.07	0.01	-7.29	<0.001
R thalamus	0.24	-0.20	0.03	-6.69	<0.001
R pericalcarine	0.12	-0.11	0.02	-5.82	<0.001
R rostral middle frontal gyrus	0.10	-0.07	0.02	-3.77	0.006

Table 3.2: Group differences in vertex strength. List of vertices for which vertex strength was significantly different ($p < 0.05$ determined by linear models and permutation testing) between groups. Group differences greater than 0 indicate higher values in the control group compared to Fontans. The β values are parameter estimates for the *Group* predictor, shown along with their associated standard errors, t-statistics, and P-values.

L: left; R: right

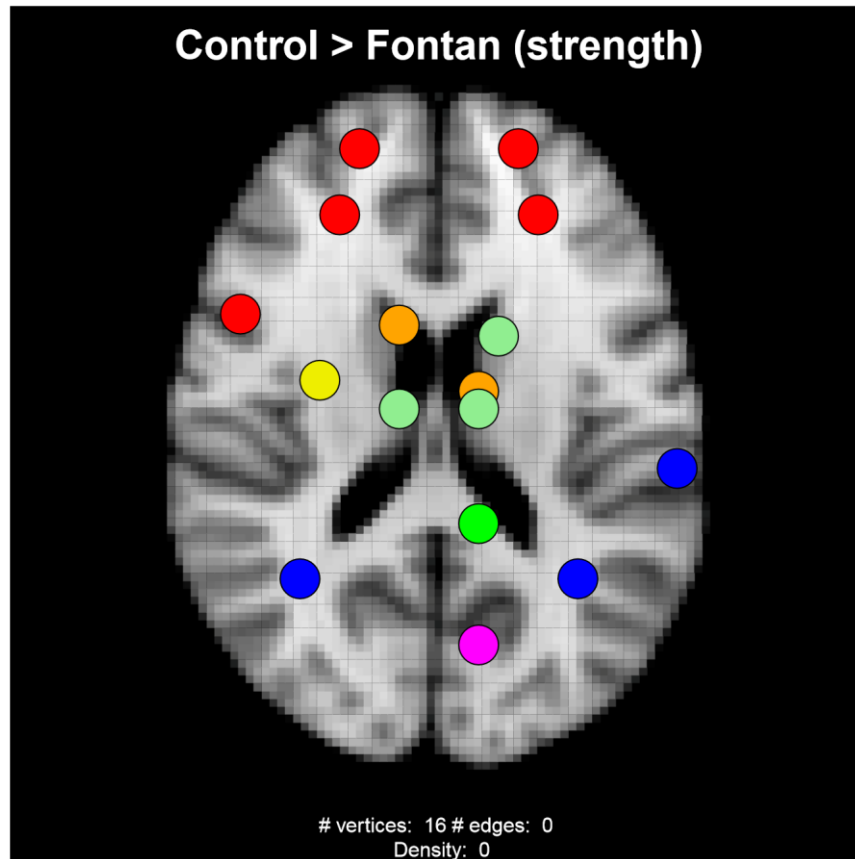


Figure 3.2: **Group differences in vertex strength.** The vertices shown are those which had significantly higher strength in the control group than the Fontan group. Significance was determined by permutation testing; $p < 0.05$. Vertex color corresponds to lobe membership (red: frontal; green: parietal; blue: occipital; yellow: insula; orange: cingulate; light green: subcortical). The left hemisphere is displayed on the left side of the figure.

Region	Group diff.	β	Std. error	T	P-value
L amygdala	0.73	-0.86	0.14	-6.29	<0.001
L entorhinal	0.30	-0.45	0.09	-4.93	<0.001
L fusiform	1.33	-1.64	0.25	-6.49	<0.001
L insula	0.35	-0.59	0.14	-4.26	<0.001
L inferior parietal lobule	0.16	-0.19	0.05	-3.71	0.003
L inferior temporal gyrus	0.13	-0.26	0.09	-2.93	0.04
L lingual	0.10	-0.24	0.07	-3.23	0.01
L lateral orbitofrontal	0.30	-0.57	0.09	-6.19	<0.001
L lateral occipital gyrus	0.41	-0.53	0.07	-7.26	<0.001
L middle temporal gyrus	0.09	-0.14	0.03	-4.64	<0.001
L parahippocampal	0.91	-1.16	0.25	-4.67	<0.001
L putamen	1.32	-1.66	0.30	-5.59	<0.001
L superior frontal gyrus	0.61	-0.80	0.06	-13.42	<0.001
L thalamus	1.81	-1.97	0.17	-11.91	<0.001
L transverse temporal	0.08	-0.22	0.07	-3.33	0.01
L caudal middle frontal gyrus	0.36	-0.50	0.07	-6.90	<0.001
L pars opercularis	0.60	-0.76	0.07	-10.15	<0.001
L pars orbitalis	0.18	-0.36	0.09	-4.14	<0.001
L precentral	0.16	-0.32	0.08	-4.13	<0.001
L rostral anterior cingulate cortex	0.48	-0.66	0.07	-9.81	<0.001
L rostral middle frontal gyrus	0.68	-0.91	0.07	-13.03	<0.001

Table 3.3: **Group differences in vertex weighted nodal efficiency (L)** List of vertices for which vertex weighted nodal efficiency was significantly different ($p < 0.05$ determined by linear models and permutation testing) between groups. Group differences greater than 0 indicate higher values in the control group compared to Fontans. The β values are parameter estimates for the *Group* predictor, shown along with their associated standard errors, t-statistics, and p-values. L: left; R: right

Region	Group diff.	β	Std. error	T	P-value
R amygdala	0.74	-0.93	0.18	-5.32	<0.001
R entorhinal	0.37	-0.52	0.09	-5.74	<0.001
R lateral orbitofrontal	0.22	-0.43	0.09	-4.85	<0.001
R middle temporal gyrus	1.24	-1.33	0.07	-18.33	<0.001
R pallidum	0.48	-0.59	0.11	-5.56	<0.001
R superior frontal gyrus	0.48	-0.65	0.06	-10.98	<0.001
R thalamus	1.74	-1.94	0.19	-9.97	<0.001
R transverse temporal	0.13	-0.23	0.08	-2.93	0.04
R caudal middle frontal gyrus	0.42	-0.55	0.11	-4.85	<0.001
R pars opercularis	0.43	-0.58	0.12	-4.96	<0.001
R pars orbitalis	0.21	-0.34	0.09	-3.91	0.001
R pericalcarine	0.76	-0.85	0.07	-11.63	<0.001
R precentral	0.23	-0.36	0.08	-4.47	<0.001
R rostral anterior cingulate cortex	0.04	-0.21	0.07	-2.84	0.05
R rostral middle frontal gyrus	0.42	-0.58	0.08	-7.33	<0.001

Table 3.4: **Group differences in vertex weighted nodal efficiency (R)** List of vertices for which vertex weighted nodal efficiency was significantly different ($p < 0.05$ determined by linear models and permutation testing) between groups. Group differences greater than 0 indicate higher values in the control group compared to Fontans. The β values are parameter estimates for the *Group* predictor, shown along with their associated standard errors, t-statistics, and p-values. L: left; R: right

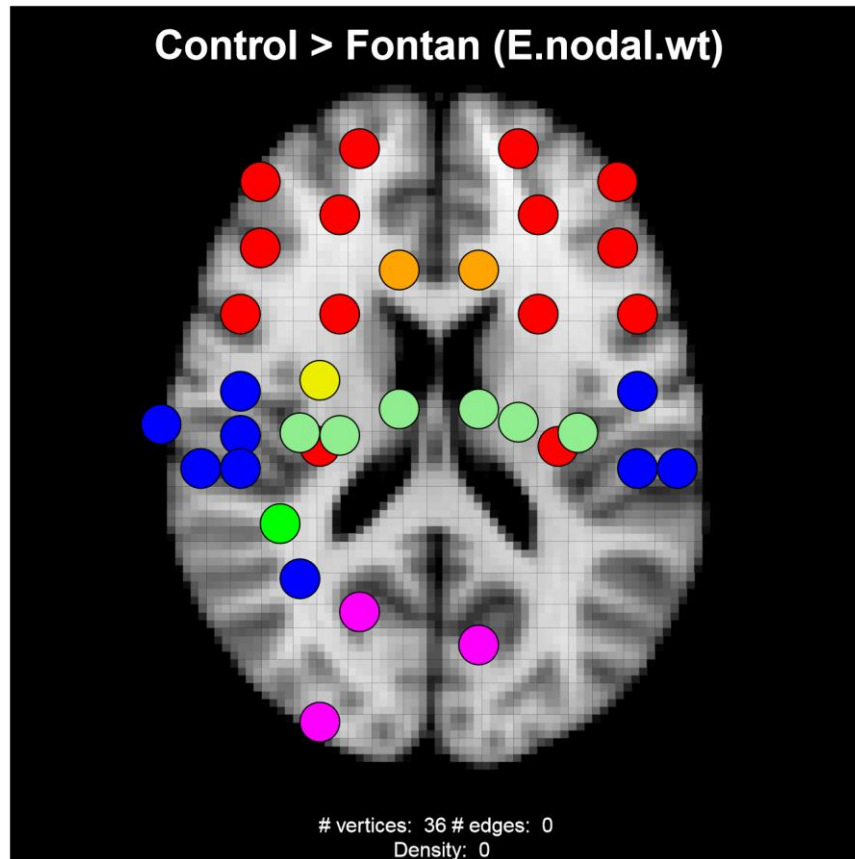


Figure 3.3: **Group differences in vertex weighted nodal efficiency.** The vertices shown are those which had significantly higher weighted nodal efficiency. Significance was determined by permutation testing; $p < 0.05$. Vertex color corresponds to lobe membership (red: frontal; green: parietal; blue: occipital; yellow: insula; orange: cingulate; light green: subcortical). The left hemisphere is displayed on the left side of the figure.

Region	Group diff.	β	Std. error	T	P-value
L nucleus accumbens	-0.03	0.05	0.01	5.19	<0.001
L amygdala	-0.13	0.15	0.01	15.86	<0.001
L caudate	-0.07	0.09	0.01	9.47	<0.001
L entorhinal	-0.08	0.11	0.01	10.74	<0.001
L fusiform	-0.09	0.11	0.01	13.00	<0.001
L hippocampus	-0.05	0.07	0.01	7.27	<0.001
L insula	-0.04	0.06	0.01	8.19	<0.001
L inferior parietal lobule	-0.05	0.06	0.01	6.22	<0.001
L inferior temporal gyrus	-0.06	0.08	0.01	8.31	<0.001
L lingual	-0.03	0.05	0.01	5.38	<0.001
L lateral orbitofrontal	-0.05	0.07	0.01	9.36	<0.001
L lateral occipital gyrus	-0.08	0.10	0.01	10.80	<0.001
L medial orbitofrontal	-0.01	0.03	0.01	3.38	0.01
L middle temporal gyrus	-0.05	0.07	0.01	6.65	<0.001
L pallidum	-0.07	0.08	0.01	7.78	<0.001
L parahippocampal	-0.13	0.16	0.01	15.13	<0.001
L posterior cingulate cortex	-0.01	0.03	0.01	3.34	0.01
L putamen	-0.12	0.14	0.01	16.64	<0.001
L superior frontal gyrus	-0.08	0.10	0.01	12.79	<0.001
L supramarginal gyrus	-0.02	0.03	0.01	3.60	0.005
L superior temporal gyrus	-0.04	0.06	0.01	7.75	<0.001
L thalamus	-0.20	0.22	0.01	20.82	<0.001
L transverse temporal	-0.03	0.05	0.01	6.56	<0.001
L caudal anterior cingulate	-0.03	0.05	0.01	6.46	<0.001
L caudal middle frontal gyrus	-0.06	0.08	0.01	10.61	<0.001
L isthmus cingulate cortex	-0.00	0.02	0.01	2.80	0.04
L pars opercularis	-0.07	0.09	0.01	11.38	<0.001
L pars orbitalis	-0.04	0.06	0.01	7.11	<0.001
L pars triangularis	-0.03	0.06	0.01	5.97	<0.001
L pericalcarine	-0.01	0.03	0.01	2.91	0.03
L precentral	-0.03	0.04	0.01	5.83	<0.001
L rostral anterior cingulate cortex	-0.05	0.08	0.01	8.59	<0.001
L rostral middle frontal gyrus	-0.08	0.10	0.01	13.14	<0.001

Table 3.5: **Group differences in vertex weighted shortest path length (L)** List of vertices for which vertex weighted shortest path length was significantly different ($p < 0.05$ determined by linear models and permutation testing) between groups. Group differences greater than 0 indicate higher values in the control group compared to Fontans. The β values are parameter estimates for the *Group* predictor, shown along with their associated standard errors, t-statistics, and p-values. L: left; R: right

Region	Group diff.	β	Std. error	T	P-value
R nucleus accumbens	-0.01	0.03	0.01	3.40	0.01
R amygdala	-0.13	0.15	0.01	14.85	<0.001
R caudate	-0.04	0.06	0.01	7.00	<0.001
R entorhinal	-0.08	0.10	0.01	10.45	<0.001
R fusiform	-0.03	0.05	0.01	6.50	<0.001
R hippocampus	-0.04	0.05	0.01	6.23	<0.001
R insula	-0.06	0.08	0.01	10.50	<0.001
R inferior parietal lobule	-0.02	0.03	0.01	3.47	0.008
R inferior temporal gyrus	-0.04	0.05	0.01	5.71	<0.001
R lateral orbitofrontal	-0.05	0.06	0.01	8.45	<0.001
R lateral occipital gyrus	-0.01	0.03	0.01	3.32	0.01
R medial orbitofrontal	-0.01	0.02	0.01	3.16	0.02
R middle temporal gyrus	-0.19	0.21	0.01	22.36	<0.001
R pallidum	-0.07	0.09	0.01	8.61	<0.001
R parahippocampal	-0.10	0.11	0.01	11.85	<0.001
R putamen	-0.08	0.10	0.01	10.37	<0.001
R superior frontal gyrus	-0.06	0.08	0.01	12.06	<0.001
R supramarginal gyrus	-0.03	0.04	0.01	5.46	<0.001
R superior temporal gyrus	-0.04	0.06	0.01	8.02	<0.001
R thalamus	-0.20	0.22	0.01	22.15	<0.001
R transverse temporal	-0.05	0.07	0.01	7.50	<0.001
R caudal anterior cingulate	-0.01	0.03	0.01	4.79	<0.001
R caudal middle frontal gyrus	-0.06	0.08	0.01	10.95	<0.001
R pars opercularis	-0.06	0.08	0.01	10.43	<0.001
R pars orbitalis	-0.06	0.07	0.01	8.16	<0.001
R pars triangularis	-0.05	0.07	0.01	7.81	<0.001
R pericalcarine	-0.08	0.10	0.01	9.95	<0.001
R precentral	-0.04	0.06	0.01	7.88	<0.001
R rostral anterior cingulate cortex	-0.01	0.03	0.01	4.86	<0.001
R rostral middle frontal gyrus	-0.06	0.08	0.01	10.18	<0.001

Table 3.6: **Group differences in vertex weighted shortest path length (R)** List of vertices for which vertex weighted shortest path length was significantly different ($p < 0.05$ determined by linear models and permutation testing) between groups. Group differences greater than 0 indicate higher values in the control group compared to Fontans. The β values are parameter estimates for the *Group* predictor, shown along with their associated standard errors, t-statistics, and p-values. L: left; R: right

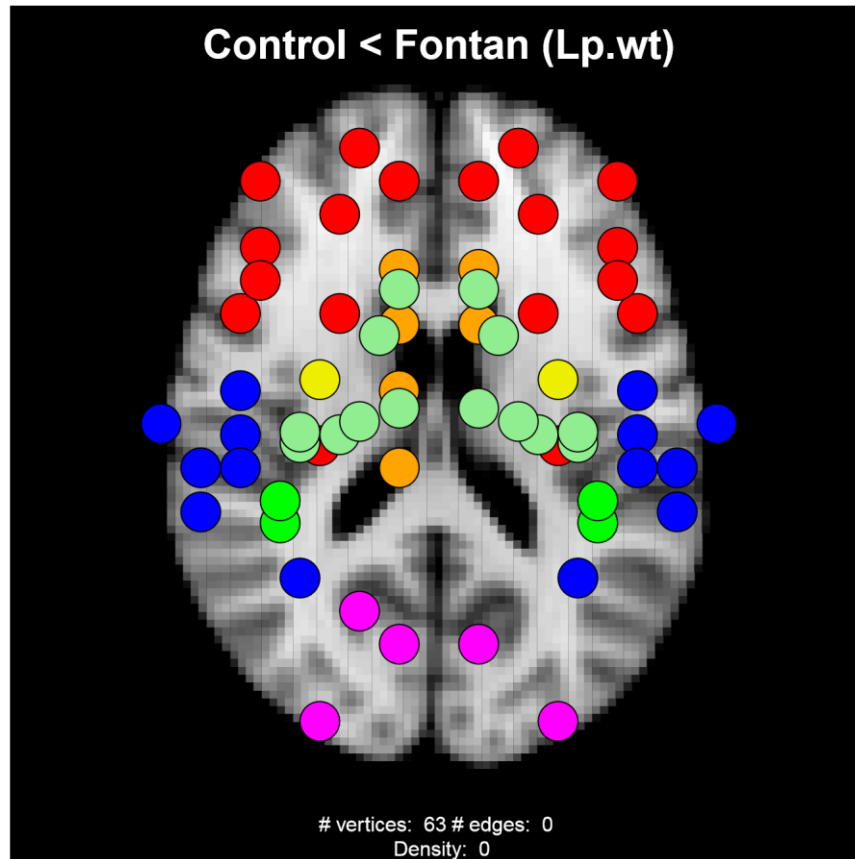


Figure 3.4: **Group differences in vertex weighted shortest path length.** The vertices shown are those which had significantly lower weighted shortest path length in the control group. Significance was determined by permutation testing; $p < 0.05$. Vertex color corresponds to lobe membership (red: frontal; green: parietal; blue: occipital; yellow: insula; orange: cingulate; light green: subcortical). The left hemisphere is displayed on the left side of the figure.

Predictor	Region	β	Std. error	T	P-value
Op. 1 type	R transverse temporal	-0.0020	0.0008	-2.58	0.006
DHCA time, min	L fusiform	-0.0000	0.0000	-2.46	0.008
	L inferior temporal gyrus	-0.0000	0.0000	-2.37	0.01
Support time, min	L fusiform	-0.0000	0.0000	-2.46	0.008
	L medial orbitofrontal	-0.0007	0.0003	-2.52	0.007
	L rostral anterior cingulate cortex	-0.0007	0.0003	-2.48	0.007
Op. 1 complications	L superior frontal gyrus	-0.0007	0.0003	-2.43	0.009
	R rostral anterior cingulate cortex	-0.0007	0.0003	-2.43	0.008
	R transverse temporal	-0.0008	0.0003	-2.98	0.002
	R insula	-0.0009	0.0003	-2.75	0.004
	L fusiform	-0.0025	0.0007	-3.38	<0.001
Norwood	L inferior temporal gyrus	-0.0018	0.0006	-3.29	<0.001
	L middle temporal gyrus	-0.0014	0.0006	-2.39	0.009
	L parahippocampal	-0.0027	0.0010	-2.59	0.005
	L hippocampus	-0.0029	0.0012	-2.42	0.009
	R transverse temporal	-0.0021	0.0008	-2.69	0.004

Table 3.7: **Associations between nodal efficiency and operative variables.** Operative variables that were significantly associated with weighted nodal efficiency in the Fontan group.

L: left; R: right; min: minutes

Predictor	Region	β	Std. error	T	P-value
Op. 1 complications	R caudal middle frontal gyrus	-0.0020	0.0008	-2.50	0.007
	R lateral orbitofrontal	-0.0014	0.0005	-2.54	0.006
	R paracentral	-0.0010	0.0004	-2.49	0.007
	R pars triangularis	-0.0028	0.0010	-2.85	0.003
Norwood	L superior temporal gyrus	-0.0023	0.0009	-2.66	0.005
	R superior temporal gyrus	-0.0026	0.0009	-2.74	0.004

Table 3.8: **Associations between local efficiency and operative variables.** Operative variables that were significantly associated with weighted local efficiency in the Fontan group.

L: left; R: right; min: minutes

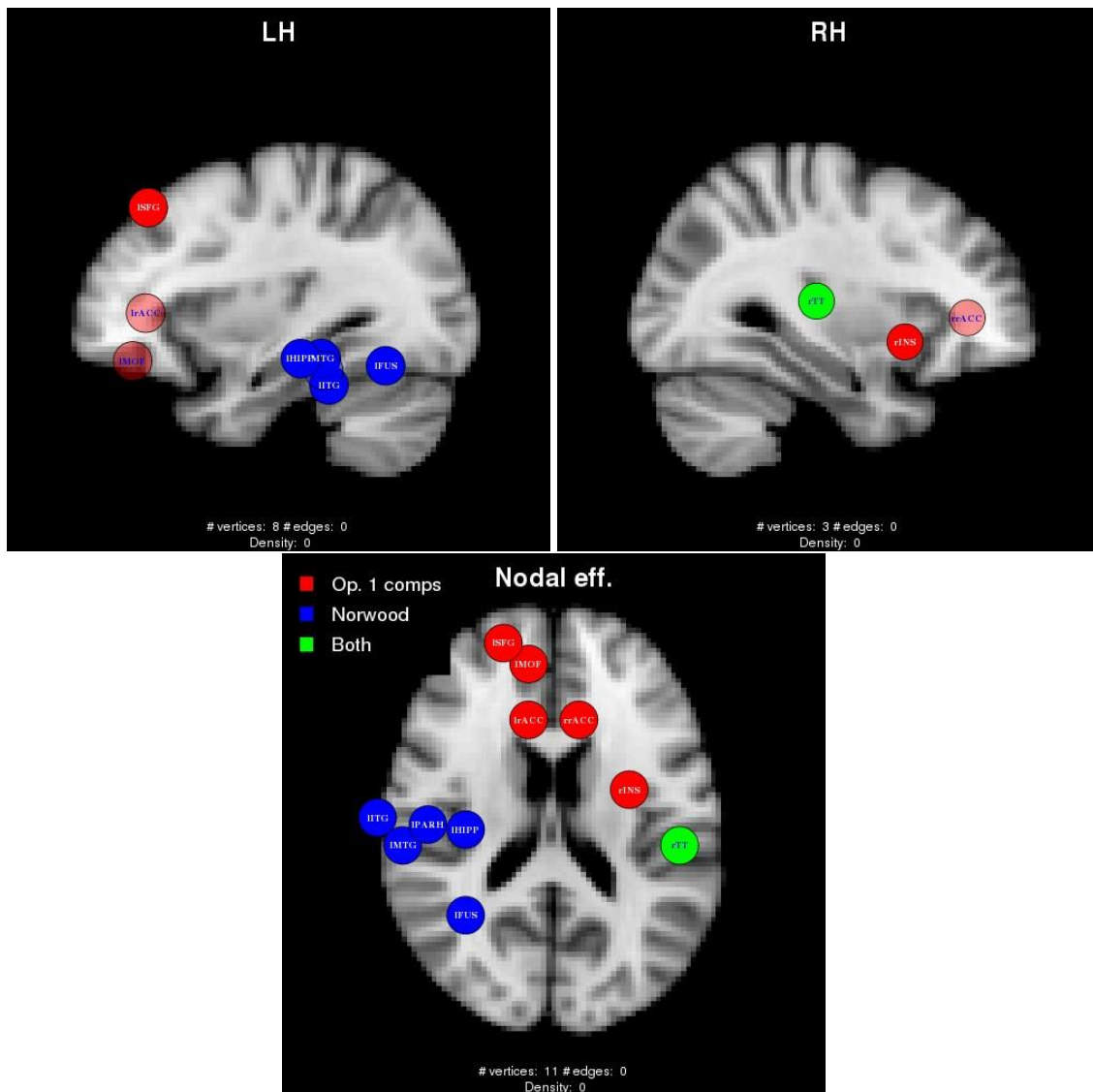


Figure 3.5: **Significant associations with nodal efficiency.** Vertices for which weighted nodal efficiency was significantly associated ($p < 0.01$) with one of the surgical variables in the Fontan group. Vertex colors denote the surgical variable of interest, with red vertices being associated with number of complications in the first operation, blue vertices with Norwood procedure, and green vertices with both.

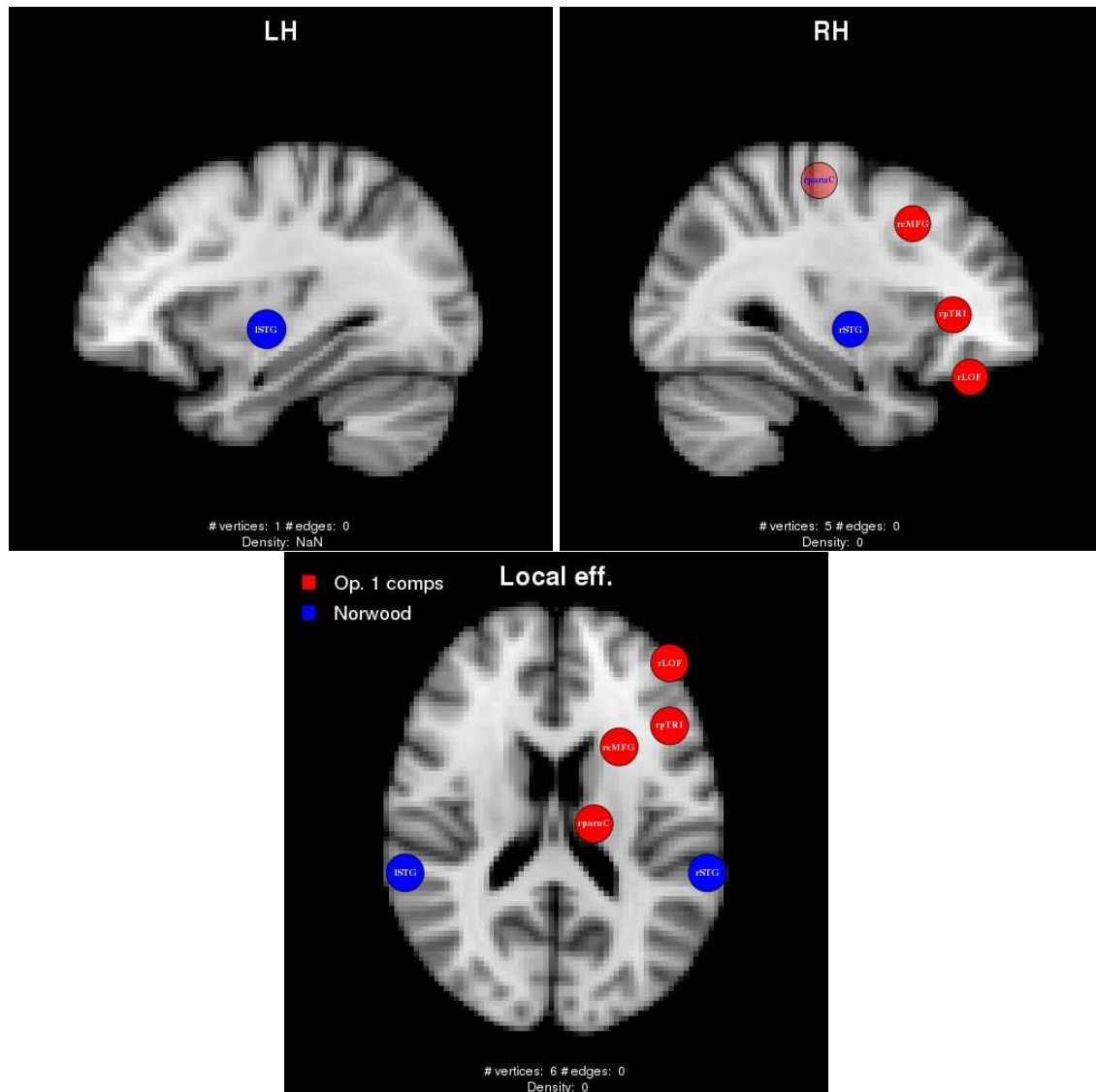


Figure 3.6: **Significant associations with local efficiency.** Vertices for which weighted local efficiency was significantly associated ($p < 0.01$) with one of the surgical variables in the Fontan group. Vertex colors denote the surgical variable of interest, with red vertices being associated with number of complications in the first operation, blue vertices with Norwood procedure, and green vertices with both.

Predictor	Region	β	Std. error	T	P-value
Op. 1 age	L transverse temporal	0.0284	0.0106	2.69	0.004
Op. 1 type	R transverse temporal	-0.0230	0.0085	-2.70	0.004
DHCA time, min	L fusiform	-0.0008	0.0003	-2.54	0.006
Support time, min	L fusiform	-0.0003	0.0001	-2.64	0.005
Op. 1 complications	R transverse temporal	-0.0077	0.0030	-2.55	0.006
	R insula	-0.0311	0.0113	-2.75	0.004
Norwood	L fusiform	-0.0546	0.0165	-3.31	<0.001

Table 3.9: **Associations between vertex strength and operative variables.** Operative variables that were significantly associated with vertex strength in the Fontan group.

L: left; R: right; min: minutes

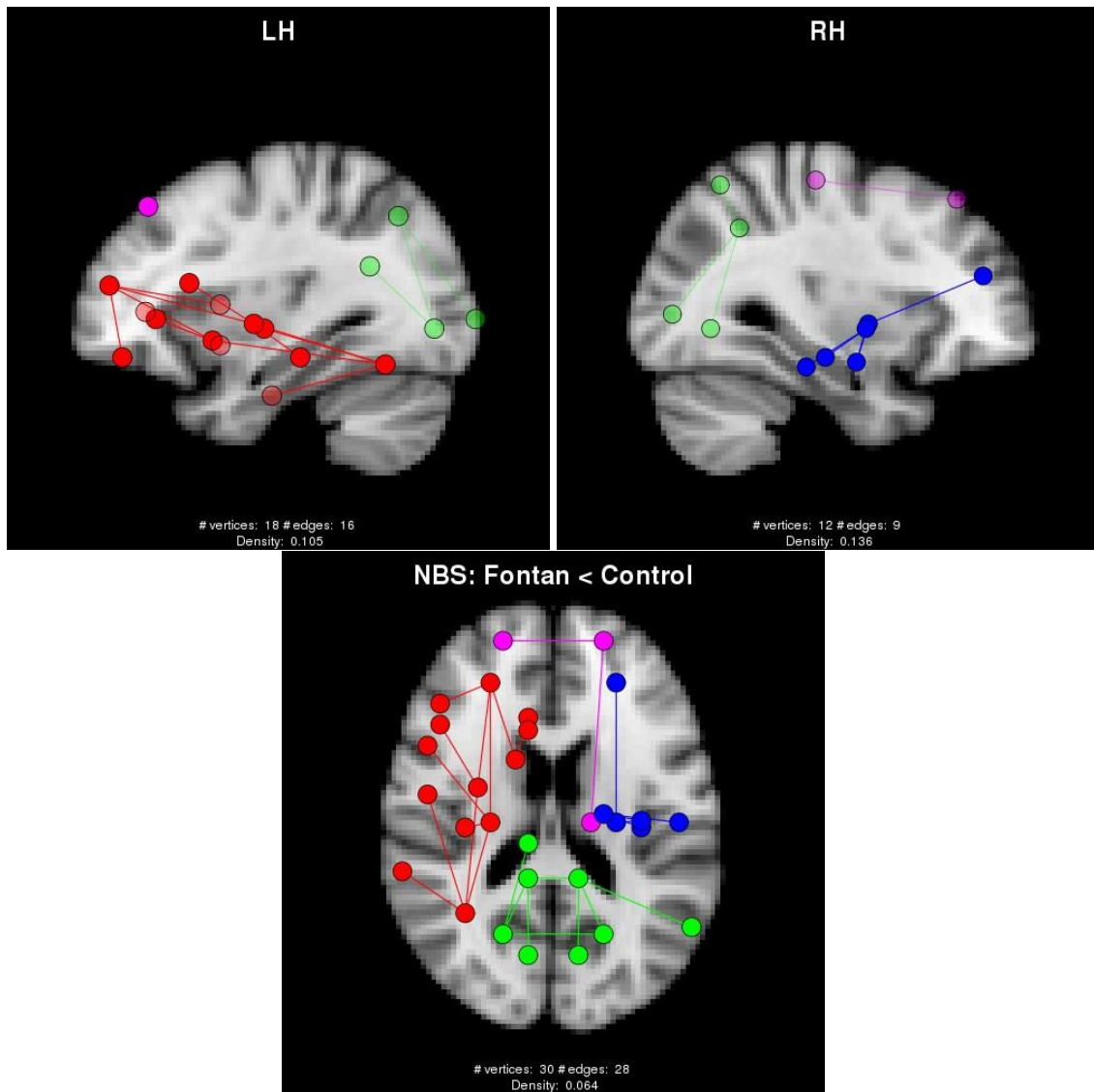


Figure 3.7: **Network-based statistic results.** Connected components with significantly lower connectivity strength in the Fontan group compared to the control group. Vertex colors are selected based on component membership, from largest to smallest: red, green, blue, magenta.

Discussion

This is the first study using probabilistic tractography and graph theory analysis in children and adolescents with single ventricle (SV) who have undergone the Fontan procedure. Our results in brain white matter networks revealed extensive differences in overall network connectivity, integration, and segregation compared to a control group. Connectivity strength and measures of network integration were lower in the Fontan group at the global level and locally in several brain regions. Measures of network segregation were higher in the Fontan group throughout the brain. Additionally, lower global and local efficiency, along with vertex-level weighted nodal and local efficiency and vertex strength were associated with increasing number of complications in the patients' first operation. Vertex strength and weighted nodal efficiency were further negatively associated with DHCA and support time, and lower in the right transverse temporal lobe for patients with an open first operation. Thus, management of complications that may arise during the initial surgery may be most beneficial to brain structural connectivity in post-Fontan SV patients.

Compared to the control group, the Fontan group demonstrated reduced connectivity strength, increased modularity (segregation), increased characteristic path length, and lower efficiency. These results are similar to our analyses of WM networks in adolescents with d-transposition of the great arteries (d-TGA) (Panigrahy et al., 2015). Furthermore, these differences were present at the regional level, across all major lobes and both hemispheres.

Given these widespread differences, and the fact that WM injury and brain immaturity are common in CHD neonates, the data support the idea of the “encephalopathy of congenital heart disease” proposed by Volpe (2014) that is evident in infancy and persists into adolescence (Volpe, 2014).

Interestingly, all regions showing altered nodal or local efficiency or vertex strength, when patients were stratified by Norwood status, were located in the temporal lobes and hippocampus bilaterally. Large portions of these regions are perfused by terminal branches of the vascular trees that subserve them and consequently could be prone to ischemic injury during periods of hemodynamic compromise (Graham, 1977; Gunn and Bennet, 2009; Malone et al., 1981). Interestingly, these areas were identified as having lower GM volumes and thicknesses in the same cohort (Watson et al., manuscript under review). In the study of CPB-related injury in animal models, immature WM—specifically pre-oligodendrocytes—were shown to be particularly vulnerable to hypoxia (Ishibashi et al., 2012); even mature oligodendrocytes that developed under conditions of hypoxia were more susceptible to injury (Agematsu et al., 2014) Chronic hypoxia alters the normally protective astrocyte response, which may add to WM injury caused by CPB (Agematsu et al., 2016). Neuronal (GM) damage is also present but not constant throughout the brain: vulnerability was dependent on the region’s vasculature and metabolic properties (Ishibashi et al., 2010). Taken together, these results suggest that exposure to chronic hypoxia and/or CPB can result in the breakdown of neural connectivity — first in white matter, since oligodendrocytes are responsible for myelination of component axons — with consequent neuronal cell death

in gray matter through Wallerian degeneration. In aggregate, this alters the normal pattern of inputs and outputs of the damaged region.

As neonates with SV have been shown to have an immature brain even before the first operation (Andropoulos et al., 2010; Lynch, 2009), the brains of SV neonates may be particularly susceptible to CPB-induced injury. Moreover, the Norwood subgroup consisted predominantly of hypoplastic left heart syndrome (HLHS) patients. Patients with HLHS have significantly lower cerebral blood flow beginning as early as the second trimester (Donofrio et al., 2003; Hahn et al., 2015; Szwasz et al., 2012). It is possible that these differences in structural brain connectivity have their origin in insufficient blood flow throughout the critical period of fetal development.

This study has some limitations. Not all patients were able to undergo MRI at 3T field strength; although we used the same acquisition parameters at both 1.5T and 3T, and included scanner field strength as a covariate in all analyses, our findings may not be as robust as those performed on a single scanner. Second, the Fontan group was not homogeneous, and includes patients with several different SV diagnoses. Some of the subgroup sizes were too small to be analyzed separately with sufficient power, and there may be variability that was not captured by our analyses. The year that the patients underwent the Fontan procedure spanned several years, and was not performed at the same hospital for all subjects. Therefore, recent advances in perioperative procedures and postoperative care may result in improved outcomes.

Conclusions

In conclusion, post-Fontan children and adolescents with SV have altered brain white matter connectivity even many years after completing the staged palliation. Some of these deficits are associated with characteristics of the initial surgery, which often occurs in the neonatal period and suggests that the early surgery adversely affects cerebral organization in adolescence. Considering this patient group has learning and behavioral difficulties throughout childhood, early interventions targeting the restoration of blood flow and protection from WM injury, in addition to better perioperative care, are important options for improving the quality-of-life in children with SV.

BRAIN STRUCTURAL CONNECTIVITY, SURGICAL HISTORY, AND NEURODEVELOPMENT IN POST-FONTAN CHILDREN AND ADOLESCENTS

Introduction

Neurodevelopmental deficits are common in children and adolescents with congenital heart disease (CHD), especially single ventricle (SV) defects (Bellinger et al., 2015, 2011; Gaynor et al., 2015). While many patients score in the low-average range on cognitive testing, a significant proportion require special educational services and have particular difficulties with attention and with visuospatial, fine motor, and executive function. As CHD is the most common congenital anomaly, this constitutes a significant burden on the educational system (Tennant et al., 2010). In a diffusion tensor imaging (DTI) study of adolescents with d-transposition of the great arteries (d-TGA), we showed that white matter (WM) microstructure is significantly lower throughout the deep WM compared to a control group, and that in a handful of WM tracts, fractional anisotropy (FA, a measure of microstructure) was significantly associated with cognitive function (Rollins et al., 2014). In the same population, graph theory analysis of DTI tractography data revealed group differences indicative of increased network segregation and decreased efficiency in the d-TGA group (Panigrahy et al., 2015). There currently are no studies using DTI tractography or structural covariance from brain magnetic resonance imaging (MRI) to illuminate the relationship between brain structure and neurodevelopment in SV children and adolescents several years after undergoing the Fontan procedure.

The properties of structural covariance networks have been shown to be associated

with relevant aspects of cognition in healthy subjects and of disease pathology in certain disease groups. Saggar et al. (2015) introduced a method for determining the contribution of a given subject to a group network, and showed that this metric was significantly associated with IQ both in typically-developing adolescents and Fragile X Syndrome patients. The direction of this relationship was such that patients who contributed more to the group network had a lower IQ (Saggar et al., 2015). Mediation analysis is a statistical technique that estimates the indirect effect of one variable on the association between a predictor and outcome variable (Baron and Kenny, 1986; MacKinnon et al., 2007). We previously applied this technique to DTI tractography networks in adolescents with d-transposition of the great arteries (d-TGA), showing that measures of network topology were mediators of cognitive outcomes, suggesting that markers of impaired connectivity mediate the relationship between CHD and cognition (Panigrahy et al., 2015). We further showed that network measures mediated outcomes specifically related to ADHD symptomatology (Schmithorst et al., 2016). Mediation analysis with graph theory has also been applied in adults with cerebral small vessel disease to show that global efficiency mediates the relationship between WM microstructure and cognition (specifically, executive function and processing speed) (Lawrence et al., 2014). Also in small vessel disease, WM fractional anisotropy (FA) of tracts with the highest centrality was a mediator between lesion volume and executive function (Reijmer et al., 2016).

In this chapter, we use graph theory data from structural covariance (cortical thickness) networks and DTI tractography networks to investigate the associations between both global and regional brain structure and neurodevelopmental outcomes in

post-Fontan children and adolescents with SV defects. We use both linear modelling and causal mediation analysis to determine whether measures of brain network structure mediate the well-known relationship between early heart surgery and impaired cognitive and behavioral function.

Methods

Subject recruitment details are the same as those outlined in Chapter 2 (“Graph theory analysis of gray matter networks in post-Fontan children and adolescents”) and Chapter 3 (“Graph theory analysis of white matter networks in post-Fontan children and adolescents”). Imaging parameters for the MP-RAGE sequence can be found in Chapter 2, and for the DTI sequence in Chapter 3.

Gray matter networks

For the volumetric data, since there are no subject-level graphs available, the *leave-one-out (LOO)* and *add-one-patient (AOP)* methods of Saggar et al. (2015) were applied to determine *individual* and *regional contributions* (IC and RC). These methods enable the calculation of either a single value for each subject (representing how much that subject “contributes” to the entire group’s graph; IC) or a vector of values for each subject (representing the amount each region contributes to the group data; RC).

LOO

With the LOO method, correlation matrices are constructed with the same procedure as in Chapter 2 (i.e., by correlating the residuals of a general linear model [GLM] between pairs of regions), except a matrix is constructed after removing one

subject from the group (this method does not iterate over subjects; i.e., each matrix reflects data from $k-1$ subjects, where k is the size of the full group). The original group matrix is compared to each of the new matrices using a Mantel test (Mantel, 1967):

$$r = \frac{1}{N-1} \sum_{i=1}^N \sum_{j=1}^N \frac{(x_{ij} - \bar{x})(y_{ij} - \bar{y})}{s_x s_y}$$

where x_{ij} and y_{ij} are the i, j^{th} entries of each matrix, \bar{x} and \bar{y} are the means of each matrix, s_x and s_y are the standard deviations, and N is the total number of distinct elements (equaling $n(n-1)/2$ if n is the number of vertices in the graph, because the matrices are symmetric and the diagonal is not considered). A Mantel test statistic closer to 1 indicate that the matrices being compared are highly similar; thus, the *individual contribution (IC)* is taken to be $1-r$, and a higher *IC* indicates a greater contribution of that subject to the group matrix. This procedure was performed separately for each group.

The *regional contribution (RC)* was taken to be the column-wise sum of the absolute value of the difference between the matrices of the full group and the group excluding each subject. This results in a single number for each brain region and subject.

AOP

With the AOP method, comparisons are made between the correlation matrix of the control group and a correlation matrix constructed from the control group in addition to each subject from the patient group. As with LOO, this is done separately for each group, and $IC = 1-r$. *RC* was defined in the same way as for LOO. This was only done for the Fontan group, as the comparisons are made against the control group.

Statistics

Associations between subjects' IC and RC (calculated using both the LOO and AOP methods) and neurodevelopmental outcomes in the Fontan group were determined using linear models. Covariates (age at MRI, sex, and scanner field strength) were not included in these models because they were already adjusted for when constructing the structural covariance networks (which were based on inter-regional correlations of model residuals). For IC, P-values were adjusted using the false discovery rate (FDR) procedure across all neurodevelopmental outcomes; for RC, P-values were adjusted using the FDR procedure across brain regions (separately for LOO and AOP). For all analyses, $p_{FDR} < 0.05$ was the criterion for statistical significance.

White matter networks

For the white matter networks created from DTI tractography data, we performed correlation, GLM, and mediation analyses. Spearman correlations were used in the case of non-normally distributed variables; otherwise, Pearson correlations were calculated. In the GLM analyses, since tractography network construction did not involve any of the covariates from Chapter 2, we adjusted for age at MRI, sex, and scanner field strength at this stage of the analysis.

Mediation analysis

Mediation models were estimated to determine the effects of the independent variable (e.g., subject group when including both the Fontan and control groups, or surgical history variables within the Fontan group alone) on the dependent variable

(neurodevelopmental outcomes; e.g., *full-scale IQ (FSIQ)*), through the *mediating* (indirect) effect of various graph measures (e.g., weighted global efficiency) (Hayes, 2009; MacKinnon et al., 2007). This is a causal model because the independent variable is hypothesized to influence the mediating variable, which in turn has an effect on the dependent variable.

In a mediation analysis, three linear models are specified (Baron and Kenny, 1986):

$$Y = i_1 + cX + e_1 \quad (4.1a)$$

$$Y = i_2 + c'X + bM + e_2 \quad (4.1b)$$

$$M = i_3 + aX + e_3 \quad (4.1c)$$

In Equations 4.1a-4.1c, i_n and e_n ($n = 1,2,3$) are the intercepts and error terms, respectively; X is the independent variable; Y is the dependent variable; and M is the mediating variable. The parameter estimates c , c' , b , and a are standard regression coefficients. To calculate a mediating effect, it is sufficient to specify only Equations 4.1b and 4.1c, as the statistic of interest is calculated from the product of parameter estimates a and b (Imai et al., 2010). This is denoted the *average causal mediation (ACME) effect* (also called the *indirect effect*).

All mediation analyses were performed using the *mediate* package in R (Tingley et al., 2014). Bias-corrected and accelerated confidence intervals were calculated based on 10,000 bootstrap samples for graph-level measures, and 1,000 samples for vertex-level measures (Efron, 1987). Several variables were examined as potential mediators:

graph-level measures (weighted global and local efficiency, weighted modularity, and strength), and vertex-level measures (weighted nodal and local efficiency, strength, weighted participation coefficient [PC], weighted within-module degree z-score, and weighted shortest path length). ACME P-values were considered significant if $p < 0.05$.

Neurodevelopmental outcomes

Several neurodevelopmental domains were chosen to be outcomes of interest based on known deficits in children and adolescents with CHD (Bellinger et al., 2015, 2011).

General intelligence

General intelligence was measured by the *Wechsler Intelligence Scale for Children –Fourth Edition (WISC-IV)* in subjects <17 years old, and the *Wechsler Adult Intelligence Scale –Fourth Edition (WAIS)* in subjects 17-19 years of age (Wechsler, 2003, 2008). There were five scores of interest: Full-Scale IQ (FSIQ), verbal comprehension, perceptual reasoning, working memory, and processing speed.

Academic achievement

Academic achievement was measured by the *Wechsler Individual Achievement Test –Second Edition (WIAT)* (Wechsler, 2005). Scores of interest were the Reading and Mathematics Composite scores.

Executive function and attention

Executive function was measured by the *Delis-Kaplan Executive Function System*

(*D-KEFS*) (Delis et al., 2001). A summary score was calculated by averaging scores on the five subtests (verbal fluency, design fluency, sorting, word context, and tower). Additionally, the *Behavior Rating Inventory of Executive Function (BRIEF)* was completed via self-report and administered to a parent and teacher (Gioia et al., 2000; Guy et al., 2004). For each subject, the General Executive Composite score from each of the three assessments was the outcome of interest. The ADHD Index T-score from the *Conners ADHD/DSM-IV Scales –Parent (CADS-P)* was used as the outcome of interest for attention (Conners, 2004).

Visuospatial function

The *Test of Visual-Perceptual Skills (nonmotor) (Upper Level) –Revised (TVPS)* was administered to assess visuospatial function (Gardner et al., 1997). Scores from the visual memory and visual closure subtests were examined, in addition to a composite score calculated from the TVPS subtests.

Social and emotional cognition

Social and emotional cognition were assessed by the *Autism Spectrum Quotient (AQ)* and the *Toronto Alexithymia Scale (TAS)* (Bagby et al., 1994; Baron-Cohen et al., 2001). From the TAS, a total score was calculated from three subscales (Difficulty Identifying Feelings, Difficulty Describing Feelings, and Externally-Oriented Thinking).

Surgical and medical history variables

Several surgical and medical history variables were investigated as potential treatment variables in the mediation analyses. These included: New York Heart

Association (NYHA) functional class, presence of a genetic abnormality (“syndromic” or “nonsyndromic”), Norwood status (“Norwood” or “non-Norwood”), history of any seizures, history of any neurologic event (stroke, seizure, choreoathetosis, and meningitis), age at first operation (“neonate” or “non-neonate”), type of first operation (“open” or “closed”), number of complications during the first operation (“zero”, “one”, or “two or more”), total number of operations (“one to two”, “three”, or “four to five”), total number of open operations (“one”, “two”, or “three or more”), total number of surgical complications (“zero”, “one to five”, or “six or more”), total number of catheterizations (“one to two”, “three to five”, or “six or more”), and total number of catheterization complications (“zero”, “one to two”, or “three or more”).

Results

Gray matter networks

In the following tables, a negative parameter estimate (β) indicates that subjects with a higher IC/RC (indicative of a greater departure from the group network) tended to have poorer scores (with the exception of the BRIEF, AQ, and TAS scores, in which higher scores are worse).

IC

For both the LOO and AOP methods, several neurodevelopmental variables were significantly associated with global network connectivity as measured by IC (see Table 4.1 and Table 4.2): general intelligence (FSIQ, processing speed, and perceptual reasoning), academic achievement (WIAT Reading and Mathematics Composite Scores), executive function (D-KEFS summary score), and social/emotional cognition (AQ). The

tables show the parameter estimates, standard errors, t-statistics, and FDR-adjusted P-values for these significant associations.

A scatterplot of IC for both LOO and AOP in the Fontan group is shown in Figure 4.1 and Figure 4.2, respectively. IC values are plotted along the y-axis, and neurodevelopmental scores along the x-axis. Each facet displays the scores for each outcome. Also included are the best-fit lines (blue) from a linear regression and 95% confidence regions (grey shading).

Outcome	β	Std. Error	T	P-value
WIAT Reading	-5015.54	1567.58	-3.20	0.009
WIAT Math	-6668.77	2111.79	-3.16	0.009
D-KEFS	-593.54	208.16	-2.85	0.02
AQ	1669.18	485.93	3.44	0.008
Perceptual reasoning	-3612.79	1464.73	-2.47	0.04
Processing speed	-5905.22	1449.81	-4.07	0.002
FSIQ	-4300.70	1520.27	-2.83	0.02

Table 4.1: **Significant associations between IC (LOO) and neurodevelopmental outcomes.** Outcome variables which were significantly ($p_{FDR} < 0.05$) associated with IC (using the LOO method) in the Fontan group. P-values are FDR-adjusted.

WIAT: Wechsler Individual Achievement Test; D-KEFS: Delis-Kaplan Executive Function System; AQ: Autism Spectrum Quotient; FSIQ: Full-Scale IQ

RC

For RC, Table 4.3 lists the outcomes and regions that are significantly associated using the LOO method, and Table 4.4 using the AOP method. For social/emotional cognition (AQ and TAS) and general intelligence (processing speed), regions were predominantly in bilateral frontal and temporal lobes.

The vertices with a significant association are displayed on an axial brain slice in Figure 4.3 (LOO) and in Figure 4.4 (AOP). Vertex colors are based on lobe membership (red: frontal; green: parietal; blue: temporal; yellow: insula; orange: cingulate). There was almost a complete overlap between both methods for AQ and processing speed.

A table of the regions in which RC (LOO method) was significantly associated ($p < 0.05$, uncorrected for multiple comparisons) with genetic abnormality is presented in Table 4.5. All estimates are positive, indicating that RC was higher in the “Syndromic” group for these regions. Results using the AOP method were similar and are not shown.

Outcome	β	Std. Error	T	P-value
WIAT Reading	-953.89	280.07	-3.41	0.004
WIAT Math	-1253.26	377.82	-3.32	0.004
D-KEFS	-115.32	37.16	-3.10	0.006
AQ	304.92	87.71	3.48	0.004
Perceptual reasoning	-813.59	258.55	-3.15	0.006
Processing speed	-1068.27	259.80	-4.11	0.001
FSIQ	-897.18	269.22	-3.33	0.004

Table 4.2: **Significant associations between IC (AOP) and neurodevelopmental outcomes.** Outcome variables which were significantly ($p_{FDR} < 0.05$) associated with IC (using the AOP method) in the Fontan group. P-values are FDR-adjusted.

WIAT: Wechsler Individual Achievement Test; D-KEFS: Delis-Kaplan Executive Function System; AQ: Autism Spectrum Quotient; FSIQ: Full-Scale IQ

White matter networks

Graph-level measures

Several of the global graph measures were significant mediators of the association between subject group and neurodevelopmental outcomes; see Table 4.6 for ACME estimates and their associated 95% confidence intervals and P-values. At the global level, weighted global efficiency was a significant mediator for general intelligence (FSIQ, working memory, and perceptual reasoning), and academic achievement (WIAT Mathematics Composite Score), weighted local efficiency was a significant mediator for general intelligence (FSIQ, working memory, and processing speed), and academic achievement (WIAT Mathematics Composite Score), weighted modularity was a significant mediator for visuospatial function (TVPS visual memory), and graph strength was a significant mediator for scores of general intelligence (FSIQ, perceptual reasoning, and processing speed) and academic achievement (WIAT Mathematics Composite Score).

Outcome	Region	β	Std. Error	T	P-value
AQ	L rostral anterior cingulate cortex	5.14	1.66	3.09	0.03
	L supramarginal gyrus	6.72	2.05	3.28	0.03
	R parahippocampal	5.33	1.82	2.93	0.04
	R precentral	7.13	1.86	3.84	0.01
	R superior frontal gyrus	7.60	2.41	3.16	0.03
	R superior temporal gyrus	7.12	2.22	3.21	0.03
TAS	L pars orbitalis	13.76	3.56	3.87	0.006
	L rostral anterior cingulate cortex	10.89	3.65	2.99	0.04
	L supramarginal gyrus	14.01	4.46	3.14	0.03
	R precentral	15.73	4.01	3.92	0.006
	R superior frontal gyrus	16.47	5.21	3.16	0.03
Processing speed	L medial orbitofrontal	-18.71	5.42	-3.45	0.02
	L rostral middle frontal gyrus	-17.91	6.09	-2.94	0.04
	L superior frontal gyrus	-17.62	6.26	-2.82	0.04
	L supramarginal gyrus	-17.95	6.29	-2.85	0.04
	R parahippocampal	-17.04	5.46	-3.12	0.04
	R pars orbitalis	-17.66	5.45	-3.24	0.03
	R precentral	-20.75	5.64	-3.68	0.02
	R superior frontal gyrus	-19.35	6.86	-2.82	0.04
	R transverse temporal	-13.73	4.89	-2.81	0.04
R insula	-14.61	5.02	-2.91	0.04	

Table 4.3: **Significant associations between RC (LOO) and neurodevelopmental outcomes.** Outcome variables which were significantly ($p_{FDR} < 0.05$) associated with RC (using the LOO method) in the Fontan group. P-values are FDR-adjusted.

AQ: Autism Spectrum Quotient; TAS: Toronto Alexithymia Scale; L: left; R: right

Vertex-level measures

At the regional level, weighted nodal efficiency was a significant mediator for academic achievement (WIAT Reading and Mathematics Composite Scores), executive function (D-KEFS summary score), social cognition (TAS score), and general intelligence (FSIQ, verbal comprehension, perceptual reasoning, and processing speed (all $p < 0.01$); see Table 4.7. The majority of regions were in the right hemisphere, and in the frontal and temporal lobes, cingulate gyrus, and subcortical gray matter.

Vertex strength was a significant mediator for academic achievement (WIAT Reading and Mathematics Composite Scores), executive function (D-KEFS summary score), visuospatial function (TVPS composite), and general intelligence (FSIQ, perceptual reasoning, processing speed, and verbal comprehension) (all $p < 0.01$); see Table 4.8. Almost all regions with a significant mediation were in the right hemisphere and subcortical gray matter, particularly the pallidum and thalamus.

Weighted local efficiency was a significant mediator for academic achievement (WIAT Reading and Mathematics Composite Scores), executive function (D-KEFS summary score), and general intelligence (FSIQ, perceptual reasoning, and processing speed) (all $p < 0.01$); see Table 4.9. All but one region with a significant mediation were the caudate and pallidum (both left and right hemispheres).

Outcome	Region	β	Std. Error	T	P-value
WIAT Reading	R pars orbitalis	-6.64	1.80	-3.69	0.02
	L middle temporal gyrus	2.23	0.71	3.15	0.03
AQ	L parahippocampal	1.77	0.59	3.01	0.04
	L supramarginal gyrus	1.69	0.52	3.27	0.03
	R parahippocampal	2.28	0.76	3.00	0.04
	R precentral	2.51	0.60	4.22	0.003
	R superior frontal gyrus	2.13	0.63	3.37	0.03
	R superior temporal gyrus	1.66	0.58	2.88	0.04
	L medial orbitofrontal	-3.62	1.31	-2.77	0.04
Processing speed	L parahippocampal	-4.82	1.77	-2.72	0.04
	L rostral middle frontal gyrus	-4.14	1.50	-2.76	0.04
	L superior frontal gyrus	-4.71	1.67	-2.82	0.04
	L supramarginal gyrus	-4.37	1.59	-2.74	0.04
	R medial orbitofrontal	-3.92	1.24	-3.17	0.04
	R pars orbitalis	-4.91	1.74	-2.82	0.04
	R precentral	-6.27	1.83	-3.42	0.04
	R superior frontal gyrus	-5.17	1.84	-2.81	0.04
	R transverse temporal	-5.85	1.86	-3.14	0.04
	R insula	-4.71	1.66	-2.83	0.04

Table 4.4: **Significant associations between RC (AOP) and neurodevelopmental outcomes.** Outcome variables which were significantly ($p_{FDR} < 0.05$) associated with RC (using the AOP method) in the Fontan group. P-values are FDR-adjusted. AQ: Autism Spectrum Quotient; TAS: Toronto Alexithymia Scale; L: left; R: right

Region	β	Std. Error	T	P-value
L medial orbitofrontal	0.14	0.05	2.73	0.007
L rostral anterior cingulate cortex	0.15	0.06	2.69	0.008
L supramarginal gyrus	0.11	0.05	2.40	0.02
R pars orbitalis	0.13	0.05	2.50	0.01
R superior temporal gyrus	0.09	0.04	2.09	0.04

Table 4.5: **Significant associations between RC (LOO) and presence of genetic abnormality.** Regions in which RC (using the LOO method), in the Fontan group, is significantly associated with the presence of a genetic abnormality. The displayed P-values are not adjusted for multiple comparisons. L: left; R: right

Mediator	Outcome	ACME (95% CI)	P-value
Global eff.	WIAT Math	2.50 (0.45, 6.27)	0.04
	Perceptual reasoning	1.50 (0.18, 3.68)	0.04
	Working memory	2.08 (0.62, 5.12)	0.009
	FSIQ	1.85 (0.44, 4.69)	0.02
Local eff.	WIAT Math	1.95 (0.21, 4.39)	0.04
	Working memory	1.56 (0.33, 3.40)	0.02
	Processing speed	1.78 (0.51, 3.47)	0.009
	FSIQ	1.61 (0.40, 3.29)	0.01
Modularity	TVPS memory	-3.99 (-9.23, -0.71)	0.02
Strength	WIAT Math	-2.30 (-5.66, -0.52)	0.02
	Perceptual reasoning	-1.49 (-3.56, -0.26)	0.03
	Processing speed	-2.27 (-5.13, -0.76)	0.002
	FSIQ	-1.99 (-4.83, -0.52)	0.009

Table 4.6: **Mediation between graph-level measures and neurodevelopmental outcomes.** Neurodevelopmental outcomes for which graph-level measures were determined to be significant mediators ($p < 0.05$), with subject group as the independent variable. The table shows point estimates for the causal mediation effect along with 95% confidence intervals and their associated P-values.

ACME: average causal mediation effect; CI: confidence interval; WIAT: Wechsler Individual Achievement Test; FSIQ: Full-Scale IQ; TVPS: Test for Visual-Perceptual Skills

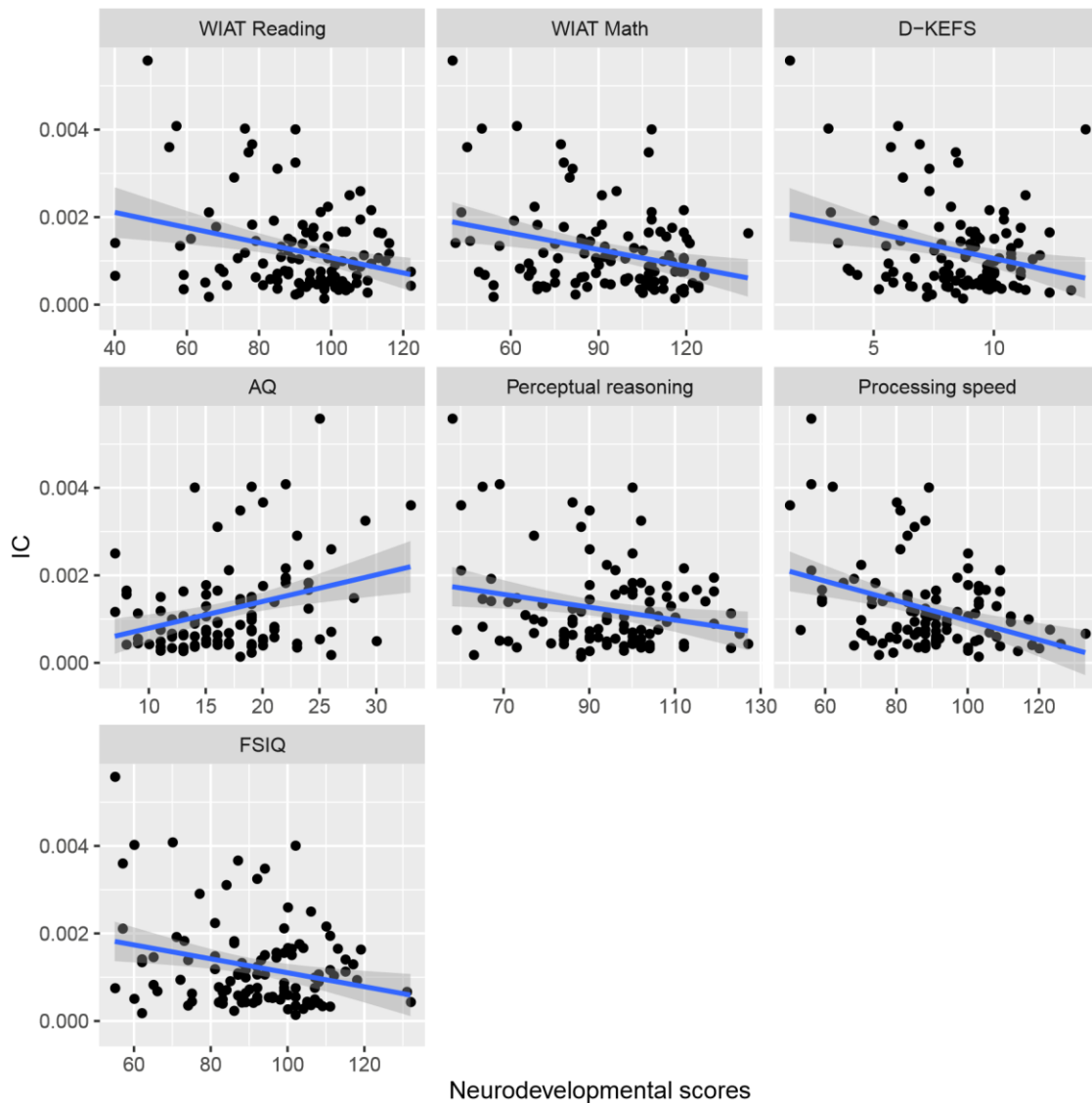


Figure 4.1: **Fontan IC (LOO) and neurodevelopmental outcomes.** Scatterplot of neurodevelopmental outcomes that are significantly (FDR-adjusted $p < 0.05$) associated to IC (LOO) in the Fontan group. The blue line is the best-fit line from a linear regression; the shaded regions represent 95% confidence intervals.

WIAT: Wechsler Individual Achievement Test; D-KEFS: Delis-Kaplan Executive Function System; AQ: Autism Spectrum Quotient; FSIQ: Full-Scale IQ

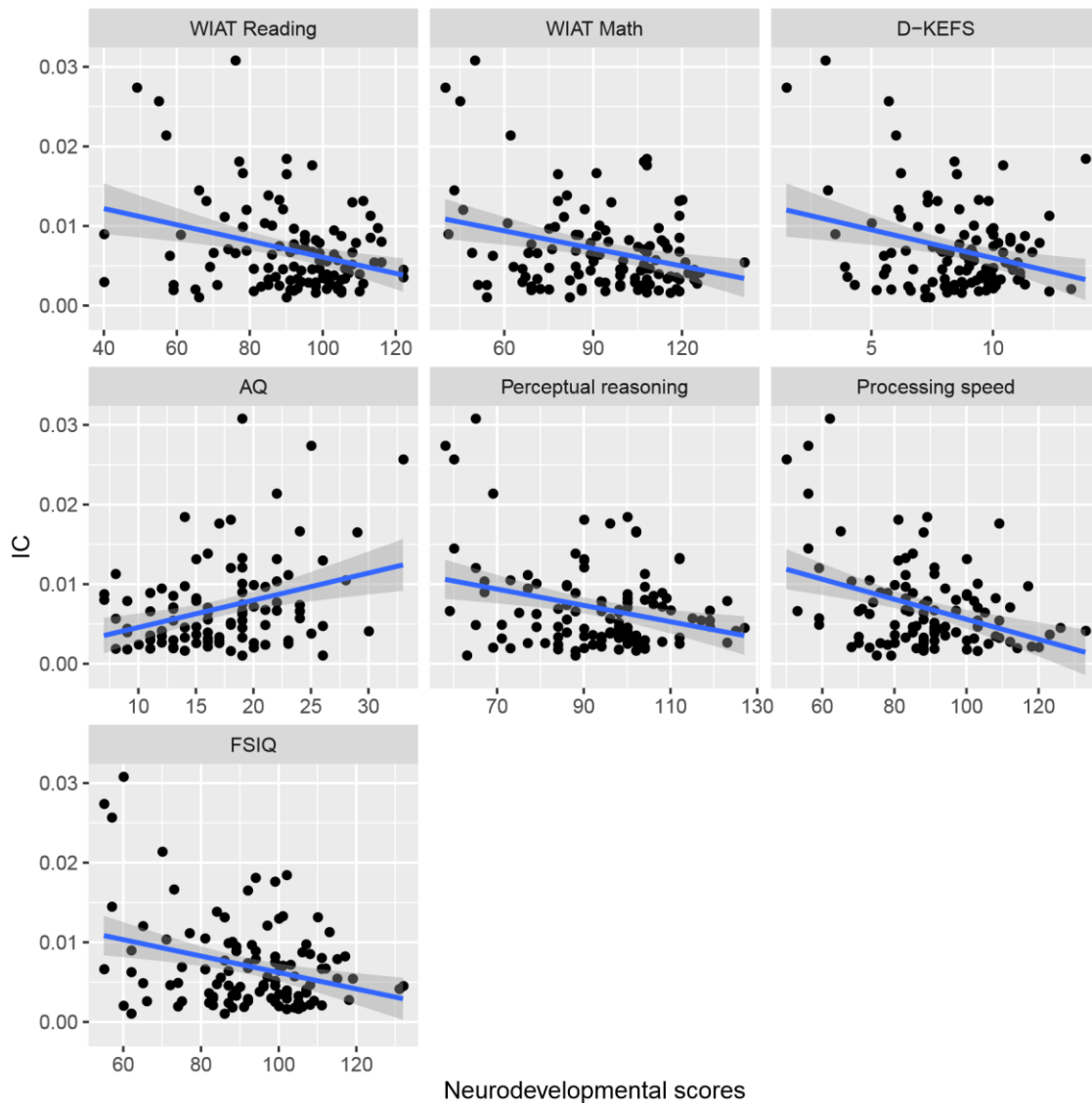


Figure 4.2: **Fontan IC (AOP) and neurodevelopmental outcomes.** Scatterplot of neurodevelopmental outcomes that are significantly (FDR-adjusted $p < 0.05$) associated to IC (AOP) in the Fontan group. The blue line is the best-fit line from a linear regression; the shaded regions represent 95% confidence intervals.

WIAT: Wechsler Individual Achievement Test; D-KEFS: Delis-Kaplan Executive Function System; AQ: Autism Spectrum Quotient; FSIQ: Full-Scale IQ

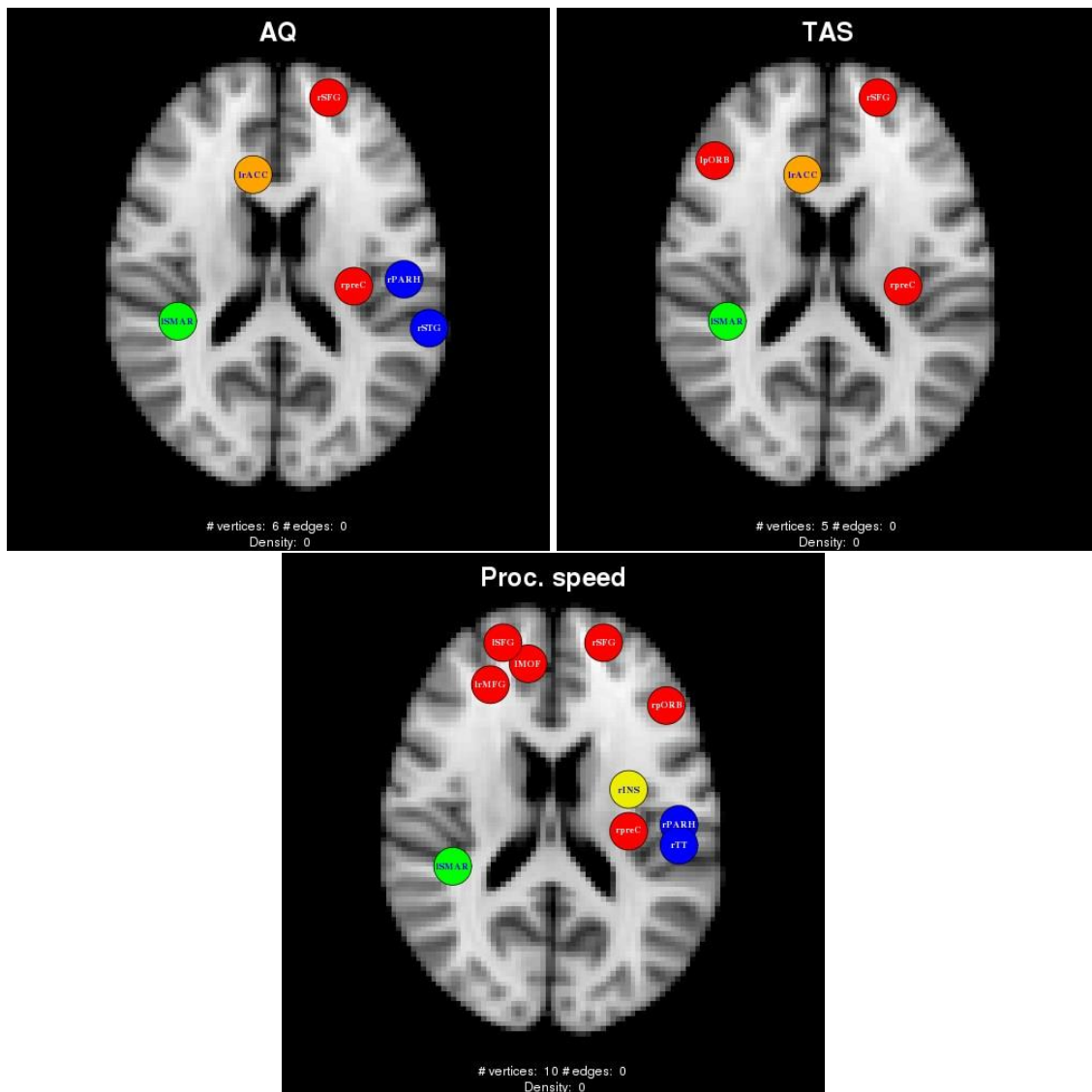


Figure 4.3: **Significant associations with RC (LOO)**. Each panel shows the vertices in which regional contribution (RC) was significantly ($p_{FDR} < 0.05$) associated with a specific neurodevelopmental outcome. Vertices are colored by lobe (red: frontal; green: parietal; blue: temporal; yellow: insula; orange: cingulate).

AQ: Autism Spectrum Quotient; TAS: Toronto Alexithymia Scale

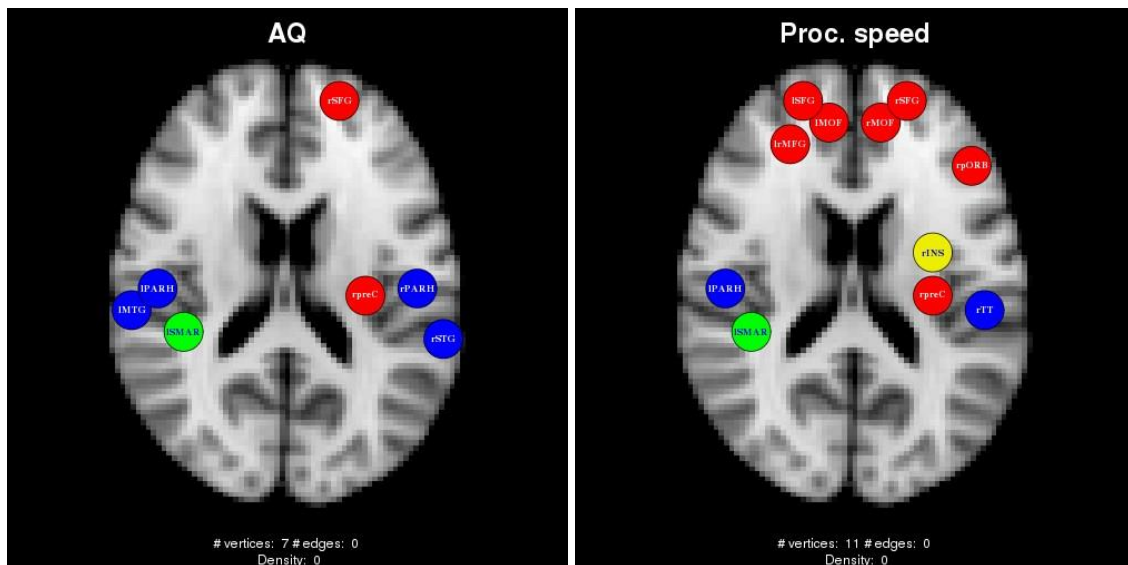


Figure 4.4: **Significant associations with RC (AOP)**. Each panel shows the vertices in which regional contribution (RC) was significantly ($p_{FDR} < 0.05$) associated with a specific neurodevelopmental outcome. Vertices are colored by lobe (red: frontal; green: parietal; blue: temporal; yellow: insula; orange: cingulate). AQ: Autism Spectrum Quotient

Outcome	Region	ACME (95% CI)	P-value
WIAT Reading	R transverse temporal	2.24 (0.72, 4.64)	0.004
	R caudal middle frontal gyrus	1.93 (0.68, 5.77)	0.004
	R pars opercularis	2.33 (1.09, 6.71)	<0.001
WIAT Math	R pallidum	4.84 (1.29, 10.13)	0.004
	R transverse temporal	3.20 (1.14, 6.29)	0.002
	R pars triangularis	2.48 (0.68, 5.91)	0.006
	R rostral middle frontal	4.47 (1.28, 8.57)	0.004
D-KEFS	R pallidum	0.58 (0.20, 1.10)	<0.001
	R transverse temporal	0.33 (0.11, 0.64)	0.002
TAS	L amygdala	-2.14 (-4.76, -0.58)	0.008
	L rostral anterior cingulate cortex	-4.22 (-7.83, -1.57)	0.004
Verbal comprehension	R transverse temporal	2.08 (0.81, 3.99)	0.002
Perceptual reasoning	R transverse temporal	1.59 (0.34, 3.63)	0.004
Processing speed	L amygdala	3.42 (1.19, 6.74)	0.002
	L rostral anterior cingulate cortex	5.14 (1.27, 10.07)	0.006
	R pallidum	4.19 (2.14, 6.78)	<0.001
FSIQ	L amygdala	3.93 (1.47, 8.47)	0.002
	R pars triangularis	1.73 (0.44, 4.32)	0.004

Table 4.7: **Mediation between weighted nodal efficiency and neurodevelopmental outcomes.** Neurodevelopmental outcomes for which *weighted nodal efficiency* was determined to be a significant mediator ($p < 0.01$), with subject group as the independent variable. The table shows point estimates for the causal mediation effect along with 95% confidence intervals and their associated P-values.

ACME: average causal mediation effect; CI: confidence interval; WIAT: Wechsler Individual Achievement Test; D-KEFS: Delis-Kaplan Executive Function System; TAS: Toronto Alexithymia Scale; FSIQ: Full-Scale IQ

Outcome	Region	ACME (95% CI)	P-value
WIAT Reading	R pallidum	-2.72 (-5.30, -0.96)	0.006
	R thalamus	-5.64 (-8.84, -2.82)	<0.001
WIAT Math	R caudate	-4.20 (-8.92, -1.54)	<0.001
	R pallidum	-3.72 (-7.27, -1.25)	0.002
	R thalamus	6.87 (-11.32, -3.06)	<0.001
D-KEFS	R pallidum	-0.40 (-0.75, -0.13)	0.006
	R thalamus	-0.76 (-1.22, -0.37)	<0.001
TVPS composite	R fusiform	-5.14 (-11.05, -1.69)	0.002
Verbal comprehension	R pallidum	-1.55 (-3.61, -0.35)	0.008
Perceptual reasoning	R pallidum	-2.64 (-5.32, -0.92)	<0.001
	R thalamus	-4.79 (-7.70, -1.92)	0.002
Processing speed	L superior frontal gyrus	-3.65 (-6.67, -1.36)	<0.001
	R pallidum	-2.81 (-5.57, -0.93)	0.002
	R thalamus	-5.88 (-9.74, -2.86)	<0.001
FSIQ	L superior frontal gyrus	-3.47 (-5.94, -1.10)	0.004
	R pallidum	-2.91 (-5.40, -0.88)	<0.001
	R thalamus	-5.62 (-9.03, -2.33)	<0.001

Table 4.8: **Mediation between strength and neurodevelopmental outcomes.** Neurodevelopmental outcomes for which *strength* was determined to be a significant mediator ($p < 0.01$), with subject group as the independent variable. The table shows point estimates for the causal mediation effect along with 95% confidence intervals and their associated P-values.

ACME: average causal mediation effect; CI: confidence interval; WIAT: Wechsler Individual Achievement Test; D-KEFS: Delis-Kaplan Executive Function System; TAS: Toronto Alexithymia Scale; FSIQ: Full-Scale IQ

Outcome	Region	ACME (95% CI)	P-value
WIAT Reading	R caudate	-2.38 (-5.39, -0.94)	0.002
	R pallidum	7.26 (3.04, 13.85)	<0.001
WIAT Math	L caudate	-4.83 (-9.03, -1.70)	<0.001
	R cuneus	-8.19 (-14.34, -4.39)	<0.001
	R pallidum	8.83 (3.32, 17.16)	0.002
D-KEFS	L caudate	-0.41 (-0.76, -0.12)	0.006
	R caudate	-0.32 (-0.60, -0.09)	0.008
	R pallidum	0.95 (0.34, 1.74)	0.004
Perceptual reasoning	L caudate	-2.41 (-4.98, -0.59)	0.008
	R pallidum	6.94 (2.99, 11.84)	<0.001
Processing speed	L caudate	-3.65 (-6.28, -1.67)	<0.001
	R pallidum	6.12 (2.65, 10.66)	<0.001
FSIQ	L caudate	-3.18 (-6.07, -1.13)	0.002
	R pallidum	7.02 (3.01, 12.12)	<0.001

Table 4.9: **Mediation between weighted local efficiency and neurodevelopmental outcomes.** Neurodevelopmental outcomes for which *weighted local efficiency* was determined to be a significant mediator ($p < 0.01$), with subject group as the independent variable. The table shows point estimates for the causal mediation effect along with 95% confidence intervals and their associated P-values.

ACME: average causal mediation effect; CI: confidence interval; WIAT: Wechsler Individual Achievement Test; D-KEFS: Delis-Kaplan Executive Function System; TAS: Toronto Alexithymia Scale; FSIQ: Full-Scale IQ

Discussion

Using linear models and causal mediation analyses to relate measures of brain structural connectivity with neurodevelopmental outcomes in children and adolescents who underwent the Fontan procedure, multiple areas of cognition and behavior were found to be significantly associated with overall contributions to structural covariance networks and with measures of network segregation and integration in white matter (WM) connectivity networks. Specifically, weighted global and local efficiency, modularity, and network strength were mediators for differences in general intelligence, academic achievement, and visuospatial function. In addition, local connectivity measures in multiple brain regions were shown to be associated with several of these neurodevelopmental outcomes. Poorer scores in the Fontan group for social/emotional cognition and processing speed were associated with network contribution bilaterally in frontal, parietal, and temporal lobe regions. The chosen outcome variables represent complex cognitive processes that require coordinated information processing across the brain. Overall, the results of these analyses show that brain structural connectivity is an important determinant of cognitive and behavioral function in single ventricle patients several years after the Fontan procedure. Strategies aimed at neuroprotection early in the perioperative period and early intervention should be emphasized in this patient group.

Patients with single ventricle (SV) heart defects show deficits in neurodevelopment beginning in infancy (Gaynor et al., 2015). These deficits continue to be present in childhood and into adolescence after the Fontan procedure is performed, and are accompanied by an increased use of special educational services and poorer

school performance (Bellinger et al., 2015; Forbess et al., 2001; Gaynor et al., 2014; Goldberg et al., 2014, 2000; Mahle et al., 2000; Wernovsky et al., 2000). As SV patients require multiple open-heart surgeries beginning as early as the neonatal period, in addition to further re-operation or catheterization procedures later in childhood, one explanation is that repeated exposure to cardiopulmonary bypass (CPB) results in brain injury that interferes with normal developmental processes (Agematsu et al., 2016, 2014; Ishibashi et al., 2012; Korotcova et al., 2015). On the other hand, abnormalities in brain structure, metabolism, blood flow, and growth have been demonstrated *in utero* and in the neonatal period, before any operations (Brossard-Racine et al., 2014; Clouchoux et al., 2013; Goff et al., 2014; Licht et al., 2009; Limperopoulos et al., 2010). Thus, it is likely that the brain immaturity in CHD neonates increases vulnerability to CPB-related injury experienced during cardiac surgery.

There are only a few reports of brain structure in SV patients after the Fontan procedure. At 5 years of age, 73% of patients had an abnormal MRI, with most lesions consistent with stroke or ischemic damage (Sarajuuri et al., 2012). The patients with the most extensive lesions had significantly worse neurodevelopmental outcomes compared to the SV patients with no/minor lesions. In an analysis of the present cohort, at age 10-19 years, we found that SV patients were 11 times more likely to have any MRI abnormality (66% vs. 6%) compared to the control group (Bellinger et al., 2015). Importantly, 13% of patients had evidence of a stroke. Associations of gross MRI abnormalities with neurodevelopmental outcomes were minor and only present between

focal infarction or atrophy and executive function, attention, and social cognition. We also performed more detailed analyses of brain structure in this cohort. In gray matter, cortical thickness and cortical and subcortical gray matter volume was significantly lower in the Fontan group throughout the brain (Watson et al., *manuscript under review*). These gray matter differences were associated with older age at first operation, total number of catheterizations, and total number of operative or catheterization complications. In white matter, measures of microstructure were different in most of the fiber tracts analyzed: fractional anisotropy (FA) and axial diffusivity (AD) were significantly lower and radial diffusivity (RD) was significantly higher in the Fontan group compared to controls. These were present bilaterally both in deep cerebral white matter and in cerebellar white matter (Watson et al., *manuscript in preparation*). We hypothesized that these differences were consistent with primary white matter injury that was pervasive and deep, and that included Wallerian degeneration to disrupt gray matter, as well. Furthermore, lower FA in the Fontan group was associated with more complications during the first operation, more operations, history of stroke, and history of any neurologic event. Taken together, these studies show that differences in brain structure are widespread, have long-term effects, and are common in the post-Fontan population.

In the present analysis, cortical thickness covariance was found to be significantly associated with neurodevelopmental outcomes in the Fontan group. *Individual contribution (IC)*, a measure representing global connectivity in the cortical thickness networks (Saggar et al., 2015), was significantly associated with scores in several neurodevelopmental domains, including academic achievement, executive function,

social cognition, and general intelligence. The direction of these relationships were such that patients with a higher IC (i.e., those who contribute more to the group network) have poorer scores. The outcomes of interest all represent broad measures of higher-order cognition and behavior, which rely on the integration of multiple connected brain regions. These results suggest that intact overall structural connectivity is important for normal cognitive functioning. Using a similar procedure to determine the contribution of individual brain regions, the most robust associations were between social cognition and processing speed present in brain regions of bilateral frontal, temporal, and parietal lobes.

In the white matter networks, measures of both global and regional connectivity were significant mediators between the relationship between subject group and neurodevelopmental outcome in several domains. The results of our mediation analyses suggest a causal link in which the well-documented deficits in cognitive and behavioral functioning in SV patients are dependent on white matter connectivity. We reported similar findings in adolescents with d-Transposition of the Great Arteries (d-TGA): lower global efficiency, higher modularity, and increased small-worldness were significant mediators of general intelligence, academic achievement, memory, executive function, and visuospatial function (Panigrahy et al., 2015). Furthermore, white matter connectivity mediated worse Attention Deficit Hyperactivity Disorder (ADHD) related outcomes, and both of these variables were affected differently in patients with different apolipoprotein E genotypes (Schmithorst et al., 2016). Although d-TGA is a different heart defect with different surgical course and outcomes, the results of these studies highlight the vital role that brain connectivity plays in the neurodevelopment of CHD patients.

Conclusions

The results of the present set of analyses show that impaired structural brain connectivity, in both gray and white matter and at the global and local levels, are predictive of poor functioning in high-level cognitive and behavioral domains. Children and adolescents with single ventricle who have undergone the Fontan procedure demonstrated patterns of aberrant brain connectivity in combination with significantly lower neurodevelopmental scores. Importantly, while interesting in their own right, these associations between brain organizational measures in both gray and white matter underscore the urgency for development of remedial treatments that take advantage of the greater cortical plasticity thought to exist in young children. Treatments and interventions that seek to restore or facilitate the normal developmental course are crucial to the improvement of the lives and reduction of cognitive morbidity in this group of children whose lives have been saved by surgical innovations of the last few decades.

CONCLUSIONS

The Fontan procedure, as well as staged palliation via the Norwood procedure for hypoplastic left heart syndrome (HLHS) and the bidirectional Glenn, represented major steps forward in the care of patients with single ventricle (SV) defects. Prior to the establishment of these procedures, survival was low: in HLHS patients, survival to 1 year of age was virtually 0%. More recently, the Single Ventricle Reconstruction Trial (SVRT) found that 3-year survival in HLHS patients was 64%; other groups have shown that 10 year survival is over 90% for all patients undergoing the Fontan procedure in the current era. Consequently, focus has turned progressively toward neurologic injury and its effects on neurodevelopmental outcomes in the aging SV population.

In this dissertation, I have presented the results from several analyses of children and adolescents (age 10-19 years) with SV defects who had undergone the Fontan procedure several years prior. In Chapter 2, I analyzed networks based on cortical thickness covariance to highlight differences both between a healthy control group and the Fontan group as a whole, and within the Fontan group, in which patients were stratified based on factors relating to their initial surgical procedure. The Fontan network was symmetric in its connections compared to a strong rightward asymmetry in the control group network. Furthermore, the distribution of hub regions (regions of high importance in a network context) showed almost no overlap across groups; the control group had predominantly right-hemispheric hubs. Several regions had significantly lower nodal efficiency and betweenness centrality (measures that represent information flow in networks) in the Fontan compared to the control group; again, most were in the

right hemisphere. Within the Fontan group, patients whose first operation was the Norwood had significantly lower betweenness centrality in several regions across both hemispheres and major lobes of the brain. These data show that the differences in gray matter covariance are, rather than being localized to one or a few brain regions, relatively widespread, and may be associated with surgical factors. In Chapter 3, I analyzed brain networks from diffusion tensor imaging (DTI) tractography data which, similar to the cortical thickness analysis, showed widespread differences in brain connectivity between groups. Once again, measures of brain connectivity were lower in the Fontan group compared to controls, both globally and locally in regions spanning all major lobes of the brain. Within the Fontan group, lower efficiency in several regions was associated with the Norwood operation and a greater number of complications in the initial operation. The regions involved were almost exclusively in frontal, temporal, cingulate, and medial cortical regions. Finally, in Chapter 4 I combined data from both the structural covariance and tractography networks along with several summary scores which measure major areas of cognitive and behavioral function. Fontan patients with a greater contribution to the structural covariance networks globally and locally had poorer neurodevelopmental outcomes in multiple domains. In the tractography networks, connectivity strength and efficiency were significant mediators of the relationship between subject group and neurodevelopmental outcomes. There was a strong tendency for the regions involved to be in frontal, temporal, and cingulate cortices along with subcortical gray matter. Similar to the results of the previous two chapters, the right hemisphere was more involved than the left.

A common theme arising from these analyses is that brain structural connectivity in post-Fontan children and adolescents tends to be more affected in the right hemisphere, and specifically in frontal, temporal, and medial cortical areas as well as the basal ganglia and thalamus. There was overlap, in associations with neurodevelopmental outcomes, between results from the gray matter covariance networks and white matter tractography networks. The probable cause in differences in brain structural connectivity in the single ventricle patient is likely to be cerebral injury that disrupts the normal trajectory of brain development due to impaired cerebral blood flow in concert with the deleterious effects of serial open heart procedures with cardiopulmonary bypass (CPB) exposure. There are known asymmetries in the vasculature and flow rates of the arteries that supply the brain with blood, such that blood flow in the right internal carotid artery is typically lower than in the left (Bogren et al., 1994). Furthermore, the affected cortical and subcortical regions are located at arterial border zones (for the cortical regions) and/or supplied by deep perforating arteries (in the case of the thalamus and basal ganglia) (Mangla et al., 2011; Tatu et al., 1998). These regions tend to be most prone to hypoxic-ischemic damage (Moody et al., 1990). Thus, it is possible that, since right carotid blood flow is lower than left, hypoperfusion leads to a more pronounced drop in cerebral oxygen delivery in the right hemisphere in SV patients. Exposure to CPB causes white matter (WM) damage, particularly among immature oligodendrocytes (Agematsu et al., 2014; Ishibashi et al., 2012). Hypoxic-ischemic damage also has secondary consequences in gray matter (GM), manifest in the loss of thalamocortical connectivity (Ishibashi et al., 2010; Leviton and Gressens, 2007; McQuillen and Ferriero, 2005). The

present analyses were not designed to be able to determine the timing of any brain injury, but given other reports in the literature, I hypothesize that initial injury likely occurred in the pre/perinatal period, and additional injuries may have resulted from factors related to neonatal open heart surgeries.

There are some general methodological considerations that should be kept in mind. First, brain MRI data do not directly measure actual neural connectivity. The structural covariance networks are based on statistical calculations, and the DTI tractography networks are based on measurements of water molecule diffusion. Thus, false positive and negative connections will always be present and these data can only be considered an approximation of the true underlying structural network. Second, network construction and comparison is not standardized in the neuroimaging literature; there are no guidelines or “best practices” as there are in functional MRI (Poldrack et al., 2008), magnetoencephalography (Gross et al., 2013), or volumetric MRI analysis (Ridgway et al., 2008). The choice of parcellation varies in number and size of regions, and may affect some measures (Bassett et al., 2011; Zalesky et al., 2010b). In structural covariance networks, a range of thresholds typically is applied to match network densities between groups. This means that the thresholds differ between groups, and the network of one group may contain statistically weaker connections (correlations) than the other group. One proposed solution is to integrate the subsequent network measures over the entire range of densities (Ginestet et al., 2011). For DTI (or other multi-subject) networks, the resulting networks can differ along (at least) two dimensions: the choice of initial matrix threshold (e.g., normalize streamline counts by ROI volumes), and the

choice of a group threshold (e.g., keep only connections that are present in at least 50% of subjects). The resultant network measures do not vary linearly across possible threshold choices (data not shown). Third, the number of statistical comparisons in this dissertation is very high, which comes with a risk of false positives due to multiple comparisons. Some of the reported P-values were adjusted for multiple comparisons (cortical thickness permutations of vertex-level measures, DTI network global- and vertexlevel measures, individual and regional contributions in cortical thickness networks), but other analyses report only uncorrected P-values (DTI regressions and mediation analyses). These results should be considered preliminary, and further investigation, possibly with a more homogeneous cohort, is warranted.

Overall, this work reinforces the large body of literature showing neurodevelopmental and structural brain deficits in children with SV defects. It adds significantly to the field in several ways. First, this is the largest cohort of CHD patients—at any age and any CHD type—from whom detailed, quantitative MRI data have been acquired. Second, the patient group comprises only those who have a SV defect and who had undergone Fontan palliation prior to study enrollment, as opposed to a group consisting of patients with a multitude of CHD types. Third, the Fontan patients also underwent several hours of neuropsychological testing, completed behavioral questionnaires, and underwent genetic evaluation. Much of the literature on neurodevelopment in SV patients addresses only one or a few testing domains. Finally, this is the only series of studies to obtain all of these forms of data in patients who are nearing the end of development, into late adolescence. These studies were not designed

to determine whether the observed differences are due to pre/perinatal physiology, genetics, or the patients' surgical course, but it is likely that there is a complex interaction between all of these factors.

The main conclusion that may be drawn is that events occurring very early in development have long-term, detrimental effects on SV patients' lives. Diagnosis early in gestation should be a goal of clinicians so that early intervention can begin when brain development increases rapidly. Fetal interventions aimed at restoring a normal level of cerebral blood flow may have the best outcomes by facilitating normal brain growth and minimizing the potential for white matter injury. Earlier diagnosis will also allow for better preparation for and planning of the patient's surgical course. More complete understanding of how the timings of Stage I, Stage II, and the Fontan operation affect brain development would better inform clinical decisions. Finally, perioperative management is of paramount importance, as is the minimization of any surgical complications and the number of procedures the patient undergoes.

BIBLIOGRAPHY

- Abu-Rustum, R. S., Ziade, M. F., Abu-Rustum, S. E., and Daou, L. S. (2016). Are there head volume alterations at 11 to 14 weeks in fetuses with congenital heart defects? a first trimester case series. *American Journal of Perinatology Reports*, 6(02):e232–e238.
- Achard, S. and Bullmore, E. (2007). Efficiency and cost of economical brain functional networks. *PLoS Computational Biology*, 3(2):e17.
- Achard, S., Salvador, R., Whitcher, B., Suckling, J., and Bullmore, E. (2006). A resilient, low-frequency, small-world human brain functional network with highly connected association cortical hubs. *The Journal of Neuroscience*, 26(1):63–72.
- Agematsu, K., Korotcova, L., Morton, P. D., Gallo, V., Jonas, R. A., and Ishibashi, N. (2016). Hypoxia diminishes the protective function of white-matter astrocytes in the developing brain. *The Journal of Thoracic and Cardiovascular Surgery*, 151(1):265–272.
- Agematsu, K., Korotcova, L., Scafidi, J., Gallo, V., Jonas, R. A., and Ishibashi, N. (2014). Effects of preoperative hypoxia on white matter injury associated with cardiopulmonary bypass in a rodent hypoxic and brain slice model. *Pediatric Research*, 75(5):618–625.
- Albert, R., Jeong, H., and Barabasi, A.-L. (2000). Error and attack tolerance of complex networks. *Nature*, 406(6794):378–382.
- Alexander-Bloch, A., Giedd, J. N., et al. (2013a). Imaging structural co-variance between human brain regions. *Nature Reviews Neuroscience*, 14(5):322–336.
- Alexander-Bloch, A., Raznahan, A., Bullmore, E., and Giedd, J. (2013b). The convergence of maturational change and structural covariance in human cortical networks. *The Journal of Neuroscience*, 33(7):2889–2899.
- Alexander-Bloch, A. F., Vertes, P. E., Stidd, R., Lalonde, F., Clasen, L., Rapoport, J., Giedd, J., Bullmore, E. T., and Gogtay, N. (2013c). The anatomical distance of functional connections predicts brain network topology in health and schizophrenia. *Cerebral Cortex*, 23(1):127–138.
- Algra, S. O., Jansen, N. J., van der Tweel, I., Schouten, A. N., Groenendaal, F., Toet, M., van Oeveren, W., van Haastert, I. C., Schoof, P. H., de Vries, L. S., et al. (2014).

- Neurological injury after neonatal cardiac surgery. a randomized, controlled trial of 2 perfusion techniques. *Circulation*, 129(2):224–233.
- Allan, C. K., Newburger, J. W., McGrath, E., Elder, J., Psinos, C., Laussen, P. C., Pedro, J., Wypij, D., and McGowan Jr, F. X. (2010). The relationship between inflammatory activation and clinical outcome after infant cardiopulmonary bypass. *Anesthesia & Analgesia*, 111(5):1244–1251.
- Almli, C., Rivkin, M., and McKinstry, R. (2007). The NIH MRI study of normal brain development (Objective-2): newborns, infants, toddlers, and preschoolers. *NeuroImage*, 35(1):308–325.
- Anderson, J. B., Beekman, R. H., Kugler, J. D., Rosenthal, G. L., Jenkins, K. J., Klitzner, T. S., Martin, G. R., Neish, S. R., Brown, D. W., Mangeot, C., et al. (2015). Improvement in interstage survival in a national pediatric cardiology learning network. *Circulation: Cardiovascular Quality and Outcomes*, 8(4):428–436.
- Anderson, P. A., Sleeper, L. A., Mahony, L., Colan, S. D., Atz, A. M., Breitbart, R. E., Gersony, W. M., Gallagher, D., Geva, T., Margossian, R., et al. (2008). Contemporary outcomes after the Fontan procedure: a Pediatric Heart Network multicenter study. *Journal of the American College of Cardiology*, 52(2):85–98.
- Andescavage, N., Yarish, A., Donofrio, M., Bulas, D., Evangelou, I., Vezina, G., McCarter, R., Limperopoulos, C., et al. (2015). 3-d volumetric MRI evaluation of the placenta in fetuses with complex congenital heart disease. *Placenta*, 36(9):1024–1030.
- Andreotti, J., Jann, K., Melie-Garcia, L., Giezendanner, S., Dierks, T., and Federspiel, A. (2014). Repeatability analysis of global and local metrics of brain structural networks. *Brain Connectivity*, 4(3):203–220.
- Andropoulos, D., Ahmad, H., Haq, T., Brady, K., Stayer, S., Meador, M., Hunter, J., Rivera, C., Voigt, R., Turcich, M., He, C., Shekerdemian, L., Dickerson, H., Fraser, C., McKenzie, E., Heinle, J., and Easley, R. (2014). The association between brain injury, perioperative anesthetic exposure, and 12-month neurodevelopmental outcomes after neonatal cardiac surgery: a retrospective cohort study. *Pediatric Anesthesia*, 24(3):266–274.
- Andropoulos, D. B., Hunter, J. V., Nelson, D. P., Stayer, S. A., Stark, A. R., McKenzie, E. D., Heinle, J. S., Graves, D. E., and Fraser, C. D. (2010). Brain immaturity is associated with brain injury before and after neonatal cardiac surgery with high-flow bypass and cerebral oxygenation monitoring. *The Journal of Thoracic and Cardiovascular Surgery*, 139(3):543–556.

- Atz, A. M., Travison, T. G., Williams, I. A., Pearson, G. D., Laussen, P. C., Mahle, W. T., Cook, A. L., Kirsh, J. A., Sklansky, M., Khaikin, S., et al. (2010). Prenatal diagnosis and risk factors for preoperative death in neonates with single right ventricle and systemic outflow obstruction: Screening data from the Pediatric Heart Network Single Ventricle Reconstruction Trial. *The Journal of Thoracic and Cardiovascular Surgery*, 140(6):1245–1250.
- Atz, A. M., Zak, V., Mahony, L., Uzark, K., Shrader, P., Gallagher, D., Paridon, S. M., Williams, R. V., Breitbart, R. E., Colan, S. D., et al. (2015). Survival data and predictors of functional outcome an average of 15 years after the Fontan procedure: the Pediatric Heart Network Fontan cohort. *Congenital Heart Disease*, 10(1):E30–E42.
- Azadbakht, H., Parkes, L. M., Haroon, H. A., Augath, M., Logothetis, N. K., de Crespigny, A., D'Arceuil, H. E., and Parker, G. J. (2015). Validation of high-resolution tractography against in vivo tracing in the macaque visual cortex. *Cerebral Cortex*, 25(11):4299–4309.
- Azaki, A., McCrindle, B. W., Van Arsdell, G., Benson, L. N., Coles, J., Hamilton, R., Freedom, R. M., and Williams, W. G. (2001). Extracardiac conduit versus lateral tunnel cavopulmonary connections at a single institution: impact on outcomes. *The Journal of Thoracic and Cardiovascular Surgery*, 122(6):1219–1228.
- Bagby, R. M., Parker, J. D., and Taylor, G. J. (1994). The twenty-item Toronto Alexithymia Scale—I. item selection and cross-validation of the factor structure. *Journal of Psychosomatic Research*, 38(1):23–32.
- Bansal, S., Khandelwal, S., and Meyers, L. A. (2009). Exploring biological network structure with clustered random networks. *BMC Bioinformatics*, 10(1):405.
- Baron, R. M. and Kenny, D. A. (1986). The moderator–mediator variable distinction in social psychological research: Conceptual, strategic, and statistical considerations. *Journal of Personality and Social Psychology*, 51(6):1173.
- Baron-Cohen, S., Wheelwright, S., Skinner, R., Martin, J., and Clubley, E. (2001). The autism-spectrum quotient (AQ): Evidence from asperger syndrome/high-functioning autism, males and females, scientists and mathematicians. *Journal of Autism and Developmental Disorders*, 31(1):5–17.
- Bassett, D. S., Brown, J. A., Deshpande, V., Carlson, J. M., and Grafton, S. T. (2011). Conserved and variable architecture of human white matter connectivity. *NeuroImage*, 54(2):1262–1279.

- Bassett, D. S., Bullmore, E., Verchinski, B. A., Mattay, V. S., Weinberger, D. R., and Meyer-Lindenberg, A. (2008). Hierarchical organization of human cortical networks in health and schizophrenia. *The Journal of Neuroscience*, 28(37):9239–9248.
- Bastiani, M., Shah, N. J., Goebel, R., and Roebroek, A. (2012). Human cortical connectome reconstruction from diffusion weighted MRI: the effect of tractography algorithm. *NeuroImage*, 62(3):1732–1749.
- Beaulieu, C. (2002). The basis of anisotropic water diffusion in the nervous system—a technical review. *NMR in Biomedicine*, 15(7-8):435–455.
- Beca, J., Gunn, J. K., Coleman, L., Hope, A., Reed, P. W., Hunt, R. W., Finucane, K., Brizard, C., Dance, B., and Shekerdemian, L. S. (2013). New white matter brain injury after infant heart surgery is associated with diagnostic group and the use of circulatory arrest. *Circulation*, 127(9):971–979.
- Behrens, T., Berg, H. J., Jbabdi, S., Rushworth, M., and Woolrich, M. (2007). Probabilistic diffusion tractography with multiple fibre orientations: What can we gain? *NeuroImage*, 34(1):144–155.
- Behrens, T., Woolrich, M., Jenkinson, M., Johansen-Berg, H., Nunes, R., Clare, S., Matthews, P., Brady, J., and Smith, S. (2003). Characterization and propagation of uncertainty in diffusion-weighted MR imaging. *Magnetic Resonance in Medicine*, 50(5):1077–1088.
- Bellinger, D. C., Jonas, R. A., Rappaport, L. A., Wypij, D., Wernovsky, G., Kuban, K. C., Barnes, P. D., Holmes, G. L., Hickey, P. R., Strand, R. D., et al. (1995). Developmental and neurologic status of children after heart surgery with hypothermic circulatory arrest or low-flow cardiopulmonary bypass. *New England Journal of Medicine*, 332(9):549–555.
- Bellinger, D. C., Watson, C. G., Rivkin, M. J., Robertson, R. L., Roberts, A. E., Stopp, C., Dunbar-Masterson, C., Bernson, D., DeMaso, D. R., Wypij, D., et al. (2015). Neuropsychological status and structural brain imaging in adolescents with single ventricle who underwent the Fontan procedure. *Journal of the American Heart Association*, 4(12):e002302.
- Bellinger, D. C., Wypij, D., duPlessis, A. J., Rappaport, L. A., Jonas, R. A., Wernovsky, G., and Newburger, J. W. (2003). Neurodevelopmental status at eight years in children with dextro-transposition of the great arteries: the boston circulatory arrest trial. *The Journal of Thoracic and Cardiovascular Surgery*, 126(5):1385–1396.

- Bellinger, D.C., Wypij, D., Kuban, K.C., Rappaport, L.A., Hickey, P.R., Wernovsky, G., Jonas, R.A., and Newburger, J.W. (1999). Developmental and neurological status of children at 4 years of age after heart surgery with hypothermic circulatory arrest or low-flow cardiopulmonary bypass. *Circulation*, 100(5):526–532.
- Bellinger, D.C., Wypij, D., Rivkin, M.J., DeMaso, D.R., Robertson, R.L., DunbarMasterson, C., Rappaport, L.A., Wernovsky, G., Jonas, R.A., and Newburger, J.W. (2011). Adolescents with d-transposition of the great arteries corrected with the arterial switch procedure neuropsychological assessment and structural brain imaging. *Circulation*, 124(12):1361–1369.
- Berg, C., Gembruch, O., Gembruch, U., and Geipel, A. (2009). Doppler indices of the middle cerebral artery in fetuses with cardiac defects theoretically associated with impaired cerebral oxygen delivery in utero: is there a brain-sparing effect? *Ultrasound in Obstetrics & Gynecology*, 34(6):666–672.
- Bernhardt, B.C., Chen, Z., He, Y., Evans, A.C., and Bernasconi, N. (2011). Graphtheoretical analysis reveals disrupted small-world organization of cortical thickness correlation networks in temporal lobe epilepsy. *Cerebral Cortex*, 21(9):2147–2157.
- Blalock, A. and Taussig, H. B. (1945). The surgical treatment of malformations of the heart: in which there is pulmonary stenosis or pulmonary atresia. *Journal of the American Medical Association*, 128(3):189–202.
- Block, A., McQuillen, P., Chau, V., Glass, H., Poskitt, K., Barkovich, A., Esch, M., Soulikias, W., Azakie, A., Campbell, A., et al. (2010). Clinically silent preoperative brain injuries do not worsen with surgery in neonates with congenital heart disease. *The Journal of Thoracic and Cardiovascular Surgery*, 140(3):550–557.
- Blondel, V.D., Guillaume, J.-L., Lambiotte, R., and Lefebvre, E. (2008). Fast unfolding of communities in large networks. *Journal of Statistical Mechanics: Theory and Experiment*, 2008(10):P10008.
- Bogren, H.G., Buonocore, M.H., and Gu, W.Z. (1994). Carotid and vertebral artery blood flow in left- and right-handed healthy subjects measured with MR velocity mapping. *Journal of Magnetic Resonance Imaging*, 4(1):37-42.
- Bohlken, M.M., Brouwer, R.M., Mandl, R.C., Van den Heuvel, M.P., Hedman, A.M., De Hert, M., Cahn, W., Kahn, R.S., and Pol, H.E.H. (2016). Structural brain connectivity as a genetic marker for schizophrenia. *JAMA Psychiatry*, 73(1):11–19.

- Branthwaite, M. (1972). Neurological damage related to open-heart surgery: a clinical survey. *Thorax*, 27(6):748–753.
- Bridges, N., Lock, J., and Castaneda, A. (1990). Baffle fenestration with subsequent transcatheter closure. modification of the Fontan operation for patients at increased risk. *Circulation*, 82(5):1681–1689.
- Bridges, N.D., Mayer, J., Lock, J., Jonas, R., Hanley, F., Keane, J., Perry, S., and Castaneda, A. (1992). Effect of baffle fenestration on outcome of the modified Fontan operation. *Circulation*, 86(6):1762–1769.
- Brossard-Racine, M., du Plessis, A., Vezina, G., Robertson, R., Donofrio, M., Tworetzky, W., and Limperopoulos, C. (2016). Brain injury in neonates with complex congenital heart disease: what is the predictive value of MRI in the fetal period? *American Journal of Neuroradiology*.
- Brossard-Racine, M., Du Plessis, A.J., Vezina, G., Robertson, R., Bulas, D., Evangelou, I.E., Donofrio, M., Freeman, D., and Limperopoulos, C. (2014). Prevalence and spectrum of in utero structural brain abnormalities in fetuses with complex congenital heart disease. *American Journal of Neuroradiology*, 35(8):1593–1599.
- Buchanan, C.R., Pernet, C.R., Gorgolewski, K.J., Storkey, A.J., and Bastin, M.E. (2014). Test–retest reliability of structural brain networks from diffusion MRI. *NeuroImage*, 86:231–243.
- Calabrese, E., Badea, A., Cofer, G., Qi, Y., and Johnson, G. A. (2015). A diffusion MRI tractography connectome of the mouse brain and comparison with neuronal tracer data. *Cerebral Cortex*, 25(11):4628–4637.
- Camposilvan, S., Milanese, O., Stellin, G., Petteazzo, A., Zancan, L., and D’Antiga, L. (2008). Liver and cardiac function in the long term after Fontan operation. *The Annals of Thoracic Surgery*, 86(1):177–182.
- Cao, Q., Shu, N., An, L., Wang, P., Sun, L., Xia, M.-R., Wang, J.-H., Gong, G.-L., Zang, Y.-F., Wang, Y.-F., et al. (2013). Probabilistic diffusion tractography and graph theory analysis reveal abnormal white matter structural connectivity networks in drug-naïve boys with attention deficit/hyperactivity disorder. *The Journal of Neuroscience*, 33(26):10676–10687.
- Carey, A.S., Liang, L., Edwards, J., Brandt, T., Mei, H., Sharp, A.J., Hsu, D.T., Newburger, J.W., Ohye, R.G., Chung, W.K., et al. (2013). The impact of CNVs on

- outcomes for infants with single ventricle heart defects. *Circulation: Cardiovascular Genetics*, 6(5):444–451.
- Chen, Z., Liu, M., Gross, D., and Beaulieu, C. (2013). Graph theoretical analysis of developmental patterns of the white matter network. *Frontiers in Human Neuroscience*, 7(716).
- Chen, Z.J., He, Y., Rosa-Neto, P., Germann, J., and Evans, A.C. (2008). Revealing modular architecture of human brain structural networks by using cortical thickness from MRI. *Cerebral Cortex*, 18(10):2374–2381.
- Childs, A.-M., Ramenghi, L.A., Cornette, L., Tanner, S.F., Arthur, R.J., Martinez, D., and Levene, M.I. (2001). Cerebral maturation in premature infants: quantitative assessment using MR imaging. *American Journal of Neuroradiology*, 22(8):1577–1582.
- Clarkson, P., MacArthur, B., Barratt-Boyes, B., Whitlock, R., and Neutze, J. (1980). Developmental progress after cardiac surgery in infancy using hypothermia and circulatory arrest. *Circulation*, 62(4):855–861.
- Clauset, A., Newman, M.E., and Moore, C. (2004). Finding community structure in very large networks. *Physical Review E*, 70(6):066111.
- Clouchoux, C., du Plessis, A., Bouyssi-Kobar, M., Tworetzky, W., McElhinney, D., Brown, D., Gholipour, A., Kudelski, D., Warfield, S., McCarter, R., et al. (2013). Delayed cortical development in fetuses with complex congenital heart disease. *Cerebral Cortex*, 23(12):2932–2943.
- Cnota, J.F., Hangge, P.T., Wang, Y., Woo, J.G., Hinton, A. C., Divanovic, A. A., Michelfelder, E. C., and Hinton, R. B. (2013). Somatic growth trajectory in the fetus with hypoplastic left heart syndrome. *Pediatric Research*, 74(3):284–289.
- Coats, L., O'Connor, S., Wren, C., and O'Sullivan, J. (2014). The single-ventricle patient population: a current and future concern a population-based study in the North of England. *Heart*, 100(17):1348–1353.
- Cohen, M.S., Schultz, A.H., Tian, Z.-Y., Donaghue, D.D., Weinberg, P.M., Gaynor, J.W., and Rychik, J. (2006). Heterotaxy syndrome with functional single ventricle: does prenatal diagnosis improve survival? *The Annals of Thoracic Surgery*, 82(5):1629–1636.
- Cohen, M. S., Zak, V., Atz, A. M., Printz, B. F., Pinto, N., Lambert, L., Pemberton, V., Li, J. S., Margossian, R., Dunbar-Masterson, C., et al. (2010). Anthropometric

- measures after Fontan procedure: implications for suboptimal functional outcome. *American Heart Journal*, 160(6):1092–1098.
- Conners, C.K. (2004). *Conners' rating scales-revised: CRS-R*. MHS, Multi-Health Systems.
- Crossley, N. A., Mechelli, A., Scott, J., Carletti, F., Fox, P. T., McGuire, P., and Bullmore, E. T. (2014). The hubs of the human connectome are generally implicated in the anatomy of brain disorders. *Brain*, 137(8):2382–2395.
- Csardi, G. and Nepusz, T. (2006). The igraph software package for complex network research. *InterJournal, Complex Systems*, 1695(5):1–9.
- Dabal, R. J., Kirklin, J. K., Kukreja, M., Brown, R. N., Cleveland, D. C., Eddins, M. C., and Lau, Y. (2014). The modern Fontan operation shows no increase in mortality out to 20 years: A new paradigm. *The Journal of Thoracic and Cardiovascular Surgery*, 148(6):2517–2524.
- Dale, A. M., Fischl, B., and Sereno, M. I. (1999). Cortical surface-based analysis: I. segmentation and surface reconstruction. *NeuroImage*, 9(2):179–194.
- de Leval, M. R., Kilner, P., Gewillig, M., and Bull, C. (1988). Total cavopulmonary connection: a logical alternative to atriopulmonary connection for complex fontan operations. *The Journal of Thoracic and Cardiovascular Surgery*, 96(5):682–695.
- de Reus, M. A. and van den Heuvel, M. P. (2013a). Estimating false positives and negatives in brain networks. *NeuroImage*, 70:402–409.
- de Reus, M. A. and van den Heuvel, M. P. (2013b). Rich club organization and intermodule communication in the cat connectome. *The Journal of Neuroscience*, 33(32):12929–12939.
- Dehaes, M., Cheng, H. H., Buckley, E. M., Lin, P.-Y., Ferradal, S., Williams, K., Vyas, R., Hagan, K., Wigmore, D., McDavitt, E., et al. (2015). Perioperative cerebral hemodynamics and oxygen metabolism in neonates with single-ventricle physiology. *Biomedical Optics Express*, 6(12):4749–4767.
- Delis, D. C., Kaplan, E., and Kramer, J. H. (2001). *Delis-Kaplan executive function system (D-KEFS)*. Psychological Corporation.
- DeMaso, D. R., Labella, M., Taylor, G. A., Forbes, P. W., Stopp, C., Bellinger, D. C., Rivkin, M. J., Wypij, D., and Newburger, J. W. (2014). Psychiatric disorders and

- function in adolescents with d-transposition of the great arteries. *The Journal of Pediatrics*, 165(4):760–766.
- Dent, C.L., Spaeth, J.P., Jones, B.V., Schwartz, S.M., Glauser, T.A., Hallinan, B., Pearl, J.M., Khoury, P.R., and Kurth, C.D. (2006). Brain magnetic resonance imaging abnormalities after the Norwood procedure using regional cerebral perfusion. *The Journal of Thoracic and Cardiovascular Surgery*, 131(1):190–197.
- Diaz, L.K., Gaynor, J.W., Koh, S.J., Ittenbach, R.F., Gerdes, M., Bernbaum, J.C., Zackai, E.H., Clancy, R.R., Rehman, M.A., Pennington, J.W., et al. (2016). Increasing cumulative exposure to volatile anesthetic agents is associated with poorer neurodevelopmental outcomes in children with hypoplastic left heart syndrome. *The Journal of Thoracic and Cardiovascular Surgery*.
- Dick, M., Fyler, D.C., and Nadas, A.S. (1975). Tricuspid atresia: clinical course in 101 patients. *The American Journal of Cardiology*, 36(3):327–337.
- Dimitropoulos, A., McQuillen, P.S., Sethi, V., Moosa, A., Chau, V., Xu, D., Brant, R., Azakie, A., Campbell, A., Barkovich, A.J., et al. (2013). Brain injury and development in newborns with critical congenital heart disease. *Neurology*, 81(3):241–248.
- Donofrio, M., Bremer, Y., Schieken, R., Gennings, C., Morton, L., Eidem, B., Cetta, F., Falkensammer, C., Huhta, J., and Kleinman, C. (2003). Autoregulation of cerebral blood flow in fetuses with congenital heart disease: the brain sparing effect. *Pediatric Cardiology*, 24(5):436–443.
- Driscoll, D.J., Offord, K.P., Feldt, R.H., Schaff, H.V., Puga, F.J., and Danielson, G.K. (1992). Five- to fifteen-year follow-up after Fontan operation. *Circulation*, 85(2):469–496.
- d’Udekem, Y., Iyengar, A.J., Galati, J.C., Forsdick, V., Weintraub, R.G., Wheaton, G.R., Bullock, A., Justo, R.N., Grigg, L.E., Sholler, G.F., et al. (2014). Redefining expectations of long-term survival after the Fontan procedure twenty-five years of followup from the entire population of Australia and New Zealand. *Circulation*, 130(11 suppl 1):S32–S38.
- Dyrby, T. B., Sogaard, L. V., Parker, G. J., Alexander, D. C., Lind, N. M., Baare, W. F., Hay-Schmidt, A., Eriksen, N., Pakkenberg, B., Paulson, O.B., et al. (2007). Validation of in vitro probabilistic tractography. *NeuroImage*, 37(4):1267–1277.
- Efron, B. (1987). Better bootstrap confidence intervals. *Journal of the American Statistical Association*, 82(397):171–185.

- Evans, A. (2006). The NIH MRI study of normal brain development. *NeuroImage*, 30(1):184–202.
- Evans, A. C. (2013). Networks of anatomical covariance. *NeuroImage*, 80:489–504.
- Fahed, A. C., Gelb, B. D., Seidman, J., and Seidman, C. E. (2013). Genetics of congenital heart disease: The glass half empty. *Circulation Research*, 112(4):707–720.
- Fan, Y., Shi, F., Smith, J. K., Lin, W., Gilmore, J. H., and Shen, D. (2011). Brain anatomical networks in early human brain development. *NeuroImage*, 54(3):1862–1871.
- Feinstein, J. A., Benson, D. W., Dubin, A. M., Cohen, M. S., Maxey, D. M., Mahle, W. T., Pahl, E., Villafane, J., Bhatt, A. B., Peng, L. F., et al. (2012). Hypoplastic left heart syndrome: current considerations and expectations. *Journal of the American College of Cardiology*, 59(1s1):S1–S42.
- Feldt, R. H., Driscoll, D. J., Offord, K. P., Cha, R. H., Perrault, J., Schaff, H. V., Puga, F. J., and Danielson, G. K. (1996). Protein-losing enteropathy after the Fontan operation. *The Journal of Thoracic and Cardiovascular Surgery*, 112(3):672–680.
- Ferry, P. C. (1990). Neurologic sequelae of open-heart surgery in children: An 'irritating question'. *American Journal of Diseases of Children*, 144(3):369–373.
- Fiore, A. C., Turrentine, M., Rodefeld, M., Vijay, P., Schwartz, T. L., Virgo, K. S., Fischer, L. K., and Brown, J. W. (2007). Fontan operation: a comparison of lateral tunnel with extracardiac conduit. *The Annals of Thoracic Surgery*, 83(2):622–630.
- Fischl, B. and Dale, A. (2000). Measuring the thickness of human cerebral cortex from magnetic resonance images. *Proceedings of the National Academy of Sciences*, 97:11044–11049.
- Fischl, B., Sereno, M., and Dale, A. (1999). Cortical surface-based analysis ii: Inflation, flattening, and a surface-based coordinate system. *NeuroImage*, 9:195–207.
- Fischl, B., van der Kouwe, A., Destrieux, C., Halgren, E., Segonne, F., Salat, D., Busa, E., Seidman, L., Goldstein, J., Kennedy, D., Caviness, V., Makris, N., Rosen, B., and Dale, A. (2004). Automatically parcellating the human cerebral cortex. *Cerebral Cortex*, 14:11–22.
- Fontan, F. and Baudet, E. (1971). Surgical repair of tricuspid atresia. *Thorax*, 26(3):240–248.

- Fontan, F., Kirklin, J., Fernandez, G., Costa, F., Naftel, D., Tritto, F., and Blackstone, E. (1990). Outcome after a "perfect" Fontan operation. *Circulation*, 81(5):1520–1536.
- Forbess, J. M., Visconti, K. J., Bellinger, D. C., and Jonas, R. A. (2001). Neurodevelopmental outcomes in children after the Fontan operation. *Circulation*, 104(Suppl 1):I-127.
- Forbess, J. M., Visconti, K. J., Hancock-Friesen, C., Howe, R. C., Bellinger, D. C., and Jonas, R. A. (2002). Neurodevelopmental outcome after congenital heart surgery: results from an institutional registry. *Circulation*, 106(12 suppl 1):1–95.
- Fountain, D. M., Schaer, M., Mutlu, A. K., Schneider, M., Debbane, M., and Eliez, S. (2014). Congenital heart disease is associated with reduced cortical and hippocampal volume in patients with 22q11.2 deletion syndrome. *Cortex*, 57:128–142.
- Freed, M. D., Heymann, M. A., Lewis, A. B., Roehl, S. L., and Kensey, R. C. (1981). Prostaglandin E1 infants with ductus arteriosus-dependent congenital heart disease. *Circulation*, 64(5):899–905.
- Friesen, C. L. H. and Forbess, J. M. (2002). Surgical management of the single ventricle. *Progress in Pediatric Cardiology*, 16(1):47–68.
- Galli, K. K., Zimmerman, R. A., Jarvik, G. P., Wernovsky, G., Kuypers, M. K., Clancy, R. R., Montenegro, L. M., Mahle, W. T., Newman, M. F., Saunders, A. M., et al. (2004). Periventricular leukomalacia is common after neonatal cardiac surgery. *The Journal of Thoracic and Cardiovascular Surgery*, 127(3):692–704.
- Garces, P., Pereda, E., Hernandez-Tamames, J. A., Del-Pozo, F., Maestu, F., and Angel Pineda-Pardo, J. (2016). Multimodal description of whole brain connectivity: A comparison of resting state MEG, fMRI, and DWI. *Human Brain Mapping*, 37(1):20–34.
- Gardner, M. F., Falkmer, T., Vogel, K., and Gregersen, N. P. (1997). *TVPS (UL)-R: Test of Visual-perceptual Skills (non Motor)(upper Level) Revised: Manual*. Psychological and Educational Publications.
- Gaynor, J. W., Ittenbach, R. F., Gerdes, M., Bernbaum, J., Clancy, R. R., McDonald-McGinn, D. M., Zackai, E. H., Wernovsky, G., Nicolson, S. C., and Spray, T. L. (2014). Neurodevelopmental outcomes in preschool survivors of the Fontan procedure. *The Journal of Thoracic and Cardiovascular Surgery*, 147(4):1276–1283.

- Gaynor, J. W., Jarvik, G. P., Bernbaum, J., Gerdes, M., Wernovsky, G., Burnham, N. B., D'Agostino, J. A., Zackai, E., McDonald-McGinn, D. M., Nicolson, S. C., et al. (2006). The relationship of postoperative electrographic seizures to neurodevelopmental outcome at 1 year of age after neonatal and infant cardiac surgery. *The Journal of Thoracic and Cardiovascular Surgery*, 131(1):181–189.
- Gaynor, J. W., Stopp, C., Wypij, D., Andropoulos, D. B., Atallah, J., Atz, A. M., Beca, J., Donofrio, M. T., Duncan, K., Ghanayem, N. S., et al. (2015). Neurodevelopmental outcomes after cardiac surgery in infancy. *Pediatrics*, 135(5):816–825.
- Genovese, C. R., Lazar, N. A., and Nichols, T. (2002). Thresholding of statistical maps in functional neuroimaging using the false discovery rate. *NeuroImage*, 15(4):870–878.
- Gentles, T. L., Gauvreau, K., Mayer, J. E., Fishberger, S. B., Burnetta, J., Colan, S. D., Newburger, J. W., and Wernovsky, G. (1997). Functional outcome after the Fontan operation: Factors influencing late morbidity. *The Journal of Thoracic and Cardiovascular Surgery*, 114(3):392–403.
- Ghaferi, A. A. and Hutchins, G. M. (2005). Progression of liver pathology in patients undergoing the Fontan procedure: chronic passive congestion, cardiac cirrhosis, hepatic adenoma, and hepatocellular carcinoma. *The Journal of Thoracic and Cardiovascular Surgery*, 129(6):1348–1352.
- Giedd, J. N. (2004). Structural magnetic resonance imaging of the adolescent brain. *Annals of the New York Academy of Sciences*, 1021(1):77–85.
- Gilman, S. (1965). Cerebral disorders after open-heart operations. *New England Journal of Medicine*, 272(10):489–498.
- Ginestet, C. E., Nichols, T. E., Bullmore, E. T., and Simmons, A. (2011). Brain network analysis: separating cost from topology using cost-integration. *PloS One*, 6(7):e21570.
- Gioia, G. A., Isquith, P. K., Guy, S. C., and Kenworthy, L. (2000). *Behavior Rating Inventory of Executive Function: BRIEF*. Psychological Assessment Resources Odessa, FL.
- Glauser, T. A., Rorke, L. B., Weinberg, P. M., and Clancy, R. R. (1990). Congenital brain anomalies associated with the hypoplastic left heart syndrome. *Pediatrics*, 85(6):984–990.

- Glenn, W. W. (1958). Circulatory bypass of the right side of the heart: shunt between superior vena cava and distal right pulmonary artery—report of clinical application. *New England Journal of Medicine*, 259(3):117–120.
- Glessner, J. T., Bick, A. G., Ito, K., Homsy, J. G., Rodriguez-Murillo, L., Fromer, M., Mazaika, E., Vardarajan, B., Italia, M., Leipzig, J., et al. (2014). Increased frequency of de novo copy number variants in congenital heart disease by integrative analysis of single nucleotide polymorphism array and exome sequence data. *Circulation Research*, 115(10):884–896.
- Goff, D. A., Blume, E. D., Gauvreau, K., Mayer, J. E., Lock, J. E., and Jenkins, K. J. (2000). Clinical outcome of fenestrated Fontan patients after closure: the first 10 years. *Circulation*, 102(17):2094–2099.
- Goff, D. A., Shera, D. M., Tang, S., Lavin, N. A., Durning, S. M., Nicolson, S. C., Montenegro, L. M., Rome, J. J., Gaynor, J. W., Spray, T. L., et al. (2014). Risk factors for preoperative periventricular leukomalacia in term neonates with hypoplastic left heart syndrome are patient related. *The Journal of Thoracic and Cardiovascular Surgery*, 147(4):1312–1318.
- Goldberg, C. S., Bove, E. L., Devaney, E. J., Mollen, E., Schwartz, E., Tindall, S., Nowak, C., Charpie, J., Brown, M. B., Kulik, T. J., et al. (2007). A randomized clinical trial of regional cerebral perfusion versus deep hypothermic circulatory arrest: outcomes for infants with functional single ventricle. *The Journal of Thoracic and Cardiovascular Surgery*, 133(4):880–887.
- Goldberg, C. S., Lu, M., Sleeper, L. A., Mahle, W. T., Gaynor, J. W., Williams, I. A., Mussatto, K. A., Ohye, R. G., Graham, E. M., Frank, D. U., et al. (2014). Factors associated with neurodevelopment for children with single ventricle lesions. *The Journal of Pediatrics*, 165(3):490–496.
- Goldberg, C. S., Schwartz, E. M., Brunberg, J. A., Mosca, R. S., Bove, E. L., Schork, M. A., Stetz, S. P., Cheatham, J. P., and Kulik, T. J. (2000). Neurodevelopmental outcome of patients after the Fontan operation: a comparison between children with hypoplastic left heart syndrome and other functional single ventricle lesions. *The Journal of Pediatrics*, 137(5):646–652.
- Gong, G., He, Y., Chen, Z. J., and Evans, A. C. (2012). Convergence and divergence of thickness correlations with diffusion connections across the human cerebral cortex. *NeuroImage*, 59(2):1239–1248.

- Gong, G., Rosa-Neto, P., Carbonell, F., Chen, Z. J., He, Y., and Evans, A. C. (2009). Age-and gender-related differences in the cortical anatomical network. *The Journal of Neuroscience*, 29(50):15684–15693.
- Graham, D. (1977). Pathology of hypoxic brain damage in man. *Journal of Clinical Pathology. Supplement (Royal College of Pathologists)*, 11:170–180.
- Grayson, D. S., Ray, S., Carpenter, S., Iyer, S., Dias, T. G. C., Stevens, C., Nigg, J. T., and Fair, D. A. (2014). Structural and functional rich club organization of the brain in children and adults. *PloS One*, 9(2):e88297.
- Greicius, M. D., Supekar, K., Menon, V., and Dougherty, R. F. (2009). Resting-state functional connectivity reflects structural connectivity in the default mode network. *Cerebral Cortex*, 19(1):72–78.
- Gross, J., Baillet, S., Barnes, G. R., Henson, R. N., Hillebrand, A., Jensen, O., Jerbi, K., Litvak, V., Maess, B., Oostenveld, R., et al. (2013). Good practice for conducting and reporting MEG research. *NeuroImage*, 65:349–363.
- Gunn, A. J. and Bennet, L. (2009). Fetal hypoxia insults and patterns of brain injury: insights from animal models. *Clinics in Perinatology*, 36(3):579–593.
- Guy, S. C., Gioia, G. A., and Isquith, P. K. (2004). *Behavior Rating Inventory of Executive Function: Self-report Version*. Psychological Assessment Resources.
- Hagmann, P., Cammoun, L., Gigandet, X., Meuli, R., Honey, C. J., Wedeen, V. J., and Sporns, O. (2008). Mapping the structural core of human cerebral cortex. *PLoS Biol*, 6(7):e159.
- Hagmann, P., Kurant, M., Gigandet, X., Thiran, P., Wedeen, V. J., Meuli, R., and Thiran, J.-P. (2007). Mapping human whole-brain structural networks with diffusion MRI. *PloS One*, 2(7):e597.
- Hahn, E., Szwaast, A., Cnota, J., Levine, J. C., Fifer, C. G., Jaeggi, E., Andrews, H., and Williams, I. A. (2015). The association of fetal growth, cerebral blood flow, and neurodevelopmental outcome in single ventricle fetuses. *Ultrasound in Obstetrics & Gynecology*.
- Han, X., Jovicich, J., Salat, D., van der Kouwe, A., Quinn, B., Czanner, S., Busa, E., Pacheco, J., Albert, M., Killiany, R., et al. (2006). Reliability of MRI-derived measurements of human cerebral cortical thickness: the effects of field strength, scanner upgrade and manufacturer. *NeuroImage*, 32(1):180–194.

- Hayes, A. F. (2009). Beyond Baron and Kenny: statistical mediation analysis in the new millennium. *Communication Monographs*, 76(4):408–420.
- He, Y., Chen, Z., and Evans, A. (2008). Structural insights into aberrant topological patterns of large-scale cortical networks in Alzheimer's disease. *The Journal of Neuroscience*, 28(18):4756–4766.
- He, Y., Chen, Z. J., and Evans, A. C. (2007). Small-world anatomical networks in the human brain revealed by cortical thickness from MRI. *Cerebral Cortex*, 17(10):2407–2419.
- He, Y., Dagher, A., Chen, Z., Charil, A., Zijdenbos, A., Worsley, K., and Evans, A. (2009). Impaired small-world efficiency in structural cortical networks in multiple sclerosis associated with white matter lesion load. *Brain*, 132(12):3366–3379.
- Hehir, D. A., Dominguez, T. E., Ballweg, J. A., Ravishankar, C., Marino, B. S., Bird, G. L., Nicolson, S. C., Spray, T. L., Gaynor, J. W., and Tabbutt, S. (2008). Risk factors for interstage death after stage 1 reconstruction of hypoplastic left heart syndrome and variants. *The Journal of Thoracic and Cardiovascular Surgery*, 136(1):94–99.
- Hinton, R. B., Andelfinger, G., Sekar, P., Hinton, A. C., Gendron, R. L., Michelfelder, E. C., Robitaille, Y., and Benson, D. W. (2008). Prenatal head growth and white matter injury in hypoplastic left heart syndrome. *Pediatric Research*, 64(4):364–369.
- Hirsch, J. C., Goldberg, C., Bove, E. L., Salehian, S., Lee, T., Ohye, R. G., and Devaney, E. J. (2008). Fontan operation in the current era: a 15-year single institution experience. *Annals of Surgery*, 248(3):402–410.
- Hoffman, G. M., Brosig, C. L., Mussatto, K. A., Tweddell, J. S., and Ghanayem, N. S. (2013). Perioperative cerebral oxygen saturation in neonates with hypoplastic left heart syndrome and childhood neurodevelopmental outcome. *The Journal of Thoracic and Cardiovascular Surgery*, 146(5):1153–1164.
- Hoffman, G. M., Mussatto, K. A., Brosig, C. L., Ghanayem, N. S., Musa, N., Fedderly, R. T., Jaquiss, R. D., and Tweddell, J. S. (2005). Systemic venous oxygen saturation after the Norwood procedure and childhood neurodevelopmental outcome. *The Journal of Thoracic and Cardiovascular Surgery*, 130(4):1094–1100.
- Hoffman, J. I. and Kaplan, S. (2002). The incidence of congenital heart disease. *Journal of the American College of Cardiology*, 39(12):1890–1900.
- Holl, N., Noblet, V., Rodrigo, S., Dietemann, J. L., Mekhbi, M. B., Kehrl, P., WolframGabel, R., Braun, M., and Kremer, S. (2011). Temporal lobe association fiber

- tractography as compared to histology and dissection. *Surgical and Radiologic Anatomy*, 33(8):713–722.
- Hollingshead, A. B. et al. (1975). Four factor index of social status.
- Homsy, J., Zaidi, S., Shen, Y., Ware, J. S., Samocha, K. E., Karczewski, K. J., DePalma, S. R., McKean, D., Wakimoto, H., Gorham, J., et al. (2015). De novo mutations in congenital heart disease with neurodevelopmental and other congenital anomalies. *Science*, 350(6265):1262–1266.
- Honey, C., Sporns, O., Cammoun, L., Gigandet, X., Thiran, J.-P., Meuli, R., and Hagmann, P. (2009). Predicting human resting-state functional connectivity from structural connectivity. *Proceedings of the National Academy of Sciences*, 106(6):2035–2040.
- Hopkins, R., Armstrong, B. E., Serwer, G., Peterson, R., and Oldham Jr, H. (1985). Physiological rationale for a bidirectional cavopulmonary shunt. a versatile complement to the Fontan principle. *The Journal of Thoracic and Cardiovascular Surgery*, 90(3):391–398.
- Hosein, R. B., Clarke, A. J., McGuirk, S. P., Griselli, M., Stumper, O., De Giovanni, J. V., Barron, D. J., and Brawn, W. J. (2007). Factors influencing early and late outcome following the Fontan procedure in the current era. the 'Two Commandments'? *European Journal of Cardio-Thoracic Surgery*, 31(3):344–353.
- Hosseini, S. H., Hoefft, F., and Kesler, S. R. (2012). GAT: a graph-theoretical analysis toolbox for analyzing between-group differences in large-scale structural and functional brain networks. *PloS One*, 7(7):e40709.
- Hosseini, S. H. and Kesler, S. R. (2013a). Comparing connectivity pattern and small-world organization between structural correlation and resting-state networks in healthy adults. *NeuroImage*, 78:402–414.
- Hosseini, S. H. and Kesler, S. R. (2013b). Influence of choice of null network on smallworld parameters of structural correlation networks. *PLoS One*, 8(6):e67354.
- Humphries, M. D. and Gurney, K. (2008). Network 'small-world-ness': a quantitative method for determining canonical network equivalence. *PLoS One*, 3(4):e0002051.
- Huttenlocher, P. R. (1990). Morphometric study of human cerebral cortex development. *Neuropsychologia*, 28(6):517–527.

- Huttenlocher, P. R. and Dabholkar, A. S. (1997). Regional differences in synaptogenesis in human cerebral cortex. *Journal of Comparative Neurology*, 387(2):167–178.
- Ibuki, K., Watanabe, K., Yoshimura, N., Kakimoto, T., Matsui, M., Yoshida, T., Origasa, H., and Ichida, F. (2012). The improvement of hypoxia correlates with neuroanatomic and developmental outcomes: comparison of midterm outcomes in infants with transposition of the great arteries or single-ventricle physiology. *The Journal of Thoracic and Cardiovascular Surgery*, 143(5):1077–1085.
- Imai, K., Keele, L., and Tingley, D. (2010). A general approach to causal mediation analysis. *Psychological Methods*, 15(4):309.
- Inder, T. E., Huppi, P. S., Warfield, S., Kikinis, R., Zientara, G. P., Barnes, P. D., Jolesz, F., and Volpe, J. J. (1999). Periventricular white matter injury in the premature infant is followed by reduced cerebral cortical gray matter volume at term. *Annals of Neurology*, 46(5):755–760.
- Ishibashi, N., Iwata, Y., Okamura, T., Zurakowski, D., Lidov, H. G., and Jonas, R. A. (2010). Differential neuronal vulnerability varies according to specific cardiopulmonary bypass insult in a porcine survival model. *The Journal of Thoracic and Cardiovascular Surgery*, 140(6):1408–1415.
- Ishibashi, N., Scafidi, J., Murata, A., Korotcova, L., Zurakowski, D., Gallo, V., and Jonas, R. A. (2012). White matter protection in congenital heart surgery. *Circulation*, 125(7):859–871.
- Iturria-Medina, Y., Canales-Rodriguez, E., Melie-Garcia, L., Valdes-Hernandez, P., Martinez-Montes, E., Aleman-Gomez, Y., and Sanchez-Bornot, J. (2007). Characterizing brain anatomical connections using diffusion weighted MRI and graph theory. *NeuroImage*, 36(3):645–660.
- Iturria-Medina, Y., Sotero, R. C., Canales-Rodriguez, E. J., Aleman-Gomez, Y., and Melie-Garcia, L. (2008). Studying the human brain anatomical network via diffusion-weighted MRI and graph theory. *NeuroImage*, 40(3):1064–1076.
- Jacobs, M. L., Rychik, J., Rome, J. J., Apostolopoulou, S., Pizarro, C., Murphy, J. D., and Norwood, W. I. (1996). Early reduction of the volume work of the single ventricle: the hemi-Fontan operation. *The Annals of Thoracic Surgery*, 62(2):456–462.
- Jbabdi, S. and Johansen-Berg, H. (2011). Tractography: where do we go from here? *Brain Connectivity*, 1(3):169–183.

- Jbabdi, S., Lehman, J. F., Haber, S. N., and Behrens, T. E. (2013). Human and monkey ventral prefrontal fibers use the same organizational principles to reach their targets: tracing versus tractography. *The Journal of Neuroscience*, 33(7):3190–3201.
- Jbabdi, S., Woolrich, M., Andersson, J., and Behrens, T. (2007). A bayesian framework for global tractography. *NeuroImage*, 37(1):116–129.
- Jeurissen, B., Leemans, A., Tournier, J.-D., Jones, D. K., and Sijbers, J. (2013). Investigating the prevalence of complex fiber configurations in white matter tissue with diffusion magnetic resonance imaging. *Human Brain Mapping*, 34(11):2747–2766.
- Jonas, R. A. (2002). Deep hypothermic circulatory arrest: current status and indications. In *Seminars in Thoracic and Cardiovascular Surgery: Pediatric Cardiac Surgery Annual*, volume 5, pages 76–88. Elsevier.
- Kaltman, J., Di, H., Tian, Z., and Rychik, J. (2005). Impact of congenital heart disease on cerebrovascular blood flow dynamics in the fetus. *Ultrasound in Obstetrics & Gynecology*, 25(1):32–36.
- Kaufman, J., Birmaher, B., Brent, D., Rao, U., Flynn, C., Moreci, P., Williamson, D., and Ryan, N. (1997). Schedule for affective disorders and schizophrenia for school-age children-present and lifetime version (K-SADS-PL): initial reliability and validity data. *Journal of the American Academy of Child & Adolescent Psychiatry*, 36(7):980–988.
- Kern, J. H., Hinton, V. J., Nereo, N. E., Hayes, C. J., and Gersony, W. M. (1998). Early developmental outcome after the Norwood procedure for hypoplastic left heart syndrome. *Pediatrics*, 102(5):1148–1152.
- Khairy, P., Fernandes, S. M., Mayer, J. E., Triedman, J. K., Walsh, E. P., Lock, J. E., and Landzberg, M. J. (2008). Long-term survival, modes of death, and predictors of mortality in patients with fontan surgery. *Circulation*, 117(1):85–92.
- Khairy, P., Ionescu-Ittu, R., Mackie, A. S., Abrahamowicz, M., Pilote, L., and Marelli, A. J. (2010). Changing mortality in congenital heart disease. *Journal of the American College of Cardiology*, 56(14):1149–1157.
- Khundrakpam, B. S., Reid, A., Brauer, J., Carbonell, F., Lewis, J., Ameis, S., Karama, S., Lee, J., Chen, Z., Das, S., and Evans, A. C. (2013). Developmental changes in organization of structural brain networks. *Cerebral Cortex*, 23(9):2072–2085.

- Kiesewetter, C. H., Sheron, N., Vettukattill, J. J., Hacking, N., Stedman, B., MillwardSadler, H., Haw, M., Cope, R., Salmon, A. P., Sivaprakasam, M. C., et al. (2007). Hepatic changes in the failing Fontan circulation. *Heart*, 93(5):579–584.
- Kim, S.-G., Jung, W. H., Kim, S. N., Jang, J. H., and Kwon, J. S. (2013). Disparity between dorsal and ventral networks in patients with obsessive-compulsive disorder: evidence revealed by graph theoretical analysis based on cortical thickness from MRI. *Frontiers in Human Neuroscience*, 7.
- Kinney, H. C., Panigrahy, A., Newburger, J. W., Jonas, R. A., and Sleeper, L. A. (2005). Hypoxic-ischemic brain injury in infants with congenital heart disease dying after cardiac surgery. *Acta Neuropathologica*, 110(6):563–578.
- Klein, A. and Tourville, J. (2012). 101 labeled brain images and a consistent human cortical labeling protocol. *Frontiers in Neuroscience*, 6.
- Knosche, T. R., Anwander, A., Liptrot, M., and Dyrby, T. B. (2015). Validation of tractography: comparison with manganese tracing. *Human Brain Mapping*, 36(10):4116–4134.
- Kolaczyk, E. (2009). *Statistical Analysis of Network Data, volume 69 of Springer Series in Statistics*. Springer New York.
- Kolaczyk, E. D. and Csardi, G. (2014). *Statistical analysis of network data with R*, volume 65. Springer.
- Korotcova, L., Kumar, S., Agematsu, K., Morton, P. D., Jonas, R. A., and Ishibashi, N. (2015). Prolonged white matter inflammation after cardiopulmonary bypass and circulatory arrest in a juvenile porcine model. *The Annals of Thoracic Surgery*, 100(3):1030–1037.
- Kostovic, I. and Jovanov-Milosevic, N. (2006). The development of cerebral connections during the first 20–45 weeks gestation. In *Seminars in Fetal and Neonatal Medicine*, volume 11, pages 415–422. Elsevier.
- Kumar, R. K., Newburger, J. W., Gauvreau, K., Kamenir, S. A., and Hornberger, L. K. (1999). Comparison of outcome when hypoplastic left heart syndrome and transposition of the great arteries are diagnosed prenatally versus when diagnosis of these two conditions is made only postnatally. *The American Journal of Cardiology*, 83(12):1649–1653.

- Kumar, S. P., Rubinstein, C. S., Simsic, J. M., Taylor, A. B., Saul, J. P., and Bradley, S. M. (2003). Lateral tunnel versus extracardiac conduit Fontan procedure: a concurrent comparison. *The Annals of Thoracic Surgery*, 76(5):1389–1397.
- Kurth, C. D., Steven, J. L., Montenegro, L. M., Watzman, H. M., Gaynor, J. W., Spray, T. L., and Nicolson, S. C. (2001). Cerebral oxygen saturation before congenital heart surgery. *The Annals of Thoracic Surgery*, 72(1):187–192.
- Lawrence, A. J., Chung, A. W., Morris, R. G., Markus, H. S., and Barrick, T. R. (2014). Structural network efficiency is associated with cognitive impairment in small-vessel disease. *Neurology*, 83(4):304–311.
- Lemler, M. S., Scott, W. A., Leonard, S. R., Stromberg, D., and Ramaciotti, C. (2002). Fenestration improves clinical outcome of the Fontan procedure: a prospective, randomized study. *Circulation*, 105(2):207–212.
- Lerch, J. P., Worsley, K., Shaw, W. P., Greenstein, D. K., Lenroot, R. K., Giedd, J., and Evans, A. C. (2006). Mapping anatomical correlations across cerebral cortex (MACACC) using cortical thickness from MRI. *NeuroImage*, 31(3):993–1003.
- Leviton, A. and Gressens, P. (2007). Neuronal damage accompanies perinatal white-matter damage. *Trends in Neurosciences*, 30(9):473–478.
- Licht, D. J., Shera, D. M., Clancy, R. R., Wernovsky, G., Montenegro, L. M., Nicolson, S. C., Zimmerman, R. A., Spray, T. L., Gaynor, J. W., and Vossough, A. (2009). Brain maturation is delayed in infants with complex congenital heart defects. *The Journal of Thoracic and Cardiovascular Surgery*, 137(3):529–537.
- Lim, J. M., Saini, B., Chau, V., Post, M., Blaser, S., Macgowan, C., Miller, S. P., Seed, M., et al. (2016). Cerebral oxygen delivery is reduced in newborns with congenital heart disease. *The Journal of Thoracic and Cardiovascular Surgery*.
- Limperopoulos, C., Tworetzky, W., McElhinney, D. B., Newburger, J. W., Brown, D. W., Robertson, R. L., Guizard, N., McGrath, E., Geva, J., Annese, D., et al. (2010). Brain volume and metabolism in fetuses with congenital heart disease evaluation with quantitative magnetic resonance imaging and spectroscopy. *Circulation*, 121(1):26–33.
- Longmuir, P. E., Banks, L., and McCrindle, B. W. (2012). Cross-sectional study of motor development among children after the Fontan procedure. *Cardiology in the Young*, 22(04):443–450.
- Lynch, J. (2009). Epidemiology and classification of perinatal stroke. *Seminars in Fetal & Neonatal Medicine*, 14:245–249.

- Lynch, J. M., Buckley, E. M., Schwab, P. J., McCarthy, A. L., Winters, M. E., Busch, D. R., Xiao, R., Goff, D. A., Nicolson, S. C., Montenegro, L. M., et al. (2014). Time to surgery and preoperative cerebral hemodynamics predict postoperative white matter injury in neonates with hypoplastic left heart syndrome. *The Journal of Thoracic and Cardiovascular Surgery*, 148(5):2181–2188.
- MacKinnon, D. P., Fairchild, A. J., and Fritz, M. S. (2007). Mediation analysis. *Annual Review of Psychology*, 58:593–614.
- Madsen, N. L., Schwartz, S. M., Lewin, M. B., and Mueller, B. A. (2013). Prepregnancy body mass index and congenital heart defects among offspring: A population-based study. *Congenital Heart Disease*, 8(2):131–141.
- Mahle, W. T., Clancy, R. R., McGaurn, S. P., Goin, J. E., and Clark, B. J. (2001). Impact of prenatal diagnosis on survival and early neurologic morbidity in neonates with the hypoplastic left heart syndrome. *Pediatrics*, 107(6):1277–1282.
- Mahle, W. T., Clancy, R. R., Moss, E. M., Gerdes, M., Jobes, D. R., and Wernovsky, G. (2000). Neurodevelopmental outcome and lifestyle assessment in school-aged and adolescent children with hypoplastic left heart syndrome. *Pediatrics*, 105(5):1082–1089.
- Mahle, W. T., Matthews, E., Kanter, K. R., Kogon, B. E., Hamrick, S. E., and Strickland, M. J. (2014). Inflammatory response after neonatal cardiac surgery and its relationship to clinical outcomes. *The Annals of Thoracic Surgery*, 97(3):950–956.
- Mahle, W. T., Tavani, F., Zimmerman, R. A., Nicolson, S. C., Galli, K. K., Gaynor, J. W., Clancy, R. R., Montenegro, L. M., Spray, T. L., Chiavacci, R. M., et al. (2002). An MRI study of neurological injury before and after congenital heart surgery. *Circulation*, 106(12 suppl 1):I–109.
- Mahle, W. T., Visconti, K. J., Freier, M. C., Kanne, S. M., Hamilton, W. G., Sharkey, A. M., Chinnock, R. E., Jenkins, K. J., Isquith, P. K., Burns, T. G., et al. (2006). Relationship of surgical approach to neurodevelopmental outcomes in hypoplastic left heart syndrome. *Pediatrics*, 117(1):e90–e97.
- Mair, D. D., Puga, F. J., and Danielson, G. K. (2001). The Fontan procedure for tricuspid atresia: early and late results of a 25-year experience with 216 patients. *Journal of the American College of Cardiology*, 37(3):933–939.
- Malone, M., Prior, P., and Scholtz, C. (1981). Brain damage after cardiopulmonary bypass: correlations between neurophysiological and neuropathological findings. *Journal of Neurology, Neurosurgery & Psychiatry*, 44(10):924–931.

- Mangla, R., Kolar, B., Almast, J., and Ekholm, S.E. (2011). Border zone infarcts: pathophysiologic and imaging characteristics. *Radiographics*, 31(5):1201-1214.
- Mantel, N. (1967). The detection of disease clustering and a generalized regression approach. *Cancer Research*, 27(2 Part 1):209–220.
- Marcelletti, C., Corno, A., Giannico, S., and Marino, B. (1990). Inferior vena cavapulmonary artery extracardiac conduit. a new form of right heart bypass. *The Journal of Thoracic and Cardiovascular Surgery*, 100(2):228–232.
- Marelli, A., Mackie, A., Ionescu-Ittu, R., Rahme, E., and Pilote, L. (2007). Congenital heart disease in the general population: changing prevalence and age distribution. *Circulation*, 115(2):163–172.
- Maslov, S. and Sneppen, K. (2002). Specificity and stability in topology of protein networks. *Science*, 296(5569):910–913.
- Masoller, N., Sanz-Cortes, M., Crispi, F., Gomez, O., Bennasar, M., Egana-Ugrinovic, G., Bargallo, N., Martinez, J., and Gratacos, E. (2016). Fetal brain doppler and biometry at mid-gestation for the early prediction of abnormal brain development at birth in congenital heart disease. *Ultrasound in Obstetrics & Gynecology*, 47(1):65–73.
- Matthiesen, N. B., Agergaard, P., Henriksen, T. B., Bach, C. C., Gaynor, J. W., Hjortdal, V., and Østergaard, J. R. (2016). Congenital heart defects and measures of fetal growth in newborns with down syndrome or 22q11.2 deletion syndrome. *The Journal of Pediatrics*.
- McConnell, J. R., Fleming, W. H., Chu, W.-K., Hahn, F. J., Sarafian, L. B., Hofschire, P. J., and Kugler, J. D. (1990). Magnetic resonance imaging of the brain in infants and children before and after cardiac surgery: a prospective study. *American Journal of Diseases of Children*, 144(3):374–378.
- McCordle, B. W., Williams, R. V., Mitchell, P. D., Hsu, D. T., Paridon, S. M., Atz, A. M., Li, J. S., Newburger, J. W., Investigators, P. H. N., et al. (2006). Relationship of patient and medical characteristics to health status in children and adolescents after the Fontan procedure. *Circulation*, 113(8):1123–1129.
- McQuillen, P. and Ferriero, D. (2005). Perinatal subplate neuron injury: implications for cortical development and plasticity. *Brain Pathology*, 15(3):250–260.
- McQuillen, P. S. and Miller, S. P. (2010). Congenital heart disease and brain development. *Annals of the New York Academy of Sciences*, 1184(1):68–86.

- Mechelli, A., Friston, K. J., Frackowiak, R. S., and Price, C. J. (2005). Structural covariance in the human cortex. *The Journal of Neuroscience*, 25(36):8303–8310.
- Mertens, L., Hagler, D. J., Sauer, U., Somerville, J., and Gewillig, M. (1998). Protein-losing enteropathy after the Fontan operation: an international multicenter study. *The Journal of Thoracic and Cardiovascular Surgery*, 115(5):1063–1073.
- Mlczoch, E., Brugger, P., Ulm, B., Novak, A., Frantal, S., Prayer, D., and Salzer-Muhar, U. (2013). Structural congenital brain disease in congenital heart disease: results from a fetal MRI program. *European Journal of Paediatric Neurology*, 17(2):153–160.
- Monagle, P. and Karl, T. R. (2002). Thromboembolic problems after the Fontan operation. In *Seminars in Thoracic & Cardiovascular Surgery: Pediatric Cardiac Surgery Annual*, volume 5, pages 36–47. Elsevier.
- Moody, D., Bell, M., and Challa, V. (1990). Features of the cerebral vascular pattern that predict vulnerability to perfusion or oxygenation deficiency: an anatomic study. *American Journal of Neuroradiology*, 11(3):431–439.
- Moons, P., Van Deyk, K., De Geest, S., Gewillig, M., and Budts, W. (2005). Is the severity of congenital heart disease associated with the quality of life and perceived health of adult patients? *Heart*, 91(9):1193–1198.
- Mori, S. and van Zijl, P. (2002). Fiber tracking: principles and strategies—a technical review. *NMR in Biomedicine*, 15(7-8):468–480.
- Mulkey, S. B., Ou, X., Ramakrishnaiah, R. H., Glasier, C. M., Swearingen, C. J., Melguizo, M. S., Yap, V. L., Schmitz, M. L., and Bhutta, A. T. (2014). White matter injury in newborns with congenital heart disease: a diffusion tensor imaging study. *Pediatric Neurology*, 51(3):377–383.
- Mulkey, S. B., Swearingen, C. J., Melguizo, M. S., Schmitz, M. L., Ou, X., Ramakrishnaiah, R. H., Glasier, C. M., Schaefer, G. B., and Bhutta, A. T. (2013). Multi-tiered analysis of brain injury in neonates with congenital heart disease. *Pediatric Cardiology*, 34(8):1772–1784.
- Mussatto, K. A., Hoffmann, R. G., Hoffman, G. M., Tweddell, J. S., Bear, L., Cao, Y., and Brosig, C. (2014). Risk and prevalence of developmental delay in young children with congenital heart disease. *Pediatrics*, 133(3):e570–e577.
- Nagaraj, U. D., Evangelou, I. E., Donofrio, M. T., Vezina, L. G., McCarter, R., du Plessis, A. J., and Limperopoulos, C. (2015). Impaired global and regional cerebral

- perfusion in newborns with complex congenital heart disease. *The Journal of Pediatrics*, 167(5):1018–1024.
- Newburger, J. W., Jonas, R. A., Wernovsky, G., Wypij, D., Hickey, P. R., Kuban, K., Farrell, D. M., Holmes, G. L., Helmers, S. L., Constantinou, J., et al. (1993). A comparison of the perioperative neurologic effects of hypothermic circulatory arrest versus low-flow cardiopulmonary bypass in infant heart surgery. *New England Journal of Medicine*, 329(15):1057–1064.
- Newburger, J. W., Sleeper, L. A., Bellinger, D. C., Goldberg, C. S., Tabbutt, S., Lu, M., Mussatto, K. A., Williams, I. A., Gustafson, K. E., and Mital, S. e. a. (2012). Early developmental outcome in children with hypoplastic left heart syndrome and related anomalies: The single ventricle reconstruction trial. *Circulation*, 125(17):2081–2091.
- Newburger, J. W., Sleeper, L. A., Frommelt, P. C., Pearson, G. D., Mahle, W. T., Chen, S., Dunbar-Masterson, C., Mital, S., Williams, I. A., Ghanayem, N. S., et al. (2014). Transplantation-free survival and interventions at 3 years in the Single Ventricle Reconstruction Trial. *Circulation*, 129(20):2013–2020.
- Newman, M. (2003). Mixing patterns in networks. *Physical Review E*, 67(2):026126.
- Newman, M. E. (2010). *Networks: an introduction*. Oxford University Press, Oxford.
- Nichols, T. E. and Holmes, A. P. (2002). Nonparametric permutation tests for functional neuroimaging: a primer with examples. *Human Brain Mapping*, 15(1):1–25.
- Nie, J., Li, G., and Shen, D. (2013). Development of cortical anatomical properties from early childhood to early adulthood. *NeuroImage*, 76:216–224.
- Norwood, W. I., Kirklin, J. K., and Sanders, S. P. (1980). Hypoplastic left heart syndrome: experience with palliative surgery. *The American Journal of Cardiology*, 45(1):87–91.
- Ohye, R. G., Sleeper, L. A., Mahony, L., Newburger, J. W., Pearson, G. D., Lu, M., Goldberg, C. S., Tabbutt, S., Frommelt, P. C., Ghanayem, N. S., et al. (2010). Comparison of shunt types in the norwood procedure for single-ventricle lesions. *New England Journal of Medicine*, 362(21):1980–1992.
- O’Leary, P. W. (2002). Prevalence, clinical presentation and natural history of patients with single ventricle. *Progress in Pediatric Cardiology*, 16(1):31–38.
- Ono, M., Boethig, D., Goerler, H., Lange, M., Westhoff-Bleck, M., and Breymann, T. (2006). Clinical outcome of patients 20 years after Fontan operation: Effect of

- fenestration on late morbidity. *European Journal of Cardio-thoracic Surgery*, 30(6):923–929.
- Ortinou, C., Alexopoulos, D., Dierker, D., Van Essen, D., Beca, J., and Inder, T. (2013). Cortical folding is altered before surgery in infants with congenital heart disease. *The Journal of Pediatrics*, 163(5):1507–1510.
- Ortinou, C., Beca, J., Lambeth, J., Ferdman, B., Alexopoulos, D., Shimony, J. S., Wallendorf, M., Neil, J., and Inder, T. (2012). Regional alterations in cerebral growth exist preoperatively in infants with congenital heart disease. *The Journal of Thoracic and Cardiovascular Surgery*, 143(6):1264–1270.
- Oster, M. E., Lee, K. A., Honein, M. A., Riehle-Colarusso, T., Shin, M., and Correa, A. (2013). Temporal trends in survival among infants with critical congenital heart defects. *Pediatrics*, 131(5):e1502–e1508.
- Owen, J. P., Ziv, E., Bukshpun, P., Pojman, N., Wakahiro, M., Berman, J. I., Roberts, T. P., Friedman, E. J., Sherr, E. H., and Mukherjee, P. (2013). Test–retest reliability of computational network measurements derived from the structural connectome of the human brain. *Brain Connectivity*, 3(2):160–176.
- Owen, M., Shevell, M., Donofrio, M., Majnemer, A., McCarter, R., Vezina, G., BouyssiKobar, M., Evangelou, I., Freeman, D., Weisenfeld, N., et al. (2014). Brain volume and neurobehavior in newborns with complex congenital heart defects. *The Journal of Pediatrics*, 164(5):1121–1127.
- Panigrahy, A., Schmithorst, V. J., Wisnowski, J. L., Watson, C. G., Bellinger, D. C., Newburger, J. W., and Rivkin, M. J. (2015). Relationship of white matter network topology and cognitive outcome in adolescents with d-transposition of the great arteries. *NeuroImage: Clinical*, 7:438–448.
- Pardoe, H., Pell, G. S., Abbott, D. F., Berg, A. T., and Jackson, G. D. (2008). Multi-site voxel-based morphometry: methods and a feasibility demonstration with childhood absence epilepsy. *NeuroImage*, 42(2):611–616.
- Parker, G. J., Haroon, H. A., and Wheeler-Kingshott, C. A. (2003). A framework for a streamline-based probabilistic index of connectivity (PICO) using a structural interpretation of MRI diffusion measurements. *Journal of Magnetic Resonance Imaging*, 18(2):242–254.
- Pereira, J. B., Aarsland, D., Ginestet, C. E., Lebedev, A. V., Wahlund, L.-O., Simmons, A., Volpe, G., and Westman, E. (2015). Aberrant cerebral network topology and mild

- cognitive impairment in early parkinson's disease. *Human Brain Mapping*, 36(8):2980–2995.
- Peyvandi, S., De Santiago, V., Chakkarapani, E., Chau, V., Campbell, A., Poskitt, K. J., Xu, D., Barkovich, A. J., Miller, S., and McQuillen, P. (2016). Association of prenatal diagnosis of critical congenital heart disease with postnatal brain development and the risk of brain injury. *JAMA Pediatrics*, 170(4):e154450–e154450.
- Phipson, B. and Smyth, G. K. (2010). Permutation P-values should never be zero: calculating exact P-values when permutations are randomly drawn. *Statistical Applications in Genetics and Molecular Biology*, 9(1):1–16.
- Poldrack, R. A., Fletcher, P. C., Henson, R. N., Worsley, K. J., Brett, M., and Nichols, T. E. (2008). Guidelines for reporting an fMRI study. *NeuroImage*, 40(2):409–414.
- Porayette, P., Madathil, S., Sun, L., Jaeggi, E., Grosse-Wortmann, L., Yoo, S.-J., Hickey, E., Miller, S. P., Macgowan, C. K., and Seed, M. (2016). Mri reveals hemodynamic changes with acute maternal hyperoxygenation in human fetuses with and without congenital heart disease. *Prenatal Diagnosis*.
- Pundi, K., Dearani, J., Pundi, K., Johnson, J., and Li, Z. (2015). 40 years of the Fontan operation: long-term outcome of 1,052 patients. *Journal of the American College of Cardiology*, 65(10 S).
- Pundi, K., Pundi, K. N., Kamath, P. S., Cetta, F., Li, Z., Poterucha, J. T., Driscoll, D. J., and Johnson, J. N. (2016). Liver disease in patients after the Fontan operation. *The American Journal of Cardiology*, 117(3):456–460.
- Qin, J., Wei, M., Liu, H., Yan, R., Luo, G., Yao, Z., and Lu, Q. (2014). Abnormal brain anatomical topological organization of the cognitive-emotional and the frontoparietal circuitry in major depressive disorder. *Magnetic Resonance in Medicine*, 72(5):1397–1407.
- R Core Team (2015). *R: A Language and Environment for Statistical Computing*. R Foundation for Statistical Computing, Vienna, Austria.
- Raissadati, A., Nieminen, H., Jokinen, E., and Sairanen, H. (2015). Progress in late results among pediatric cardiac surgery patients: a population-based 6-decade study with 98% follow-up. *Circulation*, 131(4):347–353.
- Ramakrishnan, K., Alfares, F., Hammond-Jack, K., Endicott, K., Nettleton, M., Zurakowski, D., Jonas, R. A., and Nath, D. S. (2016). Optimal timing of pulmonary

- banding for newborns with single ventricle physiology and unrestricted pulmonary blood flow. *Pediatric Cardiology*, 37:606–609.
- Reijmer, Y. D., Fotiadis, P., Piantoni, G., Boulouis, G., Kelly, K. E., Gurol, M. E., Leemans, A., O’Sullivan, M. J., Greenberg, S. M., and Viswanathan, A. (2016). Small vessel disease and cognitive impairment: The relevance of central network connections. *Human Brain Mapping*, 37(7):2446–2454.
- Ridgway, G. R., Henley, S. M., Rohrer, J. D., Scahill, R. I., Warren, J. D., and Fox, N. C. (2008). Ten simple rules for reporting voxel-based morphometry studies. *NeuroImage*, 40(4):1429–1435.
- Rivkin, M. J., Watson, C. G., Scoppettuolo, L. A., Wypij, D., Vajapeyam, S., Bellinger, D. C., DeMaso, D. R., Robertson Jr, R. L., and Newburger, J. W. (2013). Adolescents with d-transposition of the great arteries repaired in early infancy demonstrate reduced white matter microstructure associated with clinical risk factors. *The Journal of Thoracic and Cardiovascular Surgery*, 146(3):543–549.
- Rogers, B., Msall, M., Buck, G., Lyon, N., Norris, M., Roland, J.-M., Gingell, R., Cleveland, D., and Pieroni, D. (1995). Neurodevelopmental outcome of infants with hypoplastic left heart syndrome. *The Journal of Pediatrics*, 126(3):496–498.
- Rogers, L. S., Glatz, A. C., Ravishankar, C., Spray, T. L., Nicolson, S. C., Rychik, J., Rush, C. H., Gaynor, J. W., and Goldberg, D. J. (2012). 18 years of the fontan operation at a single institution: results from 771 consecutive patients. *Journal of the American College of Cardiology*, 60(11):1018–1025.
- Rollins, C. K., Watson, C. G., Asaro, L. A., Wypij, D., Vajapeyam, S., Bellinger, D. C., DeMaso, D. R., Robertson, R. L., Newburger, J. W., and Rivkin, M. J. (2014). White matter microstructure and cognition in adolescents with congenital heart disease. *The Journal of Pediatrics*, 165(5):936–944.
- Romero-Garcia, R., Atienza, M., Clemmensen, L. H., and Cantero, J. L. (2012). Effects of network resolution on topological properties of human neocortex. *NeuroImage*, 59(4):3522–3532.
- Rosenthal, D. N., Friedman, A. H., Kleinman, C. S., Kopf, G. S., Rosenfeld, L. E., and Hellenbrand, W. E. (1995). Thromboembolic complications after Fontan operations. *Circulation*, 92(9):287–293.

- Rosenthal, G. L. (1996). Patterns of prenatal growth among infants with cardiovascular malformations: possible fetal hemodynamic effects. *American Journal of Epidemiology*, 143(5):505–513.
- Rossi, R., Ekroth, R., Lincoln, C., Jackson, A., Thompson, R., Scallan, M., and Tsang, V. (1986). Detection of cerebral injury after total circulatory arrest and profound hypothermia by estimation of specific creatine kinase isoenzyme levels using monoclonal antibody techniques. *The American Journal of Cardiology*, 58(13):1236–1241.
- Rubinov, M. and Sporns, O. (2010). Complex network measures of brain connectivity: uses and interpretations. *NeuroImage*, 52(3):1059–1069.
- Rychik, J., Veldtman, G., Rand, E., Russo, P., Rome, J. J., Krok, K., Goldberg, D. J., Cahill, A. M., and Wells, R. G. (2012). The precarious state of the liver after a Fontan operation: summary of a multidisciplinary symposium. *Pediatric Cardiology*, 33(7):1001–1012.
- Saggar, M., Hosseini, S. H., Bruno, J. L., Quintin, E.-M., Raman, M. M., Kesler, S. R., and Reiss, A. L. (2015). Estimating individual contribution from group-based structural correlation networks. *NeuroImage*, 120:274–284.
- Sananes, R., Manlhiot, C., Kelly, E., Hornberger, L. K., Williams, W. G., MacGregor, D., Buncic, R., and McCrindle, B. W. (2012). Neurodevelopmental outcomes after open heart operations before 3 months of age. *The Annals of Thoracic Surgery*, 93(5):1577–1583.
- Sarajuuri, A., Jokinen, E., Mildh, L., Tujulin, A.-M., Mattila, I., Valanne, L., and Lonnqvist, T. (2012). Neurodevelopmental burden at age 5 years in patients with univentricular heart. *Pediatrics*, 130(6):e1636–e1646.
- Sarajuuri, A., Jokinen, E., Puosi, R., Eronen, M., Mildh, L., Mattila, I., Valanne, L., and Lonnqvist, T. (2007). Neurodevelopmental and neuroradiologic outcomes in patients with univentricular heart aged 5 to 7 years: related risk factor analysis. *The Journal of Thoracic and Cardiovascular Surgery*, 133(6):1524–1532.
- Sarajuuri, A., Jokinen, E., Puosi, R., Mildh, L., Mattila, I., Lano, A., and Lonnqvist, T. (2010). Neurodevelopment in children with hypoplastic left heart syndrome. *The Journal of Pediatrics*, 157(3):414–420.
- Sarajuuri, A., Lonnqvist, T., Mildh, L., Rajantie, I., Eronen, M., Mattila, I., and Jokinen, E. (2009). Prospective follow-up study of children with univentricular heart:

- neurodevelopmental outcome at age 12 months. *The Journal of Thoracic and Cardiovascular Surgery*, 137(1):139–145.
- Schaer, M., Glaser, B., Cuadra, M. B., Debbane, M., Thiran, J.-P., and Eliez, S. (2009). Congenital heart disease affects local gyrification in 22q11. 2 deletion syndrome. *Developmental Medicine & Child Neurology*, 51(9):746–753.
- Schaer, M., Glaser, B., Ottet, M.-C., Schneider, M., Cuadra, M. B., Debbane, M., Thiran, J.-P., and Eliez, S. (2010). Regional cortical volumes and congenital heart disease: a MRI study in 22q11. 2 deletion syndrome. *Journal of Neurodevelopmental Disorders*, 2(4):224–234.
- Scheinost, D., Kwon, S. H., Lacadie, C., Vohr, B. R., Schneider, K. C., Papademetris, X., Constable, R. T., and Ment, L. R. (2015). Alterations in anatomical covariance in the prematurely born. *Cerebral Cortex*, page bhv248.
- Schmithorst, V. J., Panigrahy, A., Gaynor, J. W., Watson, C. G., Lee, V., Bellinger, D. C., Rivkin, M. J., and Newburger, J. W. (2016). Organizational topology of brain and its relationship to ADHD in adolescents with d-transposition of the great arteries. *Brain and Behavior*.
- Seehaus, A. K., Roebroek, A., Chiry, O., Kim, D.-S., Ronen, I., Bratzke, H., Goebel, R., and Galuske, R. A. (2013). Histological validation of DW-MRI tractography in human postmortem tissue. *Cerebral Cortex*, 23(2):442–450.
- Seeley, W. W., Crawford, R. K., Zhou, J., Miller, B. L., and Greicius, M. D. (2009). Neurodegenerative diseases target large-scale human brain networks. *Neuron*, 62(1):42– 52.
- Sethi, V., Tabbutt, S., Dimitropoulos, A., Harris, K. C., Chau, V., Poskitt, K., Campbell, A., Azakie, A., Xu, D., Barkovich, A. J., et al. (2013). Single-ventricle anatomy predicts delayed microstructural brain development. *Pediatric Research*, 73(5):661–667.
- Shaw, P., Lalonde, F., Lepage, C., Rabin, C., Eckstrand, K., Sharp, W., Greenstein, D., Evans, A., Giedd, J., and Rapoport, J. (2009). Development of cortical asymmetry in typically developing children and its disruption in attention-deficit/hyperactivity disorder. *Archives of General Psychiatry*, 66(8):888–896.
- Shillingford, A. J., Glanzman, M. M., Ittenbach, R. F., Clancy, R. R., Gaynor, J. W., and Wernovsky, G. (2008). Inattention, hyperactivity, and school performance in a

- population of school-age children with complex congenital heart disease. *Pediatrics*, 121(4):e759–e767.
- Shillingford, A. J., Ittenbach, R. F., Marino, B. S., Rychik, J., Clancy, R. R., Spray, T. L., Gaynor, J. W., and Wernovsky, G. (2007). Aortic morphometry and microcephaly in hypoplastic left heart syndrome. *Cardiology in the Young*, 17(02):189–195.
- Sistino, J. J. and Bonilha, H. S. (2012). Improvements in survival and neurodevelopmental outcomes in surgical treatment of hypoplastic left heart syndrome: a meta-analytic review. *The Journal of Extra-corporeal Technology*, 44(4):216–223.
- Sivarajan, V., Penny, D. J., Filan, P., Brizard, C., and Shekerdemian, L. S. (2009). Impact of antenatal diagnosis of hypoplastic left heart syndrome on the clinical presentation and surgical outcomes: the Australian experience. *Journal of Paediatrics and Child Health*, 45(3):112–117.
- Skudlarski, P., Jagannathan, K., Calhoun, V. D., Hampson, M., Skudlarska, B. A., and Pearlson, G. (2008). Measuring brain connectivity: diffusion tensor imaging validates resting state temporal correlations. *NeuroImage*, 43(3):554–561.
- Smith, S. M., Jenkinson, M., Johansen-Berg, H., Rueckert, D., Nichols, T. E., Mackay, C. E., Watkins, K. E., Ciccarelli, O., Cader, M. Z., Matthews, P. M., et al. (2006). Tractbased spatial statistics: voxelwise analysis of multi-subject diffusion data. *NeuroImage*, 31(4):1487–1505.
- Smith, S. M., Jenkinson, M., Woolrich, M. W., Beckmann, C. F., Behrens, T. E., Johansen-Berg, H., Bannister, P. R., De Luca, M., Drobnjak, I., Flitney, D. E., et al. (2004). Advances in functional and structural MR image analysis and implementation as FSL. *NeuroImage*, 23:S208–S219.
- Soman, S., Prasad, G., Hitchner, E., Massaband, P., Moseley, M. E., Zhou, W., and Rosen, A. C. (2016). Brain structural connectivity distinguishes patients at risk for cognitive decline after carotid interventions. *Human Brain Mapping*, 37(6):2185–2194.
- Sporns, O., Chialvo, D., Kaiser, M., and Hilgetag, C. (2004). Organization, development and function of complex brain networks. *Trends in Cognitive Sciences*, 8(9):418–425.
- Sporns, O., Tononi, G., and Kotter, R. (2005). The human connectome: a structural description of the human brain. *PLoS Computational Biology*, 1(4):e42.
- Stephenson, E. A., Lu, M., Berul, C. I., Etheridge, S. P., Idriss, S. F., Margossian, R., Reed, J. H., Prakash, A., Sleeper, L. A., Vetter, V. L., et al. (2010). Arrhythmias in a

- contemporary Fontan cohort: prevalence and clinical associations in a multicenter cross-sectional study. *Journal of the American College of Cardiology*, 56(11):890–896.
- Stocker, C. F., Shekerdemian, L. S., Visvanathan, K., Skinner, N., Brizard, C. P., Carlin, J. B., Horton, S. B., and Penny, D. J. (2004). Cardiopulmonary bypass elicits a prominent innate immune response in children with congenital heart disease. *The Journal of Thoracic and Cardiovascular Surgery*, 127(5):1523–1525.
- Stonnington, C. M., Tan, G., Kloppel, S., Chu, C., Draganski, B., Jack Jr, C. R., Chen, K., Ashburner, J., and Frackowiak, R. S. (2008). Interpreting scan data acquired from multiple scanners: a study with Alzheimer’s disease. *NeuroImage*, 39(3):1180–1185.
- Sugimoto, A., Ota, N., Ibuki, K., Miyakoshi, C., Murata, M., Tosaka, Y., Yamazaki, T., and Sakamoto, K. (2013). Risk factors for adverse neurocognitive outcomes in schoolaged patients after the fontan operation. *European Journal of Cardio-Thoracic Surgery*, 44(3):454.
- Sun, L., Macgowan, C. K., Sled, J. G., Yoo, S.-J., Manlhiot, C., Porayette, P., GrosseWortmann, L., Jaeggi, E., McCrindle, B. W., Hickey, E., et al. (2015). Reduced fetal cerebral oxygen consumption is associated with smaller brain size in fetuses with congenital heart disease. *Circulation*, 131(15):1313–1323.
- Szwast, A., Tian, Z., McCann, M., Soffer, D., and Rychik, J. (2012). Comparative analysis of cerebrovascular resistance in fetuses with single-ventricle congenital heart disease. *Ultrasound in Obstetrics & Gynecology*, 40(1):62–67.
- Tabbutt, S., Nord, A. S., Jarvik, G. P., Bernbaum, J., Wernovsky, G., Gerdes, M., Zackai, E., Clancy, R. R., Nicolson, S. C., Spray, T. L., et al. (2008). Neurodevelopmental outcomes after staged palliation for hypoplastic left heart syndrome. *Pediatrics*, 121(3):476–483.
- Tabtabai, S., Yeh, D. D., Stefanescu, A., Kennedy, K., Yeh, R. W., and Bhatt, A. B. (2015). National trends in hospitalizations for patients with single-ventricle anatomy. *The American Journal of Cardiology*, 116(5):773–778.
- Tassani, P., Barankay, A., Haas, F., Paek, S., Heilmaiera, M., Hess, J., Lange, R., and Richter, J. (2002). Cardiac surgery with deep hypothermic circulatory arrest produces less systemic inflammatory response than low-flow cardiopulmonary bypass in newborns. *The Journal of Thoracic and Cardiovascular Surgery*, 123(4):648–654.
- Tatu, L., Moulin, T., Bogousslavsky, J., and Duvernoy, H. (1998). Arterial territories of the human cerebral hemispheres. *Neurology*, 50(6):1699-1708.

- Tchervenkov, C. I., Jacobs, J. P., Weinberg, P. M., Aiello, V. D., Beland, M. J., Colan, S. D., Elliott, M. J., Franklin, R. C., Gaynor, J. W., Krogmann, O. N., et al. (2006). The nomenclature, definition and classification of hypoplastic left heart syndrome. *Cardiology in the Young*, 16(04):339–368.
- Teicher, M. H., Anderson, C. M., Ohashi, K., and Polcari, A. (2014). Childhood maltreatment: altered network centrality of cingulate, precuneus, temporal pole and insula. *Biological Psychiatry*, 76(4):297–305.
- Telesford, Q. K., Joyce, K. E., Hayasaka, S., Burdette, J. H., and Laurienti, P. J. (2011). The ubiquity of small-world networks. *Brain Connectivity*, 1(5):367–375.
- Tennant, P. W., Pearce, M. S., Bythell, M., and Rankin, J. (2010). 20-year survival of children born with congenital anomalies: a population-based study. *The Lancet*, 375(9715):649–656.
- Terplan, K. L. (1973). Patterns of brain damage in infants and children with congenital heart disease: association with catheterization and surgical procedures. *American Journal of Diseases of Children*, 125(2):175–185.
- Terplan, K. L. (1976). Brain changes in newborns, infants and children with congenital heart disease in association with cardiac surgery. additional observations. *Journal of Neurology*, 212(3):225–236.
- Thomas, C., Frank, Q. Y., Irfanoglu, M. O., Modi, P., Saleem, K. S., Leopold, D. A., and Pierpaoli, C. (2014). Anatomical accuracy of brain connections derived from diffusion MRI tractography is inherently limited. *Proceedings of the National Academy of Sciences*, 111(46):16574–16579.
- Tijms, B. M., Moller, C., Vrenken, H., Wink, A. M., de Haan, W., van der Flier, W. M., Stam, C. J., Scheltens, P., and Barkhof, F. (2013). Single-subject grey matter graphs in Alzheimer's disease. *PloS One*, 8(3):e58921.
- Tingley, D., Yamamoto, T., Hirose, K., Keele, L., and Imai, K. (2014). mediaton: R package for causal mediation analysis. *Journal of Statistical Software*, 59(5):1–38.
- Tononi, G., Edelman, G., and Sporns, O. (1998). Complexity and coherency: integrating information in the brain. *Trends in Cognitive Sciences*, 2(12):474–484.
- Uzark, K., Lincoln, A., Lamberti, J. J., Mainwaring, R. D., Spicer, R. L., and Moore, J. W. (1998). Neurodevelopmental outcomes in children with Fontan repair of functional single ventricle. *Pediatrics*, 101(4):630–633.

- Vaessen, M., Hofman, P., Tijssen, H., Aldenkamp, A., Jansen, J., and Backes, W. H. (2010). The effect and reproducibility of different clinical DTI gradient sets on small world brain connectivity measures. *NeuroImage*, 51(3):1106–1116.
- van den Heuvel, M. P., de Reus, M. A., Feldman Barrett, L., Scholtens, L. H., Coopmans, F. M., Schmidt, R., Preuss, T. M., Rilling, J. K., and Li, L. (2015). Comparison of diffusion tractography and tract-tracing measures of connectivity strength in rhesus macaque connectome. *Human Brain Mapping*, 36(8):3064–3075.
- van den Heuvel, M. P. and Sporns, O. (2011). Rich-club organization of the human connectome. *The Journal of Neuroscience*, 31(44):15775–15786.
- van der Bom, T., Zomer, A. C., Zwinderman, A. H., Meijboom, F. J., Bouma, B. J., and Mulder, B. J. (2011). The changing epidemiology of congenital heart disease. *Nature Reviews Cardiology*, 8(1):50–60.
- van der Linde, D., Konings, E. E., Slager, M. A., Witsenburg, M., Helbing, W. A., Takkenberg, J. J., and Roos-Hesselink, J. W. (2011). Birth prevalence of congenital heart disease worldwide: a systematic review and meta-analysis. *Journal of the American College of Cardiology*, 58(21):2241–2247.
- Vasa, F., Griffa, A., Scariati, E., Schaer, M., Urban, S., Eliez, S., and Hagmann, P. (2016). An affected core drives network integration deficits of the structural connectome in 22q11.2 deletion syndrome. *NeuroImage: Clinical*, 10:239–249.
- Viger, F. and Latapy, M. (2015). Efficient and simple generation of random simple connected graphs with prescribed degree sequence. *Journal of Complex Networks*, page cnv013.
- Visconti, K. J., Rimmer, D., Gauvreau, K., del Nido, P., Mayer, J. E., Hagino, I., and Pigula, F. A. (2006). Regional low-flow perfusion versus circulatory arrest in neonates: one-year neurodevelopmental outcome. *The Annals of Thoracic Surgery*, 82(6):2207–2213.
- Vogt, K. N., Manlhiot, C., Van Arsdell, G., Russell, J. L., Mital, S., and McCrindle, B. W. (2007). Somatic growth in children with single ventricle physiology: Impact of physiologic state. *Journal of the American College of Cardiology*, 50(19):1876–1883.
- Volpe, J. J. (2009). Brain injury in premature infants: a complex amalgam of destructive and developmental disturbances. *The Lancet Neurology*, 8(1):110–124.
- Volpe, J. J. (2014). Encephalopathy of congenital heart disease—destructive and developmental effects intertwined. *The Journal of Pediatrics*, 164(5):962–965.

- von Rhein, M., Buchmann, A., Hagmann, C., Dave, H., Bernet, V., Scheer, I., Knirsch, W., Latal, B., Heart, Group, B. R., et al. (2015). Severe congenital heart defects are associated with global reduction of neonatal brain volumes. *The Journal of Pediatrics*, 167(6):1259–1263.
- von Rhein, M., Buchmann, A., Hagmann, C., Huber, R., Klaver, P., Knirsch, W., and Latal, B. (2014). Brain volumes predict neurodevelopment in adolescents after surgery for congenital heart disease. *Brain*, 137(1):268–276.
- Wakana, S., Caprihan, A., Panzenboeck, M. M., Fallon, J. H., Perry, M., Gollub, R. L., Hua, K., Zhang, J., Jiang, H., Dubey, P., et al. (2007). Reproducibility of quantitative tractography methods applied to cerebral white matter. *NeuroImage*, 36(3):630–644.
- Wald, R. M., Tham, E. B., McCrindle, B. W., Goff, D. A., McAuliffe, F. M., Golding, F., Jaeggi, E. T., Hornberger, L. K., Tworetzky, W., and Nield, L. E. (2007). Outcome after prenatal diagnosis of tricuspid atresia: a multicenter experience. *American Heart Journal*, 153(5):772–778.
- Wang, D., Shi, L., Liu, S., Hui, S. C., Wang, Y., Cheng, J. C., and Chu, W. C. (2013). Altered topological organization of cortical network in adolescent girls with idiopathic scoliosis. *PLoS One*, 8:83767.
- Wang, J. Y., Abdi, H., Bakhadirov, K., Diaz-Arrastia, R., and Devous, M. D. (2012). A comprehensive reliability assessment of quantitative diffusion tensor tractography. *NeuroImage*, 60(2):1127–1138.
- Warren, O. J., Smith, A. J., Alexiou, C., Rogers, P. L., Jawad, N., Vincent, C., Darzi, A. W., and Athanasiou, T. (2009). The inflammatory response to cardiopulmonary bypass: part 1—mechanisms of pathogenesis. *Journal of Cardiothoracic and Vascular Anesthesia*, 23(2):223–231.
- Watanabe, K., Matsui, M., Matsuzawa, J., Tanaka, C., Noguchi, K., Yoshimura, N., Hongo, K., Ishiguro, M., Wanatabe, S., Hirono, K., et al. (2009). Impaired neuroanatomic development in infants with congenital heart disease. *The Journal of Thoracic and Cardiovascular Surgery*, 137(1):146–153.
- Watson, C. G., Asaro, L. A., Wypij, D., Robertson, R. L., Newburger, J. W., and Rivkin, M. J. (2016). Altered gray matter in adolescents with d-transposition of the great arteries. *The Journal of Pediatrics*, 169:36–43.
- Watts, D. J. and Strogatz, S. H. (1998). Collective dynamics of “small-world” networks. *Nature*, 393(6684):440–442.

- Wechsler, D. (2003). Wechsler intelligence scale for children—fourth edition (WISC-IV). *San Antonio, TX: The Psychological Corporation.*
- Wechsler, D. (2005). *Wechsler individual achievement test (WIAT-II UK)*. Harcourt Assessment.
- Wechsler, D. (2008). *Wechsler adult intelligence scale—fourth edition*. San Antonio: Pearson.
- Wells, F., Coghill, S., Caplan, H., and Lincoln, C. (1983). Duration of circulatory arrest does influence the psychological development of children after cardiac operation in early life. *The Journal of Thoracic and Cardiovascular surgery*, 86(6):823–831.
- Wernovsky, G., Stiles, K. M., Gauvreau, K., Gentles, T. L., Bellinger, D. C., Walsh, A. Z., Burnett, J., Jonas, R. A., Mayer, J. E., Newburger, J. W., et al. (2000). Cognitive development after the Fontan operation. *Circulation*, 102(8):883–889.
- Westaby, S. (1987). Organ dysfunction after cardiopulmonary bypass. a systemic inflammatory reaction initiated by the extracorporeal circuit. *Intensive Care Medicine*, 13(2):89–95.
- Williams, I. A., Fifer, C., Jaeggi, E., Levine, J. C., Michelfelder, E. C., and Szvast, A. L. (2013). The association of fetal cerebrovascular resistance with early neurodevelopment in single ventricle congenital heart disease. *American Heart Journal*, 165(4):544–550.
- Williams, I. A., Fifer, W. P., and Andrews, H. (2015). Fetal growth and neurodevelopmental outcome in congenital heart disease. *Pediatric Cardiology*, 36(6):1135–1144.
- Wren, C., Birrell, G., and Hawthorne, G. (2003). Cardiovascular malformations in infants of diabetic mothers. *Heart*, 89(10):1217–1220.
- Wren, C. and O’Sullivan, J. (2001). Survival with congenital heart disease and need for follow up in adult life. *Heart*, 85(4):438–443.
- Wypij, D., Newburger, J. W., Rappaport, L. A., duPlessis, A. J., Jonas, R. A., Wernovsky, G., Lin, M., and Bellinger, D. C. (2003). The effect of duration of deep hypothermic circulatory arrest in infant heart surgery on late neurodevelopment: the Boston Circulatory Arrest Trial. *The Journal of Thoracic and Cardiovascular Surgery*, 126(5):1397–1403.

- Yao, Z., Zhang, Y., Lin, L., Zhou, Y., Xu, C., Jiang, T., Initiative, A. D. N., et al. (2010). Abnormal cortical networks in mild cognitive impairment and Alzheimer's disease. *PLoS Computational Biology*, 6(11):e1001006.
- Zalesky, A., Fornito, A., and Bullmore, E. (2012). On the use of correlation as a measure of network connectivity. *NeuroImage*, 60(4):2096–2106.
- Zalesky, A., Fornito, A., and Bullmore, E. T. (2010a). Network-based statistic: identifying differences in brain networks. *NeuroImage*, 53(4):1197–1207.
- Zalesky, A., Fornito, A., Harding, I. H., Cocchi, L., Yucel, M., Pantelis, C., and Bullmore, E. T. (2010b). Whole-brain anatomical networks: does the choice of nodes matter? *NeuroImage*, 50(3):970–983.
- Zeng, S., Zhou, J., Peng, Q., Tian, L., Xu, G., Zhao, Y., Wang, T., and Zhou, Q. (2015a). Assessment by three-dimensional power Doppler ultrasound of cerebral blood flow perfusion in fetuses with congenital heart disease. *Ultrasound in Obstetrics & Gynecology*, 45(6):649–656.
- Zeng, S., Zhou, Q., Zhou, J., Li, M., Long, C., and Peng, Q. (2015b). Volume of intracranial structures on three-dimensional ultrasound in fetuses with congenital heart disease. *Ultrasound in Obstetrics & Gynecology*, 46(2):174–181.
- Zhou, D., Lebel, C., Evans, A., and Beaulieu, C. (2013). Cortical thickness asymmetry from childhood to older adulthood. *NeuroImage*, 83:66–74.
- Zielinski, B. A., Gennatas, E. D., Zhou, J., and Seeley, W. W. (2010). Network-level structural covariance in the developing brain. *Proceedings of the National Academy of Sciences*, 107(42):18191–18196.

CURRICULUM VITAE

- Contact* Christopher G. Watson
 Year of birth: 1983
cgwatson@bu.edu
 Graduate Program for Neuroscience, Boston University, 677 Beacon Street, Boston, MA 02215, USA
- Education* Massachusetts Institute of Technology, B.Sc., Brain & Cognitive Sciences, September 2001 – June 2007.
 Boston University PhD candidate, September 2011 – present. Thesis advisor: Lucia M. Vaina.
- Publications*
1. Watson CG, Dehaes M, Gagoski BA, Grant PE, Rivkin MJ. *Arterial spin labeling perfusion magnetic resonance imaging performed in acute perinatal stroke reveals hyperperfusion associated with ischemic injury.* *Stroke*, 47(6):1514-1519. doi:10.1161/STROKEAHA.115.011936
 2. Schmithorst VJ, Panigrahy A, Gaynor JW, Watson CG, Lee V, Bellinger DC, Rivkin MJ, Newburger JW. *Organizational topology of brain and its relationship to ADHD in adolescents with d-transposition of the great arteries.* *Brain and Behavior*, in press. doi:10.1002/brb3.504
 3. Watson CG, Asaro LA, Wypij D, Newburger JW, Rivkin MJ. *Altered gray matter in adolescents with d-Transposition of the Great Arteries.* *Journal of Pediatrics*, 2016. 169:36-43.e1. doi:10.1016/j.jpeds.2015.09.084
 4. Bellinger DC, Watson CG, Rivkin MJ, Robertson RL, Roberts AE, Stopp C, Dunbar-Masterson C, Bernson D, DeMaso DR, Wypij D, Newburger JW. *Neuropsychological status and structural brain imaging in adolescents with critical congenital heart disease who underwent the Fontan procedure.* *Journal of the American Heart Association*, 2015. 4:e002302. doi:10.1161/JAHA.115.002302
 5. Lehman LL, Watson CG, Kapur K, Danehy AR, Rivkin MJ. *Predictors of stroke after transient ischemic attack in children.* *Stroke*, 2016. 47:88-93. doi:10.1161/STROKEAHA.115.009904
 6. Watson CG et al., *Cortical thickness networks in post-Fontan adolescents. In preparation*
 7. Panigrahy A, Schmithorst VJ, Wisnowski JL, Watson CG, Bellinger DC, Rivkin MJ, Newburger JW. *Structural network topology mediates cognitive outcome in adolescents with d-Transposition of the Great*

- Arteries corrected with neonatal arterial switch procedure.* NeuroImage: Clinical. 7 (2015), 438-448. doi:10.1016/j.nicl.2015.01.013
8. Rollins CK*, Watson CG*, Asaro LA, Wypij D, Bellinger DC, Newburger JW, Rivkin MJ. *White matter microstructure and cognition are related in adolescents with congenital heart disease.* Journal of Pediatrics. 165 no. 5 (2014), 936-944. doi:10.1016/j.jpeds.2014.07.028
9. Rivkin MJ, Watson CG, Scoppettuolo LA, Wypij D, Vajapeyam S, Bellinger DC, DeMaso DR, Robertson Jr. Newburger JW. *Adolescents with d-Transposition of the Great Arteries repaired in early infancy demonstrate reduced white matter microstructure associated with clinical risk factors.* Journal of Thoracic and Cardiovascular Surgery 146 no. 3 (2013), 543-549. doi:10.1016/j.jtcvs.2012.12.006